**Title**
Applications of Ionic Clusters in High Resolution Mass Spectrometry



**Author**
Leib, Ryan David

**Publication Date**
2010

Peer reviewed|Thesis/dissertation

# Applications of Ionic Clusters in High Resolution Mass Spectrometry

by

Ryan David Leib

A dissertation submitted in partial satisfaction of the

requirements for the degree of

Doctor of Philosophy

in

Chemistry

in the

Graduate Division

of the

University of California, Berkeley

Committee in charge:

Professor Evan R. Williams, Chair
Professor Kristie A. Boering
Professor Robert M. Glaeser

Fall 2010

Applications of Ionic Clusters in High Resolution Mass Spectrometry



by

Ryan David Leib

Abstract

Applications of Ionic Clusters in High Resolution Mass Spectrometry

by

Ryan David Leib

Doctor of Philosophy in Chemistry

University of California, Berkeley

Professor Evan R. Williams, Chair

This dissertation reports a series of experiments undertaken to determine new uses for gas-phase cluster ions by investigation of their formation and thermochemistry. Clusters of ions and neutrals can be formed from electrospray ionization of peptides, amino acids, metals, and metal complexes in solution, resulting in varied chemical distributions including both homogeneous analyte clusters and heterogeneous clusters, such as hydrated metal ions. Large hydrated ions are ideal chemical thermometers, which can be used to measure the adiabatic internal energy deposition from a gas-phase reaction simply by determining the change in mass resulting from the evaporation of water from the cluster ion. Ideally, each of these waters removes a discrete amount of energy– approximately the energy of two hydrogen bonds, or 10 kcal/mol–resulting in a "ladder" or "scale" of measured energies for a given reaction, as well as a width for the energy distribution imparted to the ion during the reaction. These robust and adjustable "nanocalorimeters" are introduced here and used to determine the thermochemistry of one-electron recombination reactions with metal ions and ion complexes. These results have key implications for the magnitude and character of the energy deposition in electron capture dissociation, a fundamental technique in top-down proteomics. Of further interest is the fact that these nanocalorimetry measurements should become more comparable to bulk measurements made in solution as cluster ion size increases. Initial experiments using these gas-phase measurements to obtain bulk values, such as the absolute value of the standard hydrogen electrode, that are not measureable in solution-phase electrochemistry are demonstrated.

Additionally, clusters of ions formed from a mixture of analyte components should be, in principle, indicative of the stoichiometry of the mixture if they are formed statistically. Here, statistical analyses of cluster ion distributions are used to obtain reasonably accurate and rapid measurements of peptide and amino acid molar fractions in solution mixtures over a three order of magnitude range in lieu of traditional standards. These measurements are not possible using individual ions, due to differences in ionization and detection efficiency of the discrete analytes which cause preferential

enhancement or suppression of mixture components. However, within a cluster composed primarily of like components, *i.e.*, a clustering agent, these differences become small, and mixtures of peptides and amino acids containing up to ten components are quantified. Taken together, these experiments reveal a robust series of applications for cluster ions previously regarded as a detriment to the efficient formation of ions.

*For Edwin Hensley and Otis Yount,*
*Two men whose great sacrifices ensured my opportunity to pursue education.*

CONTENTS

## ACKNOWLEDGEMENTS

Seeing as this dissertation serves as a record of my contributions to this field over the past few years, it is necessary for me to first give credit to those who helped make those contributions possible. I was able to attend university because of the tireless efforts of Drs. Michael A. Royal and Donna L. Nimec, who each went well beyond their professional obligations to start me on this path and fueled my interest in the promise and application of biochemical science. Drs. Dale Teeters and Gilbert N. Belofsky reinforced in me that a researcher's greatest tools were curiosity and diligence. And, of course, Dr. Evan R. Williams, whose infectious enthusiasm and ardent dedication to understanding chemistry are constant examples worthy of imitation.

In addition, I cannot forget those who fought in the trenches to push this work forward. A special thanks to Dr. Errol Robinson, who *was* involved, taking time from writing his own dissertation to ensure that I had the skills necessary to be successful in this career. I have been blessed with many talented collaborators in the Williams Group, notably Dr. W. Alex Donald, Jeremy T. O'Brien, Dr. Matthew F. Bush, James S. Prell, Tawnya G. Flick, Dr. Sanjay Krishnaswamy and Dr. Mariam ElNaggar, who have all contributed in their own way to what follows. Both Dr. Greg T. Blakney and Tony O'Brien were critical contributors to the development of the Predator DAS.

Outside the laboratory, I must thank my many dear friends and my family: my parents, Doug and Mary, and my sister Erin, who are constant reminders of what people with real jobs do, and provided much-needed frames of reference from time to time.

And finally, my deepest thanks to my wife Allison, whose patience, love and support carried me through these past few years. I cannot imagine a better partner, and could not have done this without her.

# Chapter 1

## Introduction

### 1.0 Overview.

A major analytical challenge in biophysical chemistry at the end of the 20th Century was untangling the human genome [1,2]: vast resources were leveraged and thousands toiled to decode the information held in ~20,000 genes present in each human nucleus. However, it became evident even as this task was being completed that to use the host of genomic data collected effectively, a more complex set of problems must also be solved: decoding the devilishly complex mixtures of the proteome [3-7], the glycome [8-11], and the metabolome [12-15], each a massive undertaking in their own right. At the same time as these biological questions became pertinent, other mixtures such as those common to pharmaceuticals, *i.e.*, natural products and synthetic reactions [16-22], forensics, *i.e.*, explosives and illegal drugs [22-27], and environmental sources, *i.e.*, petroleomics and pollutants [28-30], became increasingly critical to deconvolve and quantify. To address these issues, new instrumentation and techniques are constantly being developed, often stemming from two major goals: to simplify the analytical mixtures so that each target may be reliably probed [31-34], and to improve the performance of the analytical technique, particularly in terms of rapid, accurate measurements [33-35].

Mass spectrometry has been a leading technique in the analysis of mixtures due to a variety of unique advantages. Unlike most instrumental methods, the reliance on a proportionality between mass and charge to make the analytical measurement allows for a variety of physical properties, such as velocity or resonant frequency [36-40], to be used, each with unique advantages for a given set of analytes. Additionally, mass spectrometers are typically quite sensitive, inherently selective and easily coupled into multiple, orthogonal mass spectrometric steps, so-called tandem MS or $MS^n$ [41-46]. Using mass spectrometry, it is often trivial to distinguish species unambiguously based on their mass coupled with structural elucidation through fragmentation methods [46], making it ideal for sifting through complex mixtures. Through such measurements, the majority of the progress in proteomic research has been made, as well as significant utility in other forms of mixture analysis and quantitation.

This work details the development of two mass spectrometric techniques that can be used to better understand analyte reactivity, structure and mixture composition. The key difference between these techniques and those that came before is that, rather than dissociating ionic mixtures into individual components, this work focuses on the development of techniques that utilize clusters of ions as energetic and analytical tools. Noncovalent clusters offer a novel avenue to make a chemical measurement, one that often behaves more similarily to an ion in solution, as well as giving a more representative estimation of quantity than can be obtained from individual ions. First, solvated ions are used as easily manipulated reaction thermometers, providing a detailed first look at the energetics involved in gas-phase ion-electron interactions. Second, the

matrix from which ions are formed is modified to create cluster ions that can provide detailed, simultaneous and accurate quantitative information about a number of complex mixtures.

### 1.1 Mass Spectrometry.

With a simple and accurate measurement of mass, an unknown analyte's identity is often trivial to assign. Due to the sensitivity and selectivity of mass spectrometric measurements, obtaining an accurate mass has become a cornerstone of chemical analysis and given rise to a host of instruments that rely on different physical properties to obtain a mass-to-charge ratio. Simple measurements of mass can be made based on various physical properties that are easily related to mass by first principles, such as velocity measurements used in time-of-flight [36-38], or the resonant frequency of oscillation in an electric or magnetic field [39,40]. Each of these offer different advantages in terms of sensitivity and selectivity, as well as differences in dynamic range, mass resolving power and mass accuracy.

Of particular interest to this work are Fourier transform ion cyclotron resonance instruments (FT/ICR MS), which operate by trapping an ion within a static homogeneous magnetic field in two dimensions, and a electrostatic field in the third [40]. Using this arrangement, a trapped ion can be excited to a large radius using a waveform that covers a broad sweep in frequency [47], and then these excited ions will spin at their resonant cyclotron frequency within the magnetic field, which is directly related to its mass to charge ratio through the Lorentz force [40]. This mass-dependent 'ringing' of an ion is easily detected as an image current on electrodes within the cell, and simply transformed from its time-domain signal by Fourier transform into the frequency domain for ready determination of mass [40]. This class of mass spectrometers offers the highest resolving powers yet achieved, in excess of $\sim 10^6$ [48,49], and are highly mass accurate, often allowing for unambiguous identification of multiple species with the same nominal mass [50,51]. In addition, these instruments are uniquely suited to mixture analyses, as the cyclotron frequencies of each species present within the trap can be simultaneously collected and analyzed because the image current following excitation is simply a linear superposition of the individual components [40].

Like varied principles of the mass analyzers, introducing ions into the gas phase can be achieved by a variety of mechanisms. Early interest in mass spectrometry focused on the ionization of small volatile molecules, most commonly using electron impact or photoionization, although other, often selective methods such as chemical ionization were also employed [52,53]. These relatively 'hard' ionization techniques work well for many small molecules, but larger molecules remained inaccessible because it is typically kinetically favorable to undergo thermal decomposition before ionization. It wasn't until the introduction of 'soft' ionization methods, starting with fast atom bombardment [54] and later the Nobel prize-winning methods electrospray ionization [55-57] and "soft" laser desorption [58-60], that the vast majority of biological samples, such as intact complex sugars, proteins, and nucleic acids, became available for mass analysis [11,61,62]. In a typical electrospray experiment, ions are formed directly from a solution

containing the analyte. A large electric field difference between the solution, typically in a nozzle-like emitter, and the inlet to the mass spectrometer will distort the surface of the droplet and if the electric field is sufficiently strong, typically in the low 10s of kV/cm, it will overcome the surface tension, resulting in a jet of droplets emitted from the liquid surface [63-65]. Some of these droplets will contain the analyte molecule and excess surface charge, which can undergo desolvation due to collisions with atmospheric gases and the relatively low binding energies of the solvent molecules to the cluster. When a sufficient number of solvent molecules have been lost, droplet potential energies exceed the surface tension, and the resulting Coulomb explosion results in fission to form many smaller droplets. This process continues iteratively until bare ions remain, although the mechanism of these final steps is hotly debated [65,66] and likely species-dependent.

Unlike in a traditional electrospray ionization in which complete desolvation is desired, here small cluster ions will be formed. The attachment of solvent or other noncovalently attached molecules to the analyte is competitive with the desolvation process if collision energies are sufficiently low. This offers an ideal platform to study reaction energetics, through use of these weakly bound clusters as "nanocalorimeters", a new form of chemical thermometer [67,68]. Additionally, the attachment of other analytes in the matrix can be studied in much the same way, giving rise to a unique quantitative tool which has distinct advantages compared to more traditional standard-based techniques.

### 1.2 Tandem mass spectrometry methods and electron dissociation.

There is far more to mass spectrometry than simply generating a gas-phase ion and obtaining a mass. With the addition of a growing range of multidimensional mass spectrometry techniques, tailoring the experimental apparatus to suit the needs of a particular analytical inquiry has become increasingly easy. This array of tools includes chromatographic separations [69,70], mobility separations [71-73], as well as collisional and photon induced dissociations [74-77]. These methods ideally provide orthogonal separation by characterizing additional physical properties of an analyte, *e.g.*, ion mobility methods can be employed to determine the physical cross-section of an ion in addition to its mass giving an indication of conformation, and dissociation methods give detailed access to ion bond connectivity, thus enhancing formula elucidation and structural assignment.

Of particular interest to this work is a growing class of dissociation methods that rely on the interaction of an electron or electron donor with a multiply charged cation, broadly classified as electron ion recombination methods [78-80]. These techniques are commonly used in the study of protein sequence and structure [43], providing extensive or even complete sequence coverage. These methods differ significantly from the classic electron ionization methods, in which a relatively high-energy, *i.e.*, ~70 eV, electron ionizes a volatile neutral to form gaseous cations and fragments. In contrast, the typical electron capture dissociation experiment uses thermally generated electron with near-zero kinetic energy to reduce a gas-phase multiply charged cation trapped within an ion cell. The cross-section for electron capture is greatest when the energy difference between the

electrons and the target cation is small [81,82]. Thus, the attachment of an electron to a peptide or protein cation should simply release the recombination energy of this ion electron reaction, estimated for peptides and proteins to be between four and seven eV [83]. In peptides and proteins, the reduced radical cation then most often cleaves at the N-$C_\alpha$ bond, resulting in a pair of fragment ions, a N-terminal ***c*** ion and a C-terminal ***z*** ion [78,84]. Additional reactivity for cleaving disulfide bonds [83], as well as a small percentage of N-terminal ***a***, ***b*** fragment ions as well as C-terminal ***y*** fragment ions, corresponding to cleavage sites between the $C_\alpha$ and the amide carbon for the ***a*** ion, or at the amide bond for the ***b*** and ***y*** ions, are also frequently observed [83], but loss of posttranslational modifications, such as phosphates or sugars, or noncovalent ligands typically are not [85-87]. Following the introduction of this method using thermal electrons, additional techniques using negative ions [79] and neutrals [80] as the electron donor have been developed, usually obtaining similar results, as well as methods using higher kinetic energies for the captured electrons [82] to improve efficiency for the products from this reaction.

The electron capture process is, in itself, a source of much debate. Assuming little or no contribution from translationally 'hot' electrons, the attachment of an electron releases only a small fraction of the internal energy of a typical small protein ion at room temperature [83]. Although this may be sufficient energy to break a single bond, the distribution of this energy across the large number of internal modes results in a trivial increase in the internal energy of any given mode. This has led some to suggest that the energy is nonstatistically partitioned into a single mode resulting in fragmentation [78], whereas others hold that the electronic structure of the odd-electron ion is fundamentally 'weak' at the N-$C_\alpha$ bond compared to its even-electron cation precursor [88]. More recently, a third mechanism that relies on a cascade of radical reactions has been proposed that may account for the extensive cleavage observed for such a small energy deposition [89]. As is often the case, ample evidence has been provided supporting each of these mechanisms [90-94].

The first step in determining to what degree any of these mechanisms might be involved in the observed electron capture reaction resides in characterizing the energies involved in the electron capture process, and build from there a concept of how the energy might partition within a protein and result in the observed cleavages. Here, gas-phase cluster ions will be used as ion 'thermometers,' or 'nanocalorimeters,' to directly probe these ion-electron recombination energies, and will provide insight into the mechanisms involved in the electron capture process.

### 1.3 Gas-phase ion nanocalorimetry.

A number of tools to measure the thermodynamics of a gas-phase reaction have been introduced [95]. One of the most convenient approaches is to use a 'thermometer' ion [67,68], in which ideally a series of sequential fragment ions can be formed, each with well-described bond dissociation energies. By inputting an unknown amount of energy into this thermometer ion, the energy may be calculated by the appearance of resulting fragments of known bond dissociation energy. Cooks and coworkers developed

this technique [68] with the analysis of $FeCO_5$ collisions with a surface. Upon collision, sequential loss of CO molecules from the covalent precursor ion can occur, each loss with a well-defined energy [68]. Using the relative abundances of the resulting fragments, the average energy deposition was determined for different accelerations into the metal surface target [68]. While this method provided an accurate measure of the internal energy deposited during the collision, the resolution of this method is limited by the difference in the energies between each subsequent fragment; higher resolution chemical thermometers would therefore require smaller energy 'steps' between sequential fragments.

Previously, most gas-phase cluster ions were seen as contaminants to be reduced and avoided, and a great deal of effort has gone into producing more efficient and 'harsh' ion sources that assist in the desolvation process [96-99]. However, with proper tuning of the ionization source and transfer conditions, the attachment of noncovalent adducts can be carefully controlled, whether the adducts be molecules of the solvent [100-105], salts [103-108], specific noncovalent ligands from solution [109-113], nonspecific clusters of multiple analyte molecules [114-120] or some combination of all of these.

Here, a new, flexible thermometer ion system is introduced that takes advantage of hydrated ion clusters. A key improvement of this approach over previous approaches is that, once a sufficiently large cluster size is obtained, differences between dissociation energies for each sequential water loss become small and thus evenly spaced, aiding interpretation and comparison between different incident energies. Additionally, this method is inherently adiabatic, including all energies due to rearrangement following reduction of the cluster. Other important advantages include that these hydrated 'nanocalorimeters' can be easily controlled in size and composition and can be applied to any ion which can attach solvent molecules, providing a broad applicability for most conceivable systems. Operating under 'gentle' ion source conditions opens the door to a number of experiments using these cluster ions. Of particular interest is the ability of these highly resolved cluster ion fragments to elucidate differences in multiple kinetic pathways, providing insight into the kinetic landscape available to these reactions. Further, this method provides not only the average energy deposition but also a well-defined shape of the incident energy distribution and an indication as to the energy distribution resulting from kinetic energy release of the products, further describing the nature of gas-phase reactions. This work is described in Chapters three, four and five.

### 1.4 Quantitation of mixture components.

It is important to realize that the abundances of ions present in a typical mass spectrum are often not indicative of the absolute concentration of the analytes present in the sample. This is the result of a host of matrix effects [121-124], ionization efficiencies [125-128], and transfer and detection efficiencies [64,129], all of which can dramatically affect the observed abundances. In the case of electrospray ionization of analyte mixtures, relative analyte basicity, surface activity, and concentration [127,128,130-133] as well as solvent surface tension [126,131] are key factors that influence the observed spectrum.

Because of these ionization efficiency differences, a variety of techniques have been developed to obtain quantitative information from a mass spectrum, typically involving separations [18,35,134] and standards [135-138]. However, the use of separation techniques, such as liquid chromatography, prior to ionization are often unable to reduce coeluting matrix effects [124] that can distort the abundances in the mass spectrum. Standard-based techniques, such as external calibrations and internal standards, have found extensive use in quantitation by mass spectrometry; isotopically labeled internal standards often are the most reliable, with typically accuracies within 5% [139,140]. However, these methods are not without their disadvantages; it would be useful to be able to quantify the contents of an analytical mixture directly from the mass spectrum, rather than rely on costly and time-consuming separations and calibrations against traditional standards. This is particularly important in cases where standards are unavailable, either because the target analyte is chemically unidentified or is a restricted substance.

Here, cluster ions are used to provide a new analytical tool to determine mixture composition directly from the abundances found in the mass spectrum. Previous work has shown that both specific and nonspecific clusters of ions can be readily formed from metals, amino acids, peptides, and proteins [95,115-117,141]. When the formation of these clusters is nonspecific, integration of each component should simply be a reflection of its stociometry in the mixture. As a result, by adding a large, known excess of a 'clustering agent' to a solution, the composition of mixture components can be determined from the distribution of clusters observed. Further, since these clusters are formed primarily of the clustering agent and thus differ only slightly in structure, their ionization, transfer and detection efficiencies should be similar, resulting in abundances in the gas phase that correlate well with the solution composition. This method is described for a variety of systems here, and compared against more traditional approaches to quantitation. This work is described in Chapters six and seven.

## 1.5 References


[1] Lander, E. S.; Linton, L. M.; Birren, B.; Nusbaum, C.; Zody, M. C.; Baldwin, J.; Devon, K.; Dewar, K.; Doyle, M.; FitzHugh, W.; Funke, R.; Gage, D.; Harris, K.; Heaford, A.; Howland, J.; Kann, L.; Lehoczky, J.; LeVine, R.; McEwan, P.; McKernan, K.; Meldrim, J.; Mesirov, J. P.; Miranda, C.; Morris, W.; Naylor, J.; Raymond, C.; Rosetti, M.; Santos, R.; Sheridan, A.; Sougnez, C.; Stange-Thomann, N.; Stojanovic, N.; Subramanian, A.; Wyman, D.; Rogers, J.; Sulston, J.; Ainscough, R.; Beck, S.; Bentley, D.; Burton, J.; Clee, C.; Carter, N.; Coulson, A.; Deadman, R.; Deloukas, P.; Dunham, A.; Dunham, I.; Durbin, R.; French, L.; Grafham, D.; Gregory, S.; Hubbard, T.; Humphray, S.; Hunt, A.; Jones, M.; Lloyd, C.; McMurray, A.; Matthews, L.; Mercer, S.; Milne, S.; Mullikin, J. C.; Mungall, A.; Plumb, R.; Ross, M.; Shownkeen, R.; Sims, S.; Waterston, R. H.; Wilson, R. K.; Hillier, L. W.; McPherson, J. D.; Marra, M. A.; Mardis, E. R.; Fulton, L. A.; Chinwalla, A. T.; Pepin, K. H.; Gish, W. R.; Chissoe, S. L.; Wendl, M. C.; Delehaunty, K. D.; Miner, T. L.; Delehaunty, A.; Kramer, J. B.; Cook, L. L.; Fulton, R. S.; Johnson, D. L.; Minx, P. J.; Clifton, S. W.; Hawkins, T.; Branscomb, E.; Predki, P.; Richardson, P.; Wenning, S.; Slezak, T.; Doggett, N.; Cheng, J. F.; Olsen, A.; Lucas, S.; Elkin, C.; Uberbacher, E.; Frazier, M. *Nature* **2001**, *409*, 860-921.

[2] Venter, J. C.; Adams, M. D.; Myers, E. W.; Li, P. W.; Mural, R. J.; Sutton, G. G.; Smith, H. O.; Yandell, M.; Evans, C. A.; Holt, R. A.; Gocayne, J. D.; Amanatides, P.; Ballew, R. M.; Huson, D. H.; Wortman, J. R.; Zhang, Q.; Kodira, C. D.; Zheng, X. Q. H.; Chen, L.; Skupski, M.; Subramanian, G.; Thomas, P. D.; Zhang, J. H.; Miklos, G. L. G.; Nelson, C.; Broder, S.; Clark, A. G.; Nadeau, C.; McKusick, V. A.; Zinder, N.; Levine, A. J.; Roberts, R. J.; Simon, M.; Slayman, C.; Hunkapiller, M.; Bolanos, R.; Delcher, A.; Dew, I.; Fasulo, D.; Flanigan, M.; Florea, L.; Halpern, A.; Hannenhalli, S.; Kravitz, S.; Levy, S.; Mobarry, C.; Reinert, K.; Remington, K.; Abu-Threideh, J.; Beasley, E.; Biddick, K.; Bonazzi, V.; Brandon, R.; Cargill, M.; Chandramouliswaran, I.; Charlab, R.; Chaturvedi, K.; Deng, Z. M.; Di Francesco, V.; Dunn, P.; Eilbeck, K.; Evangelista, C.; Gabrielian, A. E.; Gan, W.; Ge, W. M.; Gong, F. C.; Gu, Z. P.; Guan, P.; Heiman, T. J.; Higgins, M. E.; Ji, R. R.; Ke, Z. X.; Ketchum, K. A.; Lai, Z. W.; Lei, Y. D.; Li, Z. Y.; Li, J. Y.; Liang, Y.; Lin, X. Y.; Lu, F.; Merkulov, G. V.; Milshina, N.; Moore, H. M.; Naik, A. K.; Narayan, V. A.; Neelam, B.; Nusskern, D.; Rusch, D. B.; Salzberg, S.; Shao, W.; Shue, B. X.; Sun, J. T.; Wang, Z. Y.; Wang, A. H.; Wang, X.; Wang, J.; Wei, M. H.; Wides, R.; Xiao, C. L.; Yan, C. H. *Science* **2001**, *291*, 1304-+.

[3] Anderson, N. L.; Anderson, N. G. *Mol. Cell. Proteomics* **2002**, *1*, 845-867.

[4] Rual, J. F.; Venkatesan, K.; Hao, T.; Hirozane-Kishikawa, T.; Dricot, A.; Li, N.; Berriz, G. F.; Gibbons, F. D.; Dreze, M.; Ayivi-Guedehoussou, N.; Klitgord, N.; Simon, C.; Boxem, M.; Milstein, S.; Rosenberg, J.; Goldberg, D. S.; Zhang, L. V.;

Wong, S. L.; Franklin, G.; Li, S. M.; Albala, J. S.; Lim, J. H.; Fraughton, C.; Llamosas, E.; Cevik, S.; Bex, C.; Lamesch, P.; Sikorski, R. S.; Vandenhaute, J.; Zoghbi, H. Y.; Smolyar, A.; Bosak, S.; Sequerra, R.; Doucette-Stamm, L.; Cusick, M. E.; Hill, D. E.; Roth, F. P.; Vidal, M. *Nature* **2005**, *437*, 1173-1178.

[5] Zhou, Z. L.; Licklider, L. J.; Gygi, S. P.; Reed, R. *Nature* **2002**, *419*, 182-185.

[6] Andersen, J. S.; Lyon, C. E.; Fox, A. H.; Leung, A. K. L.; Lam, Y. W.; Steen, H.; Mann, M.; Lamond, A. I. *Current Biology* **2002**, *12*, 1-+.

[7] Taylor, S. W.; Fahy, E.; Zhang, B.; Glenn, G. M.; Warnock, D. E.; Wiley, S.; Murphy, A. N.; Gaucher, S. P.; Capaldi, R. A.; Gibson, B. W.; Ghosh, S. S. *Nature Biotech.* **2003**, *21*, 281-286.

[8] Callewaert, N.; Van Vlierberghe, H.; Van Hecke, A.; Laroy, W.; Delanghe, J.; Contreras, R. *Nature Medicine* **2004**, *10*, 429-434.

[9] Ohtsubo, K.; Marth, J. D. *Cell* **2006**, *126*, 855-867.

[10] Raman, R.; Raguram, S.; Venkataraman, G.; Paulson, J. C.; Sasisekharan, R. *Nature Methods* **2005**, *2*, 817-824.

[11] Zaia, J. *Mass Spectrom. Rev.* **2004**, *23*, 161-227.

[12] Goodacre, R.; Vaidyanathan, S.; Dunn, W. B.; Harrigan, G. G.; Kell, D. B. *Trends in Biotechnology* **2004**, *22*, 245-252.

[13] Soga, T.; Ohashi, Y.; Ueno, Y.; Naraoka, H.; Tomita, M.; Nishioka, T. *J. Proteome Res.* **2003**, *2*, 488-494.

[14] Dettmer, K.; Aronov, P. A.; Hammock, B. D. *Mass Spectrom. Rev.* **2007**, *26*, 51-78.

[15] Kell, D. B. *Curr. Op. Microbiol.* **2004**, *7*, 296-307.

[16] Hoke, S. H.; Wood, J. M.; Cooks, R. G.; Li, X. H.; Chang, C. J. *Anal. Chem.* **1992**, *64*, 2313-2315.

[17] Kerns, E. H.; Volk, K. J.; Hill, S. E.; Lee, M. S. *J. Nat. Prod.* **1994**, *57*, 1391-1403.

[18] Corcoran, O.; Spraul, M. *Drug Discovery Today* **2003**, *8*, 624-631.

[19] Zeeb, D. J.; Nelson, B. C.; Albert, K.; Dalluge, J. J. *Anal. Chem.* **2000**, *72*, 5020-5026.

[20] Koehn, F. E.; Carter, G. T. *Nature Reviews Drug Discovery* **2005**, *4*, 206-220.

[21] Tao, W. A.; Gozzo, F. C.; Cooks, R. G. *Anal. Chem.* **2001**, *73*, 1692-1698.

[22] ElSohly, M. A.; Slade, D. *Life Sci.* **2005**, *78*, 539-548.

[23] Geiser, L.; Cherkaoui, S.; Veuthey, J. L. *J. Chromatogr. A* **2000**, *895*, 111-121.

[24] Skender, L.; Karacic, V.; Brcic, I.; Bagaric, A. *For. Sci. Int.* **2002**, *125*, 120-126.

[25] Asbury, G. R.; Klasmeier, J.; Hill, H. H. *Talanta* **2000**, *50*, 1291-1298.

[26] Wallenborg, S. R.; Bailey, C. G. *Anal. Chem.* **2000**, *72*, 1872-1878.

[27] Steinfeld, J. I.; Wormhoudt, J. *Annu. Rev. Phys. Chem.* **1998**, *49*, 203-232.

[28] Marshall, A. G.; Rodgers, R. P. *Acc. Chem. Res.* **2003**, *37*, 53-59.

[29] McKenna, A. M.; Blakney, G. T.; Xian, F.; Glaser, P. B.; Rodgers, R. P.; Marshall, A. G. *Energy Fuels*, *24*, 2939-2946.

[30] Perez-Estrada, L. A.; Malato, S.; Gernjak, W.; Aguera, A.; Thurman, E. M.; Ferrer, I.; Fernandez-Alba, A. R. *Environ. Sci. & Technol.* **2005**, *39*, 8300-8306.

[31] Neverova, I.; Van Eyk, J. E. *J. Chromatogr. B* **2005**, *815*, 51-63.

[32] McCormack, A. L.; Schieltz, D. M.; Goode, B.; Yang, S.; Barnes, G.; Drubin, D.; Yates, J. R. *Anal. Chem.* **1997**, *69*, 767-776.

[33] Opiteck, G. J.; Lewis, K. C.; Jorgenson, J. W.; Anderegg, R. J. *Anal. Chem.* **1997**, *69*, 1518-1524.

[34] Xu, N. X.; Lin, Y. H.; Hofstadler, S. A.; Matson, D.; Call, C. J.; Smith, R. D. *Anal. Chem.* **1998**, *70*, 3553-3556.

[35] Emmett, M. R.; White, F. M.; Hendrickson, C. L.; Shi, S. D. H.; Marshall, A. G. *J. Am. Soc. Mass Spectrom.* **1998**, *9*, 333-340.

[36] Wiley, W. C.; McLaren, I. H. *Rev. Sci. Instrum.* **1955**, *26*, 1150-1157.

[37] Cotter, R. J. *Anal. Chem.* **1992**, *64*, A1027-A1039.

[38] Guilhaus, M.; Selby, D.; Mlynski, V. *Mass Spectrom. Rev.* **2000**, *19*, 65-107.

[39] Hu, Q. Z.; Noll, R. J.; Li, H. Y.; Makarov, A.; Hardman, M.; Cooks, R. G. *J. Mass Spectrom.* **2005**, *40*, 430-443.

[40] Marshall, A. G.; Hendrickson, C. L.; Jackson, G. S. *Mass Spectrom. Rev.* **1998**, *17*, 1-35.

[41] Steen, H.; Mann, M. *Nat. Rev. Mol. Cell Biol.* **2004**, *5*, 699-711.

[42] Yates, J. R. *Ann. Rev. Biophys. Biomol. Structure* **2004**, *33*, 297-316.

[43] Cooper, H. J.; Hakansson, K.; Marshall, A. G. *Mass Spectrom. Rev.* **2005**, *24*, 201-222.

[44] Kelleher, N. L.; Lin, H. Y.; Valaskovic, G. A.; Aaserud, D. J.; Fridriksson, E. K.; McLafferty, F. W. *J. Am. Chem. Soc.* **1999**, *121*, 806-812.

[45] Breuker, K.; Jin, M.; Han, X. M.; Jiang, H. H.; McLafferty, F. W. *J. Am. Soc. Mass Spectrom.* **2008**, *19*, 1045-1053.

[46] McLafferty, F. W. *Acc. Chem. Res.* **1994**, *27*, 379-386.

[47] Guan, S. H.; Marshall, A. G. *Int. J. Mass Spectrom.* **1996**, *157*, 5-37.

[48] Shi, S. D. H.; Hendrickson, C. L.; Marshall, A. G. *Proc. Natl. Acad. Sci. U. S. A.* **1998**, *95*, 11532-11537.

[49] Marshall, A. G. *Int. J. Mass Spectrom.* **2000**, *200*, 331-356.

[50] Guan, S. H.; Marshall, A. G.; Scheppele, S. E. *Anal. Chem.* **1996**, *68*, 46-71.

[51] Kim, S.; Rodgers, R. P.; Marshall, A. G. *Int. J. Mass Spectrom.* **2006**, *251*, 260-265.

[52] Nash, D. G.; Baer, T.; Johnston, M. V. *Int. J. Mass Spectrom.* **2006**, *258*, 2-12.

[53] Grossert, J. S. *Int. J. Mass Spectrom.* **2001**, *212*, 65-79.

[54] Barber, M.; Bordoli, R. S.; Sedgwick, R. D.; Tyler, A. N. *J. Chem. Soc.-Chem. Comm.* **1981**, 325-327.

[55] Fenn, J. B. *Angew. Chem. Int. Ed.* **2003**, *42*, 3871-3894.

[56] Nguyen, S.; Fenn, J. B. *Proc. Natl. Acad. Sci. U. S. A.* **2007**, *104*, 1111-1117.

[57] Fenn, J. B. *J. Am. Soc. Mass Spectrom.* **1993**, *4*, 524-535.

[58] Hillenkamp, F.; Karas, M.; Beavis, R. C.; Chait, B. T. *Anal. Chem.* **1991**, *63*, A1193-A1202.

[59] Karas, M.; Hillenkamp, F. *Anal. Chem.* **1988**, *60*, 2299-2301.

[60] Nakanishi, T.; Okamoto, N.; Tanaka, K.; Shimizu, A. *Biol. Mass Spectrom.* **1994**, *23*, 230-233.

[61] Keshishian, H.; Addona, T.; Burgess, M.; Kuhn, E.; Carr, S. A. *Mol. Cell. Proteomics* **2007**, *6*, 2212-2229.

[62] Nordhoff, E.; Kirpekar, F.; Roepstorff, P. *Mass Spectrom. Rev.* **1996**, *15*, 67-138.

[63] Bruins, A. P. *J. Chromatogr. A* **1998**, *794*, 345-357.

[64] Page, J. S.; Kelly, R. T.; Tang, K.; Smith, R. D. *J. Am. Soc. Mass Spectrom.* **2007**, *18*, 1582-1590.

[65] Kebarle, P.; Verkerk, U. H. *Mass Spectrom. Rev.* **2009**, *28*, 898-917.

[66] Hogan, C. J.; Carroll, J. A.; Rohrs, H. W.; Biswas, P.; Gross, M. L. *Anal. Chem.* **2009**, *81*, 369-377.

[67] Steel, C.; Starov, V.; Leo, R.; John, P.; G. Harrison, R. *Chem. Phys. Lett.* **1979**, *62*, 121-124.

[68] DeKrey, M. J.; Kenttämaa, H. I.; Wysocki, V. H.; Cooks, R. G. *Org. Mass Spectrom.* **1986**, *21*, 193-195.

[69] Santos, F. J.; Galceran, M. T. *J. Chromatogr. A* **2003**, *1000*, 125-151.

[70] Lee, M. S.; Kerns, E. H. *Mass Spectrom. Rev.* **1999**, *18*, 187-279.

[71] Guevremont, R. *J. Chromatogr. A* **2004**, *1058*, 3-19.

[72] Wyttenbach, T.; Bowers, M. T. *Modern Mass Spectrom.* 2003; Vol. 225, p 207-232.

[73] Clemmer, D. E.; Jarrold, M. F. *J. Mass Spectrom.* **1997**, *32*, 577-592.

[74] Gauthier, J. W.; Trautman, T. R.; Jacobson, D. B. *Anal. Chim. Acta* **1991**, *246*, 211-225.

[75] Little, D. P.; Speir, J. P.; Senko, M. W.; O'Connor, P. B.; McLafferty, F. W. *Anal. Chem.* **1994**, *66*, 2809-2815.

[76] Price, W. D.; Schnier, P. D.; Williams, E. R. *Anal. Chem.* **1996**, *68*, 859-866.

[77] Dongre, A. R.; Somogyi, A.; Wysocki, V. H. *J. Mass Spectrom.* **1996**, *31*, 339-350.

[78] Zubarev, R. A.; Kelleher, N. L.; McLafferty, F. W. *J. Am. Chem. Soc.* **1998**, *120*, 3265-3266.

[79] Coon, J. J.; Shabanowitz, J.; Hunt, D. F.; Syka, J. E. P. *J. Am. Soc. Mass Spectrom.* **2005**, *16*, 880-882.

[80] Hvelplund, P.; Liu, B.; Nielsen, S. B.; Tomita, S. *Int. J. Mass Spectrom.* **2003**, *225*, 83-87.

[81] Polfer, N. C.; Haselmann, K. F.; Zubarev, R. A.; Langridge-Smith, P. R. R. *Rapid Commun. Mass Spectrom.* **2002**, *16*, 936-943.

[82] Kjeldsen, F.; Haselmann, K. F.; Budnik, B. A.; Jensen, F.; Zubarev, R. A. *Chem. Phys. Lett.* **2002**, *356*, 201-206.

[83] Zubarev, R. A.; Haselmann, K. F.; Budnik, B.; Kjeldsen, F.; Jensen, F. *Eur. J. Mass Spectrom.* **2002**, *8*, 337-349.

[84] Roepstorff, P.; Fohlman, J. *Biol. Mass Spectrom.* **1984**, *11*, 601-601.

[85] Kjeldsen, F.; Haselmann, K. F.; Budnik, B. A.; Sorensen, E. S.; Zubarev, R. A. *Anal. Chem.* **2003**, *75*, 2355-2361.

[86] Xie, Y. M.; Zhang, J.; Yin, S.; Loo, J. A. *J. Am. Chem. Soc.* **2006**, *128*, 14432-14433.

[87] Stensballe, A.; Jensen, O. N.; Olsen, J. V.; Haselmann, K. F.; Zubarev, R. A. *Rapid Commun. Mass Spectrom.* **2000**, *14*, 1793-1800.

[88] Syrstad, E. A.; Tureček, F. *J. Am. Soc. Mass Spectrom.* **2005**, *16*, 208-224.

[89] Belyayev, M. A.; Cournoyer, J. J.; Lin, C.; O'Connor, P. B. *J. Am. Soc. Mass Spectrom.* **2006**, *17*, 1429-1437.

[90] Breuker, K.; Oh, H. B.; Lin, C.; Carpenter, B. K.; McLafferty, F. W. *Proc. Natl. Acad. Sci. U. S. A.* **2004**, *101*, 14011-14016.

[91] Leymarie, N.; Costello, C. E.; O'Connor, P. B. *J. Am. Chem. Soc.* **2003**, *125*, 8949-8958.

[92] Li, X. J.; Cournoyer, J. J.; Lin, C.; O'Connor, P. B. *J. Am. Soc. Mass Spectrom.* **2008**, *19*, 1514-1526.

[93] Turecek, F. *J. Am. Chem. Soc.* **2003**, *125*, 5954-5963.

[94] Turecek, F.; Syrstad, E. A. *J. Am. Chem. Soc.* **2003**, *125*, 3353-3369.

[95] Armentrout, P. B. *Annu. Rev. Phys. Chem.* **2001**, *52*, 423-461.

[96] Allen, M. H.; Vestal, M. L. *J. Am. Soc. Mass Spectrom.* **1992**, *3*, 18-26.

[97] Takats, Z.; Wiseman, J. M.; Gologan, B.; Cooks, R. G. *Anal. Chem.* **2004**, *76*, 4050-4058.

[98] Wilm, M.; Mann, M. *Anal. Chem.* **1996**, *68*, 1-8.

[99] Shaffer, S. A.; Tang, K. Q.; Anderson, G. A.; Prior, D. C.; Udseth, H. R.; Smith, R. D. *Rapid Commun. Mass Spectrom.* **1997**, *11*, 1813-1817.

[100] Lee, S. W.; Freivogel, P.; Schindler, T.; Beauchamp, J. L. *J. Am. Chem. Soc.* **1998**, *120*, 11758-11765.

[101] Bush, M. F.; O'Brien, J. T.; Prell, J. S.; Wu, C. C.; Saylkally, R. J.; Williams, E. R. *J. Am. Chem. Soc.* **2009**, *131*, 13270-13277.

[102] O'Brien, J. T.; Prell, J. S.; Bush, M. F.; Williams, E. R. *J. Am. Chem. Soc.*, *132*, 8248-8249.

[103] Bush, M. F.; O'Brien, J. T.; Prell, J. S.; Saykally, R. J.; Williams, E. R. *J. Am. Chem. Soc.* **2007**, *129*, 1612-1622.

[104] Jockusch, R. A.; Lemoff, A. S.; Williams, E. R. *J. Phys. Chem. A* **2001**, *105*, 10929-10942.

[105] Lemoff, A. S.; Bush, M. F.; Williams, E. R. *J. Am. Chem. Soc.* **2003**, *125*, 13576-13584.

[106] Lee, S. W.; Kim, H. S.; Beauchamp, J. L. *J. Am. Chem. Soc.* **1998**, *120*, 3188-3195.

[107] Lee, S.; Wyttenbach, T.; Bowers, M. T. *Int. J. Mass Spectrom.* **1997**, *167*, 605-614.

[108] Robinson, E. W.; Garcia, D. E.; Leib, R. D.; Williams, E. R. *Anal. Chem.* **2006**, *78*, 2190-2198.

[109] Robinson, C. V.; Chung, E. W.; Kragelund, B. B.; Knudsen, J.; Aplin, R. T.; Poulsen, F. M.; Dobson, C. M. *J. Am. Chem. Soc.* **1996**, *118*, 8646-8653.

[110] Ruotolo, B. T.; Giles, K.; Campuzano, I.; Sandercock, A. M.; Bateman, R. H.; Robinson, C. V. *Science* **2005**, *310*, 1658-1661.

[111] Sharon, M.; Robinson, C. V. *Annu. Rev. Biochem.* **2007**, *76*, 167-193.

[112] Krishnaswamy, S. R.; Williams, E. R.; Kirsch, J. F. *Protein Sci.* **2006**, *15*, 1465-1475.

[113] Heck, A. J. R.; van den Heuvel, R. H. H. *Mass Spectrom. Rev.* **2004**, *23*, 368-389.

[114] Jurchen, J. C.; Cooper, R. E.; Williams, E. R. *J. Am. Soc. Mass Spectrom.* **2003**, *14*, 1477-1487.

[115] Jurchen, J. C.; Garcia, D. E.; Williams, E. R. *J. Am. Soc. Mass Spectrom.* **2003**, *14*, 1373-1386.

[116] Jurchen, J. C.; Garcia, D. E.; Williams, E. R. *J. Am. Soc. Mass Spectrom.* **2004**, *15*, 1408-1415.

[117] Takats, Z.; Nanita, S. C.; Cooks, R. G.; Schlosser, G.; Vekey, K. *Anal. Chem.* **2003**, *75*, 1514-1523.

[118] Hodyss, R.; Julian, R. R.; Beauchamp, J. L. *Chirality* **2001**, *13*, 703-706.

[119] Spencer, E. A. C.; Ly, T.; Julian, R. R. *Int. J. Mass Spectrom.* **2008**, *270*, 166-172.

[120] Haselmann, K. F.; Jorgensen, T. J. D.; Budnik, B. A.; Jensen, F.; Zubarev, R. A. *Rapid Commun. Mass Spectrom.* **2002**, *16*, 2260-2265.

[121] Cohen, S. L.; Chait, B. T. *Anal. Chem.* **1996**, *68*, 31-37.

[122] Iavarone, A. T.; Udekwu, O. A.; Williams, E. R. *Anal. Chem.* **2004**, *76*, 3944-3950.

[123] Matuszewski, B. K.; Constanzer, M. L.; Chavez-Eng, C. M. *Anal. Chem.* **2003**, *75*, 3019-3030.

[124] Taylor, P. J. *Clin. Biochem.* **2005**, *38*, 328-334.

[125] King, R.; Bonfiglio, R.; Fernandez-Metzler, C.; Miller-Stein, C.; Olah, T. *J. Am. Soc. Mass Spectrom.* **2000**, *11*, 942-950.

[126] Cech, N. B.; Enke, C. G. *Mass Spectrom. Rev.* **2001**, *20*, 362-387.

[127] Cech, N. B.; Enke, C. G. *Anal. Chem.* **2000**, *72*, 2717-2723.

[128] Cech, N. B.; Enke, C. G. *Anal. Chem.* **2001**, *73*, 4632-4639.

[129] Tang, K. Q.; Page, J. S.; Smith, R. D. *J. Am. Soc. Mass Spectrom.* **2004**, *15*, 1416-1423.

[130] Kebarle, P. *J. Mass Spectrom.* **2000**, *35*, 804-817.

[131] Iavarone, A. T.; Williams, E. R. *J. Am. Chem. Soc.* **2003**, *125*, 2319-2327.

[132] Cheng, J.; Vecitis, C. D.; Hoffmann, M. R.; Colussi, A. J. *J. Phys. Chem. B* **2006**, *110*, 25598-25602.

[133] Tang, L.; Kebarle, P. *Anal. Chem.* **1993**, *65*, 3654-3668.

[134] Lim, C. K.; Lord, G. *Biolog. & Pharm. Bull.* **2002**, *25*, 547-557.

[135] Gygi, S. P.; Rist, B.; Gerber, S. A.; Tureček, F.; Gelb, M. H.; Aebersold, R. *Nature Biotech.* **1999**, *17*, 994-999.

[136] Ong, S. E.; Blagoev, B.; Kratchmarova, I.; Kristensen, D. B.; Steen, H.; Pandey, A.; Mann, M. *Mol. Cell. Proteomics* **2002**, *1*, 376-386.

[137] Conrads, T. P.; Anderson, G. A.; Veenstra, T. D.; Pasa-Tolic, L.; Smith, R. D. *Anal. Chem.* **2000**, *72*, 3349-3354.

[138] Hall, M. P.; Ashrafi, S.; Obegi, I.; Petesch, R.; Peterson, J. N.; Schneider, L. V. *J. Mass Spectrom.* **2003**, *38*, 809-816.

[139] Ong, S.-E.; Foster, L. J.; Mann, M. *Methods* **2003**, *29*, 124-130.

[140] Yi, E. C.; Li, X.-J.; Cooke, K.; Lee, H.; Raught, B.; Page, A.; Aneliunas, V.; Hieter, P.; Goodlett, D. R.; Aebersold, R. *Proteomics* **2005**, *5*, 380-387.

[141] Nanita, S. C.; Cooks, R. G. *Angew. Chem. Int. Ed.* **2006**, *45*, 554-569.

# Chapter 2

## Instrumental Design

### 2.0 Overview.

The experiments described in this thesis were completed using two Fourier transform ion cyclotron resonance mass spectrometers that have been described elsewhere. Before these experiments could be completed, it was necessary to make a number of modifications to the existing instrumentation to expand their capabilities to solve the critical questions this text addresses. These modifications followed in the footsteps of previous improvements made to enhance cluster formation [1], as well as redesigns of the ion cells on both instruments to hold additional ions and control ion temperature [2,3]. The details provided here are to provide context for those following on this work into the modifications made, their purpose, and the likely areas for future improvement.

### 2.1 Electron Capture Cathode Assembly.

Gaseous thermal electrons can be generated from any number of sources, most commonly thin filaments or heated dispenser cathodes. Although they typically require high power, the key advantages of a dispenser cathode is that it can be operated at a lower temperature and it provides an easily manipulated columnated beam of electrons. By selecting a sufficiently large dispenser cathode cross section, complete overlap of the electron beam and the trapped ion cloud should be possible if the cathode is positioned axially with respect to the magnet; if the cathode is within the fringe field of the magnet, there should be minimal radial compression of the electron beam, resulting in a beam that is, to a first approximation, the same diameter as the cathode face.

Figure 2.1.1 and 2.1.2 are diagrams of the support rod assembly components used to house the cathode within the vacuum chamber. A 2 ¾" CF flange is used to complete the vacuum seal of the assembly to the instrument vacuum chamber, and electrical connections are made through a electrical feedthrough mounted axially on a concentric 1 1/3" CF flange. The 1 cm barium tungsten dispenser cathode (Heatwave Labs, Watsonville, CA) is mounted into three screw terminal couplers, so that electrical connections can be made to the positive and negative heater leads as well as the electrically isolated cathode housing. The opposite side of these screw terminals is connected to 0-80 stainless steel threaded rod, which in turn is inserted into a macor block. The advantage of this arrangement is that the position of the cathode and the spacing between the cathode electrical connections can be easily manipulated, and then held rigidly against the macor minimizing shorts and disconnects. Using thin, bare copper wire, electrical connections continue from the stainless steel threaded rod to the feedthrough with minimal capacitance.

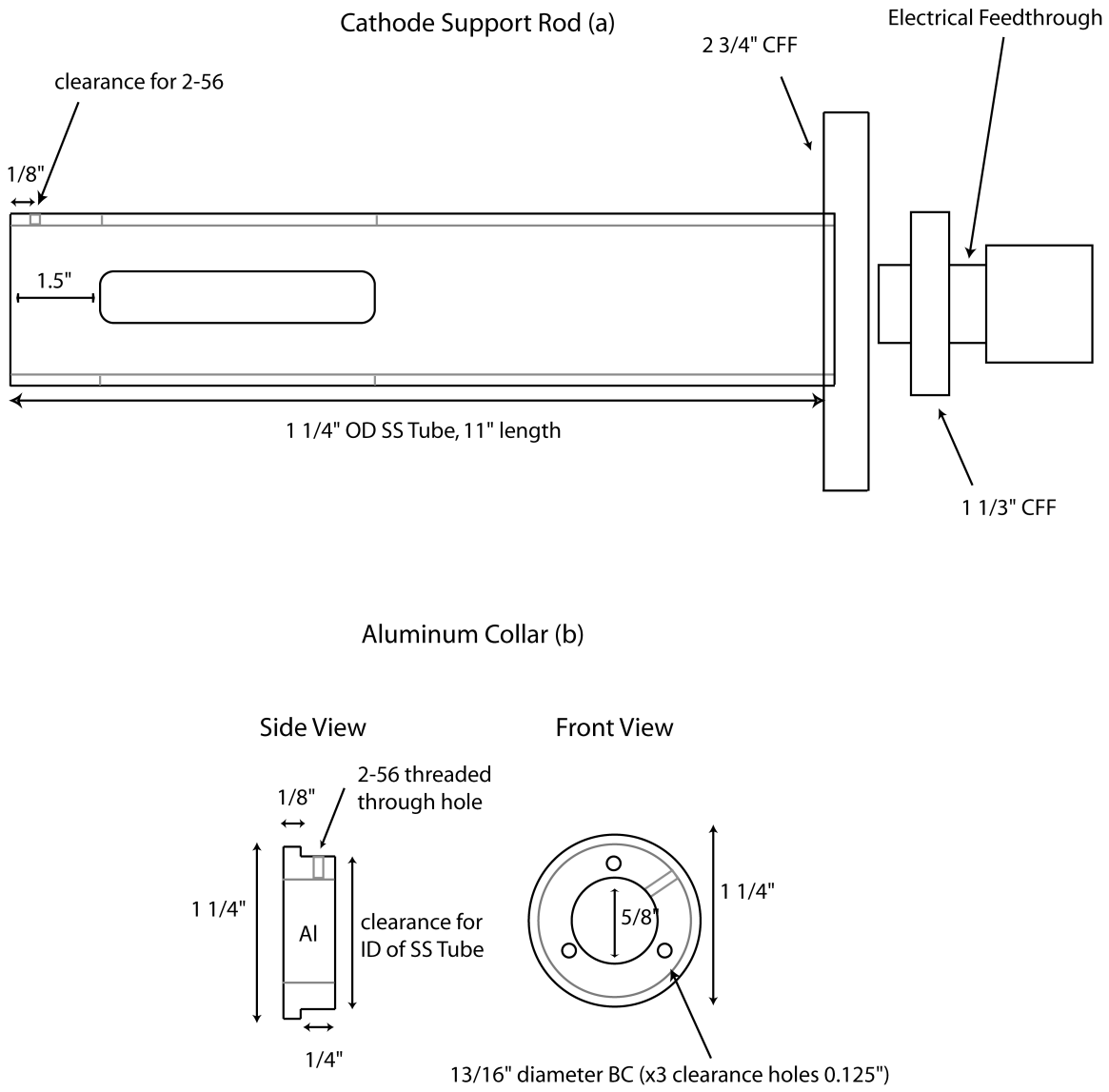


*Figure 2.1.1. (a) Schematic of the cathode support rod assembly for the ECD cathode used on the 2.7 T FT/ICR MS. (b) Schematic of the aluminum support collar used to mount the barium tungsten dispenser cathode to the support rod.*

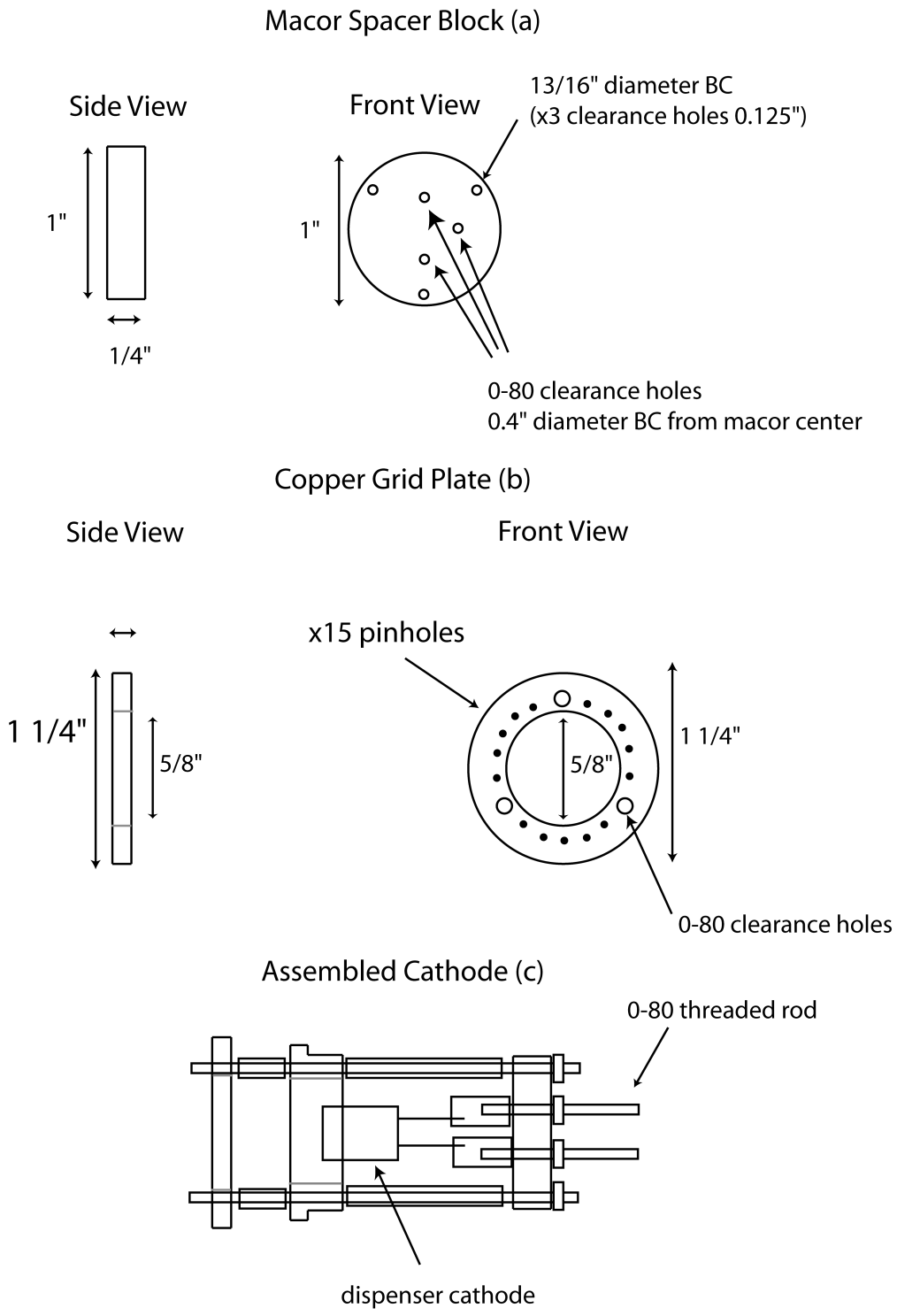


*Figure 2.1.2. (a) Schematic of the macor block used to aligned and isolate the dispenser cathode, (b) the copper grid and (c) the assembled cathode, prior to insertion into the stainless steel cathode support rod.*

An additional electrical connection is made to a copper grid, positioned ~1 cm in front of the cathode face using threaded rod and ceramic spacers. This grid consists of a thin copper ring with fine wire mesh woven over its center opening to create a uniform electricstatic surface with high electron transmittance. The grid is electrically isolated much as the wires for the dispenser cathode, and lines run through the same feedthrough to external power supplies.

The grid and macor assembly are isolated from an aluminum mounting collar, which fixes the components within the support rod. This rigid support rod extends 11" from the back of the instrument, positioning the cathode within the fringe field, and serves to help shield the cathode wiring from the rest of the vacuum chamber. Slits were added to the support rod to reduce pump down times. When mounted against the vacuum chamber, the face of the dispenser cathode is ~50 cm away from the center of the ion trapping cell.

Under typical operation, the cathode heater receives an 18 Watt (6 V, 3 A) DC current, which results in a heated cathode temperature of ~1000 °C. This temperature is sufficiently high to promote a large flux of electrons from the conduction band into free thermal electrons, typically on the order of milliamperes. A DC voltage of 9 V is applied to the grid surface to provide focusing for the electron beam. The voltage applied to the surface of the cathode can be transiently pulsed to introduce electrons into the ion cell, typically by lowering from a 10 V "off" to -2 V "on" for ~100 ms, providing sufficient electrons for efficient capture in these experiments.

### 2.2 9.4 T Datastation.

Another critical factor in completing these measurements was highly mass accurate and well-resolved mass spectral abundances. To complete this task, a new data acquisition system was built and installed, based in large part on the Predator Data Acquisition System developed at the National High Magnetic Field Laboratory. This design offers a few major improvements over the previous Bruker Daltonics Exceed system, particularly in significantly longer transient lengths (8 MB vs. 1 MB), greater control of the sampling rate, and an easily expandable interface for auxillary techniques, such as electron capture dissociation, photodissociation and ion mobility control. The longer sampling times and better control of sampling rates, coupled with selective bandpass filtering of the amplified signal result in a typical signal-to-noise increase of over an order of magnitude relative to the previous datastation, as well as significant improvements (~factor of thee) in typical resolution, particularly at larger $m/z$.

The key components of this datastation are a series of five cards, as diagrammed in Figure 2.2.1. The Data Acquisition Box (DAB), a National Instruments (NI) PXI1033, holds four of these cards, while the fifth card, a Spincore timing card, is coupled to the datastation computer (DSC) directly. Inside the DAB are a NI 5421, NI 5122, and two NI 6733s; these boards serve as an arbitrary waveform generator, analog to digital converter, and two variable DAQ and TTL outputs, respectively.

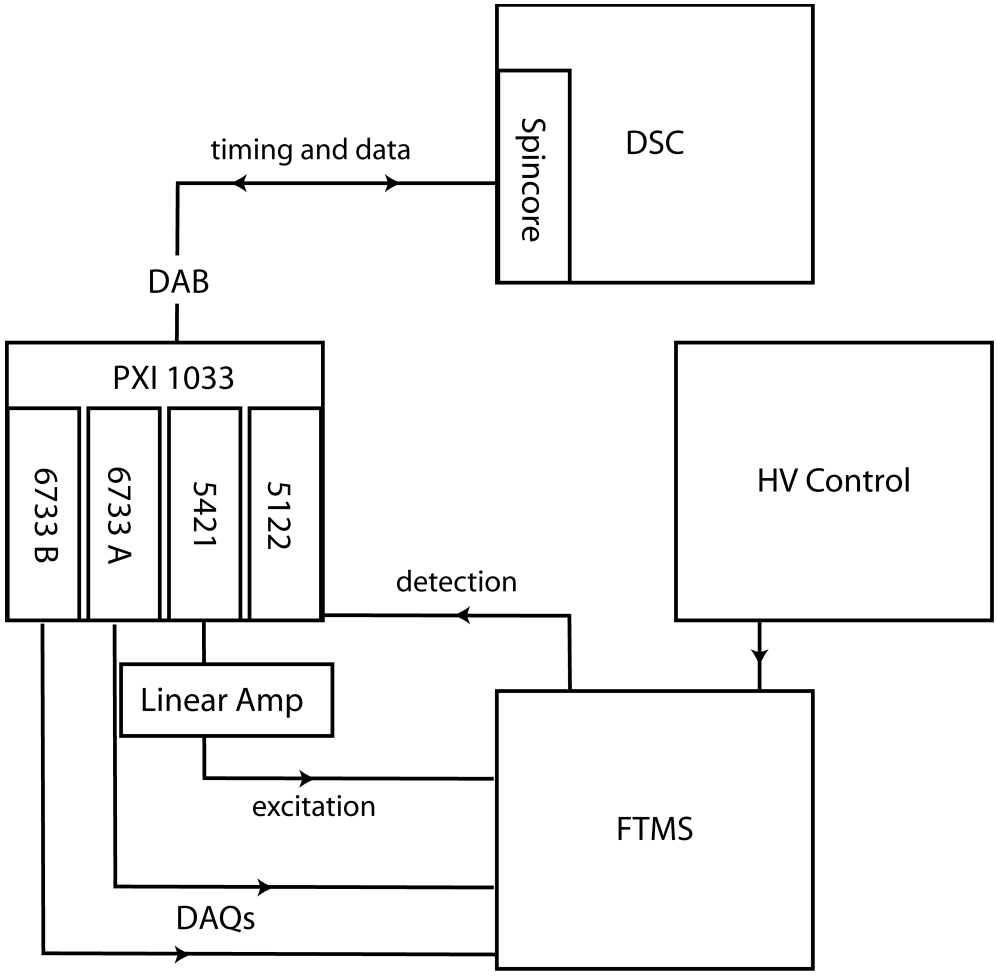


*Figure 2.2.1. Schematic diagram of the 9.4 Tesla FT/ICR MS Predator data acquisition station implementation. Relevant connections between the components are noted. See text.*

In a typical experiment, an experimental script containing all relevant pulse sequences is loaded in the DSC, and then downloaded to the DAB. When the experiment begins, timing pulses initiated from the SpinCore timing card are sent to the DAB, which then outputs the predetermined sequence of corresponding events from the script. Ultimately, this results in an ion excitation signal, sent from the NI 5421 board to the T&C Power linear amplifier and on to the cell. This happens concurrently with a trigger pulse to a reed relay, which connects the linear amplifier to the cell. The amplifier is only connected to the cell during the time window corresponding to the excitiation pulse, to eliminate broadband excitation of ions due to noise within the amplifier circuit. The coherent excitation of ions is then detected in the cell, and amplified using a custom pre-amplifier based on previous designs. The NI 5122 then detects the amplified ion current, after receiving a corresponding bit from the timing board to begin recording the ion

current signal. The resulting spectrum is then transferred back to the DSC for Fourier transform and further analysis.

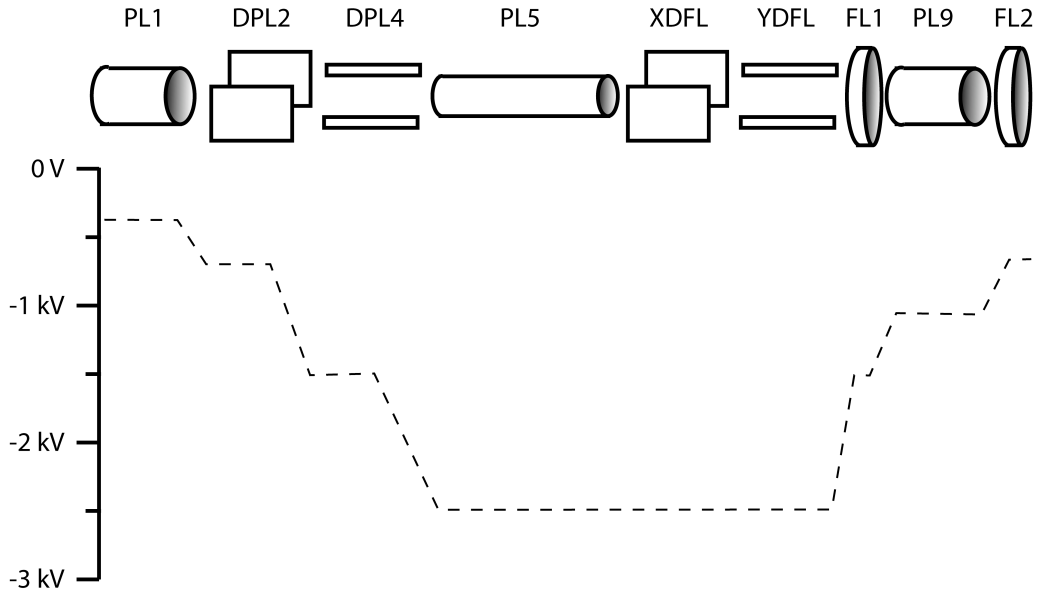


*Figure 2.2.2. Schematic of the ion transfer optics for the 9.4 Tesla FT/ICR MS, showing the thirteen lenses in the stack. Below are the typical voltages applied across each of the optics, resulting in efficient ion transmission from the external accumulator to the ion cell.*

Another key modification to the 9.4 T FTICR mass spectrometer was to replace the previous high voltage power supplies for the transfer region between the external accumulator hexapole and the ion cell. The previous supplies were prone to thermal drift, and provided significant difficulty in consistent ion transmission. This region relies on all DC fields, and ions must be accelerated past the fringe field of the magnet prior to being slowed to aid in trapping. A series of 13 elements are present in this lens stack, as are diagrammed in Figure 2.2.2. Ions are accelerated and steered by thirteen ion lenses charged by voltages provided by the high voltage control box, then decelerated and finally focused into the ion cell for trapping and storage. To minimize variation in the electric fields within the lens stack, all 13 voltages are converted off of a single 16 V power supply with a sufficiently high current (~10 A) to power all thirteen circuits with minimal droop. Ultimately, the current draw of this circuit should be quite low, and ripple is on the order of <0.2%. Further, because all thirteen voltages are amplified from the same source, any ripple should be reflected in all 13 circuits, and thus relative differences between the optics should be negligible.

A sample control circuit logic diagram is seen in Figure 2.2.3 and the DC/DC conversion logic diagram and analogous circuit diagram are present in Figure 2.2.4. The control circuit is designed to modify the output voltage into one of two possible ranges, either 0-15 V or 0-12 V to meet the demands of the respective DC/DC converters. The

DC/DC converters provide final variable voltages of 0-500, 0-1500, and 0-3000 V for corresponding regions of the instrument, allowing for acceleration and deceleration into the ion cell.

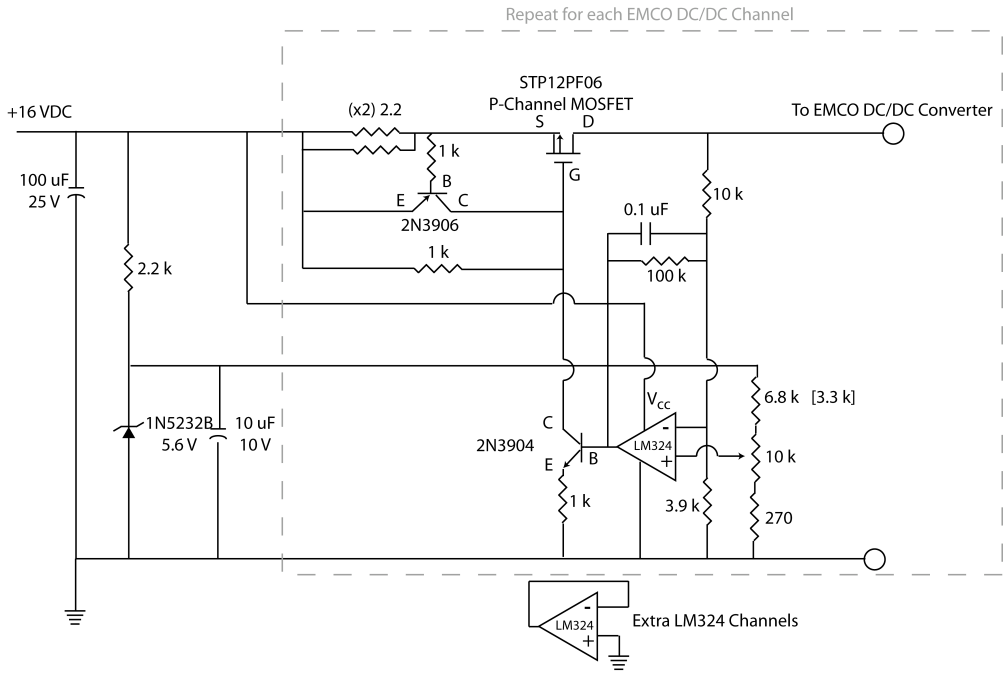


*Figure 2.2.3. Logic diagram for the electrical control circuit for the high voltage transfer optics. One of these circuits is used for each of the thirteen optics, and provides a voltage to a corresponding DC/DC conversion circuit.*

A key improvement to this system would be to modify the DC/DC conversion circuit so that negative ions could be transferred through this optic set without a major modification. A simple way to complete this task is diagrammed in Figure 2.2.5. By adding four TTL-operated switches between the HV output lines and ground, a pair of TTLs would allow for easy reversal of the output polarity. Power for the TTL could be provided internally from the existing 16 V power supply, suitably drained to the 5 V required for this task, or drawn from a spare DAQ or TTL from the DAB.

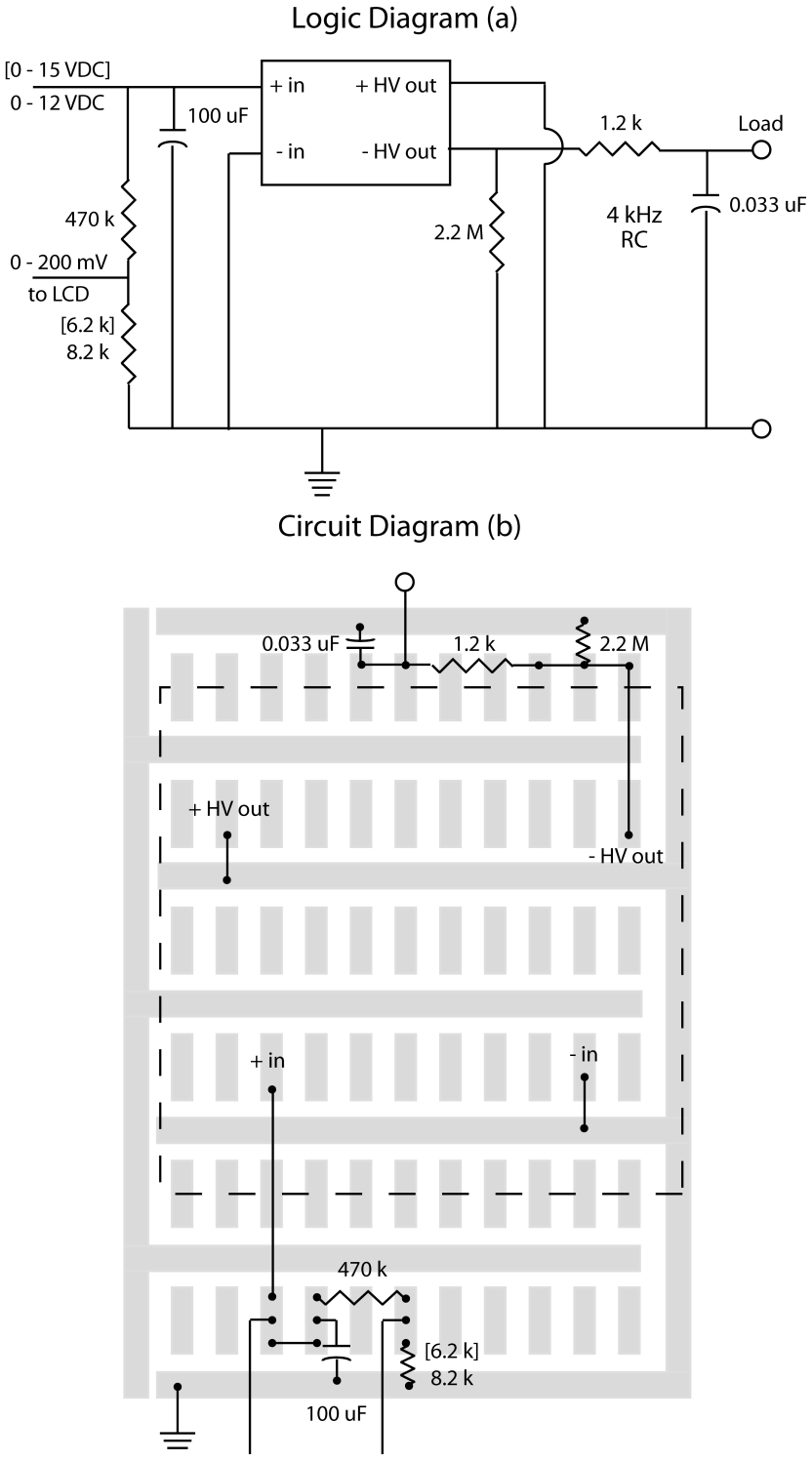


*Figure 2.2.4. (a) Logic diagram of the DC/DC conversion circuit. One of these circuits is used for each of the thirteen optics, and receives a voltage from a corresponding control circuit. (b) Schematic diagram of the same.*

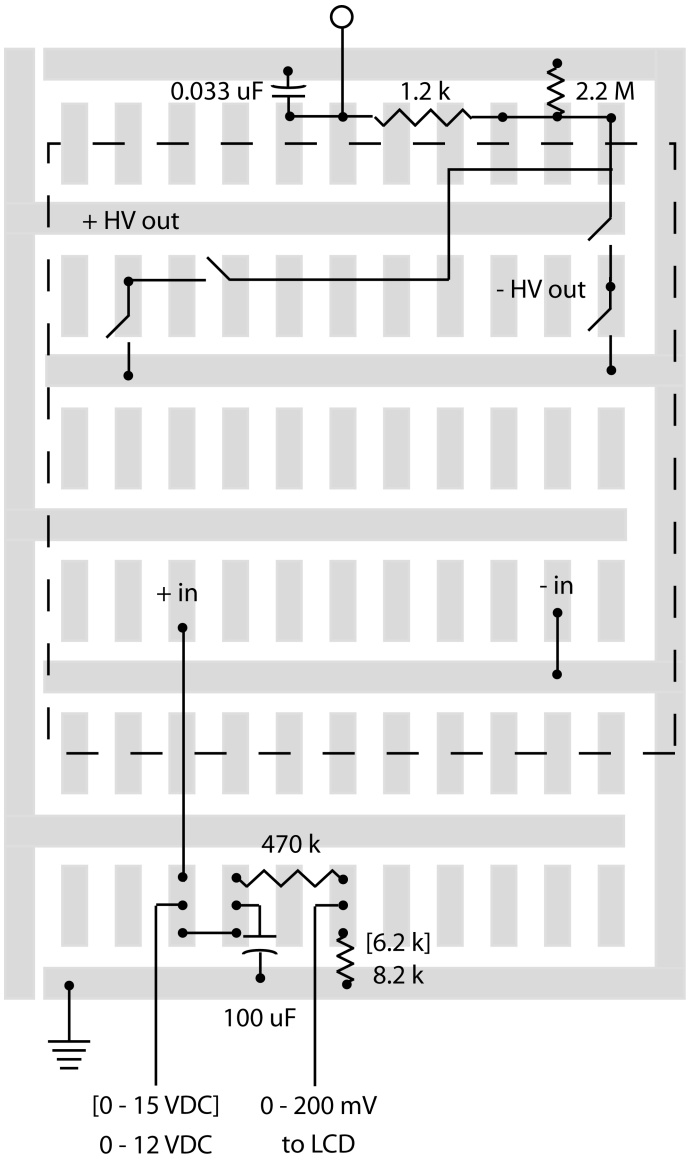


*Figure 2.2.5. Proposed modification to figure 2.2.4 b to allow for switching between positive and negative ion transmission. Four TTL switches are added for easy polarity changes on the optics.*

## 2.3 References.


[1] Rodriguez-Cruz, S. E.; Jockusch, R. A.; Williams E. R. *J. Am. Chem. Soc*. **1999**, *121*, 8898-8906.

[2] Wong, R. L.; Paech, K.; Williams E. R. *Int. J. Mass Spectrom.* **2004**, *232*, 59-66.

[3] Robinson, E. W.; Williams E. R. *J. Am. Soc. Mass Spectrom.* **2005**, *16*, 1427-1437.

## Chapter 3

### Internal Energy Deposition in Electron Capture Dissociation Measured using Hydrated Divalent Metal Ions as Nanocalorimeters



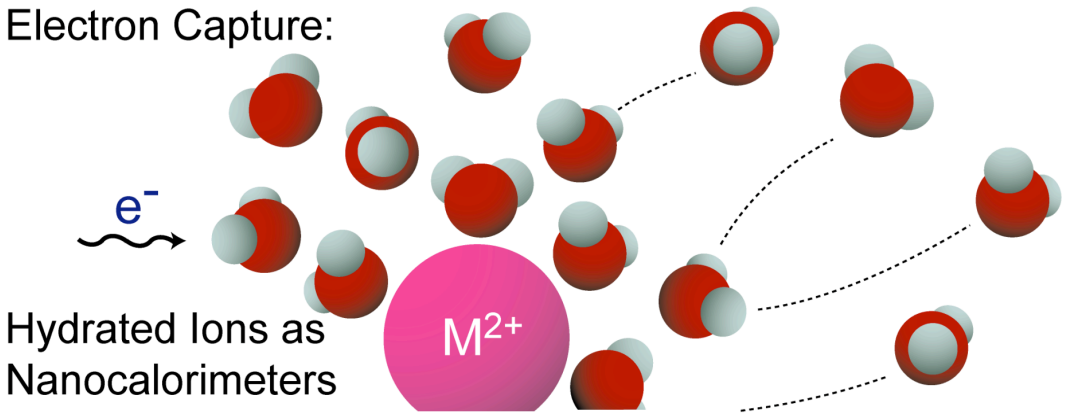


**3.0 Abstract.**

Extensively hydrated divalent metal ions are used as nanocalorimeters to measure the internal energy deposition resulting from electron capture. For $M(H_2O)_{32}^{2+}$, M = Mg, Ca, Sr and Ba, two dissociation pathways are observed: loss of a water molecule from the precursor (~6%) owing to activation from blackbody photons or collisions with residual background gas, and loss of between 9 and 11 water molecules from the reduced precursor formed by electron capture. The binding energy of a water molecule to the reduced precursor ions is estimated to be approximately 10 kcal/mol. From the distribution of water molecules lost, corrected for residual activation, the average and maximum internal energy deposited into these ions is determined to be ~4.4 and ~4.8 – 5.2 eV, respectively. The average internal energy deposition does not depend significantly on metal ion size (~0.1 eV difference for Mg to Ba) despite the large (5.0 eV) difference in second ionization energies for the isolated atoms. Similar results were obtained for $Ca(H_2O)_n^{2+}$, $n$ = 30 and 32, suggesting that neither the water binding energy nor the recombination energy changes significantly for clusters of this size. The recombination energy is roughly estimated from theory to be about 4.5 eV. These results show that these ions are not significantly activated by inelastic non-capture collisions with electrons and that the vast majority of the recombination energy resulting from electron capture is converted into internal energy of the reduced precursor ions, indicating that these ions dissociate statistically.

## 3.1 Introduction.

Capture of an electron by a multiply charged ion can produce a rich fragmentation spectrum from which ion structural information can be obtained. Electron capture (EC) can occur by collisions between ions and thermally generated free electrons (ECD) [1,2], negative ions (ETD) [3], or atoms (ECID) [4]. For peptides and proteins, these methods produce similar fragments from which substantial information can be obtained about both sequence and sites of posttranslational modifications. Since the initial report by McLafferty and coworkers on using ECD for "top-down" proteomics [1a], significant effort has been devoted to understanding how ECD fragmentation occurs. McLafferty and coworkers proposed that fragmentation proceeds via nonergodic processes originating from high-*n* Rydberg states [1c]. Tureček and coworkers have argued that the odd electron ions, resulting from EC by multiply protonated ions, have very low barriers to dissociation and that fragmentation is statistical [2]. Experimental and computational results supporting both mechanisms have been reported [1,2,5].

A key piece of information that is essential to understanding how ECD occurs is the amount of energy that is deposited into internal modes of the ion. The EC process is exothermic by a value corresponding to the recombination energy [1a,6], which is estimated to be 4 – 7 eV for multiply protonated peptides and proteins [1a,6a]. However, the extent to which this recombination energy partitions into internal modes of the precursor ion vs. translational modes of the fragmentation products is unknown. In principle, the internal energy deposited into an ion by an activation method can be obtained using "chemical thermometers," which are ions that have known fragmentation energetics [7]. The abundances of fragment ions, formed as a result of activating ions that dissociate via a linear sequence of unimolecular reactions, can be used to directly probe the distribution of internal energy deposition [7a]. A measure of internal energy deposition can also be obtained from the abundance ratio of two or more fragment ions that have different dissociation enthalpies and entropies [7b]. For larger ions, dissociation kinetics can be directly related to effective temperatures from blackbody infrared radiative dissociation (BIRD) [8] measurements and used to determine the extent of activation by other techniques [7c]. Applying these methods to activation by EC is complicated by the requirement for multiply charged ions and fragmentation pathways with known energetics; slow heating methods, such as BIRD, typically produce different fragments than ECD.

Here, extensively hydrated divalent alkaline earth metal ions are used as chemical thermometers to probe, for the first time, the internal energy deposition that occurs in ECD. The thermochemistry of hydrated monovalent ions has been extensively investigated [9a-c]. Castleman and coworkers reported DH values for the loss of a water molecule from protonated water clusters, $H(H_2O)_n^+$, $n$ = 6 – 28, and found that these values range between 9 – 11 kcal/mol for clusters with n > 10 [9a]. The heat of vaporization of water is 10.8 and 9.7 kcal/mol at 0 and 100 ºC, respectively [9d]. These results suggest that the energy required for the loss of a water molecule from these large clusters is not significantly influenced by the proton. For hydrated monovalent metal ions [9b,c], binding energies rapidly decrease with increasing cluster size; the binding energies of the 6th water molecule to hydrated $Li^+$, $Na^+$ and $K^+$ are between 12.1 and 10.0

kcal/mol [9b]. These results suggest that the loss of water from $M(H_2O)_n^+$, M = alkaline earth metal ion, formed by EC from the divalent species, should also require approximately 10 kcal/mol per water molecule that evaporates from the cluster provided that these clusters are sufficiently large. Thus, the internal energy deposition of EC can be estimated from the number and distribution of water molecules that "boil" off from the reduced precursors. Ion relaxation after EC can also occur via collisional or radiative emission processes, although such effects are expected to be small in these experiments due to the low pressure (< 10-8 Torr) and short time (50 ms) after ECD but prior to ion detection.

### 3.2 Experimental Methods.

Experiments were performed on a 2.75 Tesla Fourier-transform ion cyclotron resonance mass spectrometer with an external nanoelectrospray ionization source and an ion cell cooled to 130 K using a regulated flow of liquid nitrogen [10]. A 1.0 cm diameter heated metal cathode, located 20 cm from the ion cell center, was used to produce electrons for these experiments. A potential of -2 V was applied to the cathode to introduce electrons into the ion cell and electron radiation times of 40 ms were used.

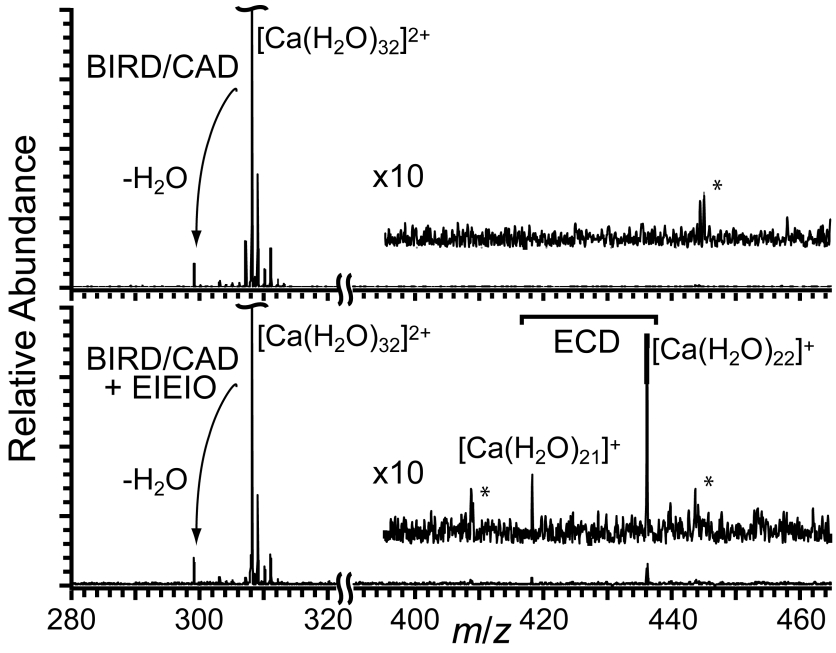


*Figure 3.1. ECD spectrum of $Ca(H_2O)_{32}^{2+}$ (bottom) showing reduced precursor ions that have lost 10 or 11 water molecules and reference spectrum (top) measured under identical conditions but with no electrons injected into the cell showing extent of BIRD and/or CAD that occurs.*

### 3.3 Results and Discussion.

In these experiments, ions dissociate via two pathways. The precursor can be activated by BIRD, collisions with residual background gas (CAD) or by inelastic non-capture collisions with electrons (EIEIO) [11] resulting in the loss of a single water molecule. The precursor may also capture an electron resulting in formation of a singly charged ion that undergoes loss of between 9 and 11 water molecules. These processes are illustrated in Figure 3.1. The spectrum of isolated $Ca(H_2O)_{32}^{2+}$, measured with identical experimental conditions as the ECD spectra but with no electrons introduced into the cell (the cathode is still heated), is shown in Figure 3.1 (top). Loss of a single water molecule (~6% total ion abundance) resulting from precursor activation by BIRD/CAD is observed. An ECD spectrum of this same ion is shown in Figure 3.1 (bottom). No additional water loss from the precursor occurs, indicating that vibrational excitation of the ions by EIEIO is negligible. Additional water loss from EIEIO can occur when higher energy electrons are used. In ECD of proteins, the observation of ***b*** and ***y*** ions, corresponding to cleavage of the amide bond of the protein backbone, has been attributed to the EIEIO process [6a]. With our nanocalorimetry method, the extent of activation by EIEIO in an ECD experiment can be quantified. Also clearly observed in this spectrum is a remarkably narrow distribution of singly charged ions that correspond to the capture of a single electron by the doubly charged precursor and loss of either 10 or 11 water molecules. The absence of an ion corresponding to loss of 12 water molecules indicates that the maximum energy deposited into these ions is approximately between 110 and 120 kcal/mol (4.8 and 5.2 eV).

*Table 3.1. Normalized abundances of ECD product ions from $M(H_2O)_{32}^{2+}$, weighted average number of water molecules lost from the reduced precursor and these latter values corrected for BIRD/CAD dissociation.*

| | Number of Molecules Lost | | | Weighted Average | |
|---|---|---|---|---|---|
| $M(H_2O)_{32}^{2+}$ | -11 | -10 | -9 | ECD | Corrected |
| Mg | 61 | 100 | <9 | 10.4 | 10.3 |
| Ca | 30 | 100 | <7 | 10.2 | 10.2 |
| Sr | 34 | 100 | 20 | 10.1 | 10.0 |
| Ba | 25 | 100 | <10 | 10.2 | 10.1 |

The second ionization energy of these alkaline earth metal atoms ranges from 15.0 eV for Mg to 10.0 eV for Ba. Results of the ECD experiments with clusters of each of these divalent metal ions with 32 water molecules are given in Table 3.1. An estimate of the average energy deposited as a function of metal ion size was obtained from a weighted average number of water molecules lost from the reduced precursor calculated using the ECD fragment ion abundances (Table 3.1). These values range from 10.4 water molecules lost for Mg to 10.2 for Ba (corresponding to 4.5 and 4.4 eV, respectively), indicating that the internal energy deposition depends only slightly on metal ion size for these extensively hydrated ions, despite the large difference in second ionization energies of the isolated atoms. This suggests that an ion-electron pair is formed in the reduced cluster. The water loss from the reduced clusters that is attributable to BIRD/CAD was estimated to be the same as that from the precursor. After this correction, the average

number of water molecules lost from the EC process ranges from 10.3 to 10.1 for Mg to Ba, respectively, and correspond to average internal energy depositions of 4.5 to 4.4 eV, respectively. From the distribution of products observed, we conclude that the average width of the energy deposition corresponds to less than ±1 water molecule or less than ±10 kcal/mol (0.4 eV). The number of water molecules lost via ECD of $Ca(H_2O)_{30}^{2+}$ is indistinguishable from that for $Ca(H_2O)_{32}^{2+}$ suggesting that neither the water binding nor the recombination energy changes significantly for clusters of this size.

Electron recombination energies correspond to the adiabatic ionization energies of the singly charged clusters formed by EC. Adiabatic ionization energies for clusters this large have not been reported, but values for $Mg(H_2O)_n^+$, $n$ = 1 – 19 have [12]; these values decrease with increasing cluster size and asymptotically approach a value between 4.0 and 4.8 eV (MP2) or between 5.1 and 5.5 eV (BLYP) for the larger clusters. In order to obtain a rough estimate of these values for larger calcium clusters, vertical recombination energies were calculated for smaller cluster of $Ca(H_2O)_n^{2+}$ and for $Mg(H_2O)_n^{2+}$ and these values were found to rapidly converge to within 0.3 eV by $n$ = 4 [13]. This indicates that recombination energies for even larger clusters of these two metal ions should be similar. Calculations for $Ca(H_2O)_{29}^{2+}$ resulted in a value of 4.5 eV, but this value must be considered only a very rough estimate. A more detailed theoretical analysis is needed. By comparison to our experimental results for even larger Ca clusters that indicate an average and maximum internal energy deposition due to just EC of ~4.4 and ~4.8 – 5.2 eV, respectively, we conclude that the majority of the recombination energy is converted into internal energy of these precursor ions.

### 3.4 Conclusions.

These results indicate that ions in an ECD experiment are not significantly activated by inelastic non-capture collisions with electrons when low electron kinetic energies are used. These results also clearly demonstrate that the vast majority of the recombination energy resulting from electron capture is converted into internal energy of the reduced precursor ions, indicating that the dissociation of these ions is statistical. Future studies on ECD of extensively hydrated ions of small organic molecules, peptides, and proteins will likely provide additional insights into the ECD processes for these species.

### 3.5 Acknowledgements.

The authors are grateful for generous financial support from NSF (CHE-041593) and from NIH (R01 GM064712-05).

### 3.6 References.


[1] a) Zubarev, R. A.; Kelleher, N. L.; McLafferty, F. W. *J. Am. Chem. Soc.* **1998**, *120*, 3265-3266.

b) Ge, Y.; Lawhorn, B. G.; ElNaggar, M.; Strauss, E.; Park, J. H.; Begley, T. P.; McLafferty, F. W. *J. Am. Chem. Soc.* **2002**, *124*, 672-678.

c) Breuker, K.; Oh, H.; Lin, C.; Carpenter, B. K.; McLafferty, F. W. *Proc. Natl. Acad. Sci. USA* **2004**, *101*, 14011-14016.

[2] a) Syrstad, E. A.; Tureček, F. *J. Am. Soc. Mass Spectrom.* **2005**, *16*, 208-224.

b) Tureček, F.; Syrstad, E. A. *J. Am. Chem. Soc.* **2003**, *125*, 3353-3369.

[3] Syka, J. E. P.; Coon, J. J.; Schroeder, M. J.; Shabanowitz, J.; Hunt, D. F. *Proc. Natl. Acad. Sci. USA* **2004**, *101*, 9528-9533.

[4] Hvelplund, P., Liu, B.; Nielsen, S. B.; Tomita, S. *Int. J. Mass Spectrom.* **2003**, *225*, 83-87.

[5] a) Robinson, E. W.; Leib, R. D.; Williams, E. R. *J. Am. Soc. Mass Spectrom*. **2006**, *17*, 1469-1479.

b) Chakraborty, T.; Holm, A. I. S.; Hvelplund, P.; Nielsen, S. B.; Poully, J. C.; Worm, E. S.; Williams, E. R. *J. Am Soc. Mass Spectrom*. **2006**, *17*, 1675-1680.

[6] a) Zubarev, R. A.; Haselmann, K. F.; Budnik, B.; Kjeldsen, F.; Jensen, F. *Eur. J. Mass Spectrom.* **2002**, *8*, 337-349.

b) Iavarone, A. T.; Paech, K.; Williams, E. R. *Anal. Chem.* **2004**, *76*, 2231-2238.

[7] a) Kenttämaa, H. I.; Cooks, R. G. *Int. J. Mass Spectrom. Ion Processes* **1985**, *64*, 79-83.

b) Griffiths, I. W.; Mukhtar, E. S.; March, R. E.; Harris, F. M.; Beynon, J. H. *Int. J. Mass Spectrom. Ion Phys.* **1981**, *39*, 125-132.

c) Schnier, P. D.; Jurchen, J. C.; Williams, E. R. *J. Phys. Chem. B* **1999**, *103*, 737-745.

[8] Price, W. D.; Schnier, P. D.; Williams, E. R. *Anal. Chem.* **1996**, *68*, 859-866.

[9] a) Shi, Z.; Ford, J. V.; Wei, S.; Castleman, A. W., Jr. *J. Chem. Phys.* **1993**, *99*, 8009-8015.

b) Dzidic, I.; Kebarle, P. *J. Phys. Chem.* **1970**, *74*, 1466-1474.

c) Dalleska, N. F.; Tjelta, B. L.; Armentrout, P. B. *J. Phys. Chem*. **1994**, *98*, 4191-4195.

d) Marsh, K. N. "Recommended Reference Materials for the Realization of Physiochemical Properties" Blackwell, Oxford, 1987.

[10] a) Bush, M. F.; Saykally, R. J.; Williams, E. R. *Int. J. Mass Spectrom*. **2006**, *253*, 256-262.

b) Wong, R. L.; Paech, K.; Williams, E. R. *Int. J. Mass Spectrom.* **2004**, *232*, 59-66.

[11] Cody, R. B.; Freiser, B. S. *Anal. Chem*. **1987**, *59*, 1056-1059.

[12] Reinhard, B. M.; Niedner-Schatteburg, G. *J. Chem. Phys*. **2003**, *118*, 3571-3582.

[13] Candidate low-energy structures were identified using Monte Carlo conformation searches with the MMFF94 force field and subsequently minimized at the B3LYP/LACVP$^{**++}$ level; single-point energies were calculated for these structures with a single electron added and used to obtain a vertical electron attachment energy.

## Chapter 4

# Reduction Potential of 1 M Aqueous Ruthenium(III) Hexaammine in the Gas Phase: A Route Towards Establishing an Absolute Electrochemical Scale

This chapter is reproduced with permission from Ryan D. Leib, William A. Donald, Jeremy T. O'Brien, Matthew F. Bush, and Evan R. Williams "Reduction Energy of 1 M Aqueous Ruthenium(III) Hexaammine in the Gas Phase: A Route Toward Establishing an Absolute Electrochemical Scale" *Journal of the American Chemical Society*. **2007**, *129*, 7716-7717. 

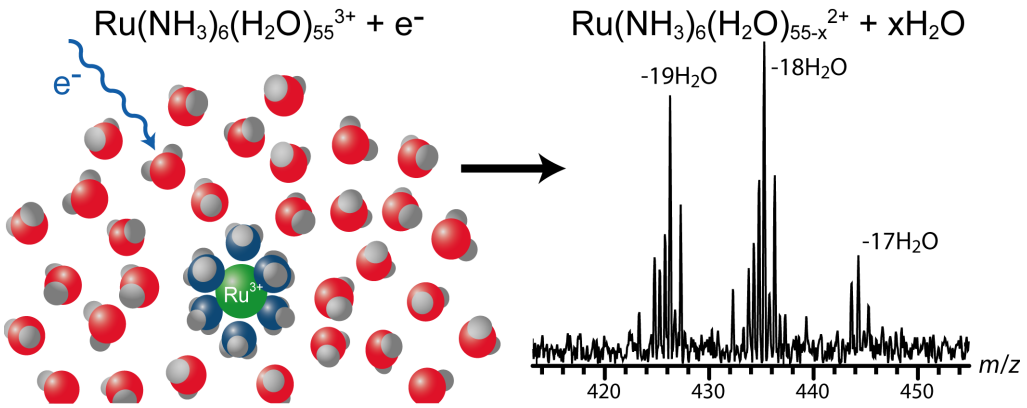


## 4.0 Abstract.

The internal energy deposited into gas-phase $Ru(NH_3)_6(H_2O)_n^{3+}$ when reduced by thermal electrons is investigated as a function of cluster size. For $n \geq 37$, reduction results exclusively in the loss of water molecules from the reduced precursor ion; loss of water is accompanied by the loss of a single ammonia molecule for smaller clusters. The average number of ligands lost from the reduced precursor decreases with cluster size for $n \leq 31$, presumably due to increased binding energy of the ligands to the smaller, doubly charged clusters. For $Ru(NH_3)_6(H_2O)_{55}^{3+}$, which corresponds to a concentration or activity of about 1 M, reduction results in a mean loss of 18.2 water molecules, from which an average and maximum energy deposition of 7.9 and ~8.2 – 8.7 eV, respectively, is determined. To the extent that the dissociation is statistical, the internal energy deposited corresponds to the reduction energy of the hydrated precursor ion by a thermal electron in the gas phase. This measured value is combined with the electron affinity of water to provide an absolute value for the reduction energy for 1 M $Ru(NH_3)_6^{3+}$ by a solvated electron in bulk water of about –4.9 eV (zero K). This gas-phase method for establishing absolute half-cell reduction potentials, which can be directly related to solution-phase values, has the advantages that effects of counter ions, solvent and chemical form can be easily controlled and quantified, and red-ox reactions not readily observed in solution can be measured.

## 4.1 Introduction.

Whereas the concept of absolute ionization potentials (or reduction potentials) of isolated gas-phase atoms, molecules and ions is well known, and extensive data have been tabulated, the concept of comparable absolute values in solution is obfuscated by several factors. In solution, electrochemical half-cell potentials are measured on a relative basis and provide a ladder or scale of thermochemical values that is anchored to the standard hydrogen electrode (SHE), which is arbitrarily assigned a value of exactly zero volts. The development of an "absolute" electrode potential has been extensively debated [1], and the concept of such a potential has been described as "necessarily something very obscure and abstruse, which certainly escapes the comprehension of average minds. Something like the origin of life in the world, the Arabian phoenix of electrochemistry" [1c].

In principle, the half-cell potentials of hydrated ions can be measured directly in the gas phase and for sufficiently large clusters, these values can potentially be related to solution-phase values. We recently demonstrated a method whereby extensively hydrated divalent ions are used as "nanocalorimeters" to measure the internal energy deposition when these ions are reduced by thermal electrons [2]. Specifically, the binding energy of a water molecule to hydrated clusters rapidly approaches a value of approximately 10 kcal/mol with increasing hydrated cluster size [2,3]. When a thermal electron in the gas phase recombines with a gas-phase cluster, energy corresponding to the recombination energy (RE) or adiabatic ionization potential of the reduced species can potentially be deposited into the ion. The resulting internal energy distribution can be obtained from the number of water molecules that evaporate from the cluster. Electron capture by $M(H_2O)_{32}^{2+}$ clusters, M = Mg, Ca, Sr, and Ba, results in the loss of on average 10.0 – 10.3 water molecules from the reduced clusters, corresponding to an average internal energy deposition of ~4.5 eV [2]. The RE does not depend significantly on ion size despite the large difference in second ionization potentials of the isolated gas-phase atoms (10.0 and 15.0 eV for Ba and Mg, respectively). This suggests that an ion-electron pair is formed in the reduced cluster. By comparison to calculated values for the RE for hydrated calcium clusters, it was demonstrated that electron capture (EC) results in statistical dissociation for these extensively hydrated ions and that the RE values obtained from this experiment correspond to gas-phase reduction potentials of the clusters.

Here, we show that the reduction potential of aqueous gas-phase nanodrops that are 1 M in $Ru(NH_3)_6^{3+}$ can be measured using our nanocalorimetry method. As with singly charged ions, the binding energy of water to divalent metal ions rapidly decreases with cluster size. For $Ca(H_2O)_n^{2+}$, $n$ = 6 to 14, the sequential water dissociation enthalpy decreases from 25.3 to 11.9 kcal/mol [4]. For larger clusters, we expect that this value approaches about 10 kcal/mol; the heat of vaporization of water is 10.8 and 9.7 kcal/mol at 0 and 100 ºC, respectively [5]. Thus, it should be possible to quantify the energy deposition resulting from reduction of extensively hydrated trivalent ions from the numbers of water molecules lost from the reduced precursor ions.

## 4.2 Experimental Methods.

Experiments were performed on a 2.75 Tesla Fourier-transform ion cyclotron resonance mass spectrometer with an external nanoelectrospray ionization source and an ion cell cooled to 130 K using a regulated flow of liquid nitrogen [6]. Thermal electrons are produced using a 1.0 cm heated cathode that is 20 cm from the cell center and 40 ms electron radiation times were used.

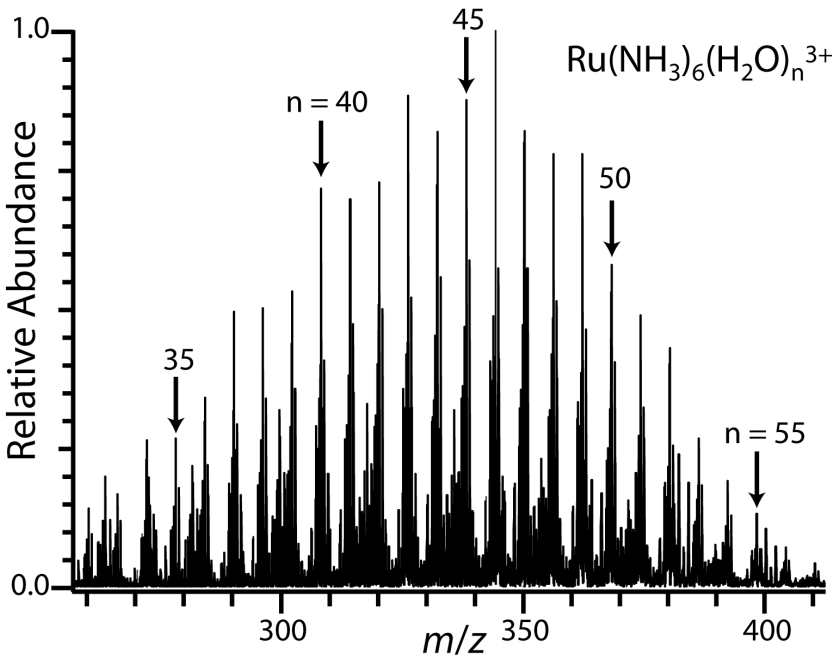


*Figure 4.1. ESI mass spectrum of ~2 mM aqueous $Ru(NH_3)_6^{3+}$ showing hydrated clusters, $Ru(NH_3)_6(H_2O)_n^{3+}$, with n indicated in the figure.*

## 4.3 Results and Discussion.

Electrospray ionization of an aqueous ~2 mM $Ru(NH_3)_6^{3+}$ solution results in a broad distribution of hydrated ions (Figure 4.1) that can be shifted to larger or smaller clusters by adjusting instrumental parameters [6b]. A nanodrop consisting of 55 water molecules and a single $Ru(NH_3)_6^{3+}$ corresponds to a concentration of about 1 M, which should be approximately the same as the activity because no other ions are present. Isolation of $Ru(NH_3)_6(H_2O)_{55}^{3+}$, followed by reduction of these ions by thermally generated electrons results in three product ions; $Ru(NH_3)_6(H_2O)_n^{2+}$, $n$ = 36, 37, and 38 (Figure 4.2). In contrast to the alkaline earth cation clusters, Ru ions are likely reduced in these clusters. These results show that a weighted average of ~18.2 water molecules are lost. Residual activation of the ions by blackbody radiation or collisions with residual gases results in a loss of < 0.1 water molecules and the average water loss from EC reported here is

corrected for this minor background dissociation. From this value, an average internal energy deposition resulting from EC by the precursor ion of 18.2 x 10 kcal/mol ≈ 182 kcal/mol (7.9 eV) is obtained. The maximum energy deposition corresponds to a value between 19 and 20 water molecules lost or ~8.2 – 8.7 eV. By comparison, the third ionization potential of isolated Ru atoms is 28.5 eV. This indicates that the ions are significantly stabilized by solvation in the nanodrop. The deposited internal energy is reflected by the distribution and the intensity of the product ions [7]. The observed distribution is very narrow and on the order of ± 15 kcal/mol (0.7 eV).

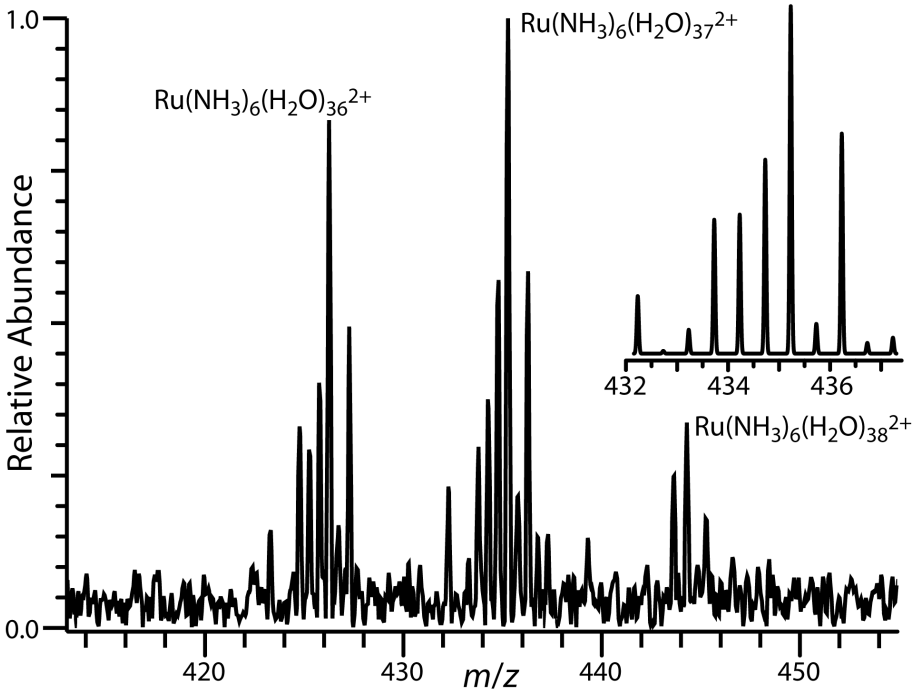


*Figure 4.2. Electron capture dissociation products resulting from reducing isolated $Ru(NH_3)_6(H_2O)_{55}^{3+}$ in the gas phase with thermally generated electrons. Inset is the calculated theoretical isotope distribution for the n = 37 product ion.*

To determine the effect of cluster size on the number of water molecules that evaporate from the cluster, EC spectra of $Ru(NH_3)_6(H_2O)_n^{3+}$ were measured for $n$ between 18 and 61. For clusters with $n \geq 40$, reduction of the precursor ion results in exclusively loss of water molecules, the average number of which reaches a broad maximum between $n = 40 – 55$ (Figure 4.3). For clusters with $n \leq 37$, a competing channel is observed where loss of one ammonia molecule accompanies water loss. The average ligand loss (including the ammonia loss channel) decreases with cluster size for $n < 37$, an effect presumably due to the higher ligand binding energy to the smaller reduced species. This effect may be counteracted by increasing RE with decreasing cluster size [2,8], but the effect of higher binding energy is more predominant. The average number of water molecules lost from the larger clusters also decreases slightly from the maximum, presumably due to

increasing degrees of freedom. For a fixed energy deposition, more degrees of freedom will result in increased lifetimes of the activated reduced species [9] and competing mechanisms for energy loss, either radiative emission or collisions with background gas can remove some energy from the clusters. These competing processes should be minimal under the conditions of these experiments (130 K, background pressure < 10-8 Torr) [10].

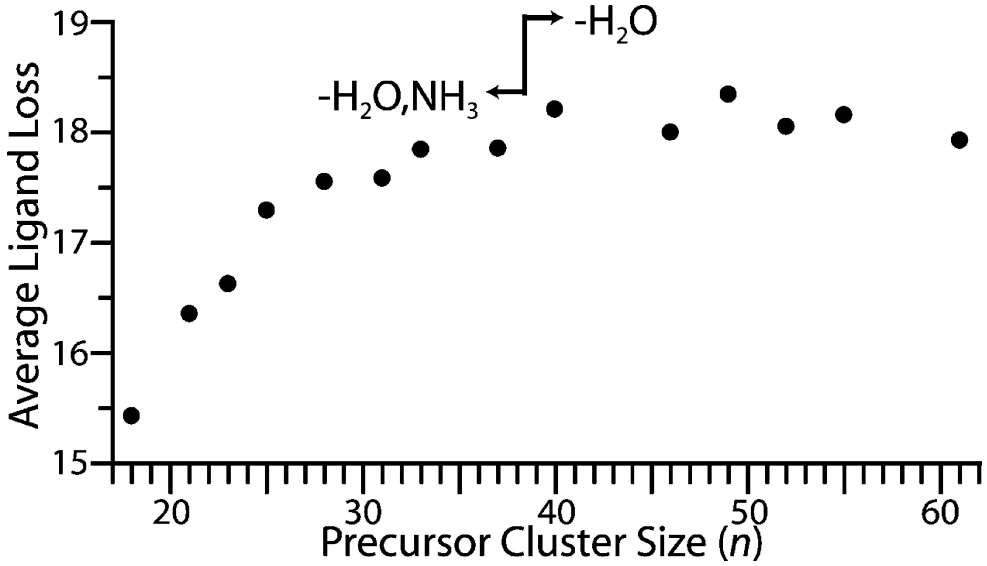


*Figure 4.3. The average number of ligands lost due to electron capture by $Ru(NH_3)_6(H_2O)_n^{3+}$ as a function of cluster size. For $n \geq 40$, loss of water is the only process observed. For $n \leq 71$, a competing channel corresponding to water loss accompanied by loss of a single ammonia molecule is observed.*

These gas phase measurements can be related to solution-phase reduction potentials at 0 K by the thermodynamic cycle described in eqs 1−5. The measured RE (eq 1), obtained from the number of water molecules lost from the reduced precursor (assuming statistical dissociation), is combined with the solvation energies of the reactant $E_{solv}(3+)$ and product $E_{solv}(2+)$ clusters (eq 2 and 3) obtained from Born theory and the adiabatic electron affinity (AEA) of water (eq 4) resulting in an approximate energy for solution-phase reduction (eq 5) referenced to an electron in aqueous solution (or a gas-phase electron by omitting eq 4).

$$Ru(NH_3)_6(H_2O)_n^{3+}{}_{(g)} + e^-_{(g)} \rightarrow Ru(NH_3)_6(H_2O)_{n-x}^{2+}{}_{(g)} + x(H_2O)_{(g)} \quad \Delta G = -RE \qquad (1)$$

$$Ru(NH_3)_6^{3+}{}_{(aq)} \rightarrow Ru(NH_3)_6(H_2O)_n^{3+}{}_{(g)} \qquad \Delta G = -E_{solv}(3+) \qquad (2)$$

$$Ru(NH_3)_6(H_2O)_n^{2+}{}_{(g)} \rightarrow Ru(NH_3)_6^{2+}{}_{(aq)} \qquad \Delta G = E_{solv}(2+) \qquad (3)$$

$$e^-_{(aq)} \rightarrow e^-_{(g)} \qquad \Delta G = AEA \qquad (4)$$

$$Ru(NH_3)_6^{3+}{}_{(aq)} + e^-_{(aq)} \rightarrow Ru(NH_3)_6^{2+}{}_{(aq)} \qquad \Delta G = -RE + AEA - \Delta E_{solv}(3+,2+) \qquad (5)$$

For gas-phase ≈1 M aqueous $Ru(NH_3)_6^{3+}$, we estimate this value to be roughly −8.2 + 3.1 + 1.3 ≈ −3.8 eV, where the 0 K AEA of water is ≈1.3 eV [11] and the $\Delta E_{soln}(3+,2+)$ is −3.1 eV. This 0 K energy can be temperature corrected to 25 °C and related to a half-cell potential ($\Delta G = -n$FE). By comparison, the one-electron reduction potential of $Ru(NH_3)_6^{3+}$ in aqueous solution, extrapolated to infinite dilution, is +0.1 eV versus the SHE [12].

**4.4 Conclusions.**

Within the limits of the approximations and uncertainties associated with our method, this suggests that eq 5 or the SHE can be assigned an absolute value to which all other half-cell potentials can be referenced. Results from additional redox couples can provide information about the accuracy of this method. Such studies, combined with temperature correction estimates, are ongoing. It should be emphasized that the reduction energy from eq 5 corresponds to reduction of the ion by a solvated electron versus an electron from a metal electrode in solution; relating these two values is made more complicated by the absence of any counterions or junction potentials in the gas phase and other factors. However, a key advantage of this approach to measuring absolute half-cell reduction potentials over methods that use solvation models and IEs of the bare ion [13] is that solute−solvent specific interactions which are poorly accounted for in solvation models [14] are accurately accounted for in our measurements. Additional advantages include that the effects of counterions, dilution, and chemical form are easily controlled and individually quantifiable, and half-cell reactions not directly observable in aqueous solution, such as a one-electron reduction of hydrated $Fe^{2+}$, can be readily measured in the gas phase.

**4.5 Acknowledgements.**

The authors thank Professors Marcin Majda, Daniel M. Neumark, and Kenneth N. Raymond for helpful discussions and NSF (CHE-041593) and NIH (R01 GM064712-05) for generous financial support.

**4.6 References.**


[1] a) Bockris, J. O'M.; Argade, S. D. *J. Chem. Phys.* **1968**, *49*, 5133-5134.

b) Bousse, L. *J. Chem. Phys.* **1982**, *76*, 5128-5133.

c) Trasatti, S. *Electrochim. Acta.* **1990**, *35*, 269-271.

[2] Leib, R. D.; Donald, W. A.; Bush, M. F.; O'Brien, J. T.; Williams, E. R. *J. Am. Chem. Soc.*, **2007**, *129*, 4894-4895.

[3] Shi, Z.; Ford, J. V.; Wei, S.; Castleman Jr., A. W. *J. Chem. Phys.* **1993**, *99*, 8009-8015.

[4] Peschke, M.; Blades, A. T.; Kebarle, P. *J. Phys. Chem. A* **1998**, *102*, 9978-9985.

[5] Marsh, K. N. "Recommended Reference Materials for the Realization of Physicochemical Properties" Blackwell, Oxford, 1987.

[6] a) Wong, R. L.; Paech, K.; Williams, E. R. *Int. J. Mass Spectrom*. **2004**, *232*, 59-66.

b) Bush, M. F.; Saykally, R. J.; Williams, E. R. *Int. J. Mass Spectrom.* **2006**, *253*, 256-262.

[7] a) DeKrey, M. J.; Kenttämaa, H. I.; Wysocki, V. H.; Cooks, R. G. *Org. Mass Spectrom.* **1986**, *21*, 193-195.

b) Kenttämaa, H. I.; Cooks, R. G. *Int. J. Mass Spectrom. Ion Processes* **1985**, *64*, 79-83.

[8] Reinhard, B. M.; Niedner-Schatteburg, G. *J. Chem Phys.* **2003**, *118*, 3571-3582.

[9] McLafferty, F. W.; Wachs, T.; Lifshitz, C.; Innorta, G.; Irving, P. *J. Am. Chem. Soc.* **1970**, *92*, 6867-6880.

[10] Price, W. D.; Williams, E. R. *J. Phys. Chem. A* **1997**, *101*, 8844-8852.

[11] Han, P.; Bartels, D. M. *J. Phys. Chem.* **1990**, *94*, 7294−7299.

[12] Meyer, T. J.; Taube, H. *Inorg. Chem.* **1968**, *7*, 2369-2379.

[13] Uudsemaa, M.; Tamm, T. *J. Phys. Chem. A* **2003**, *107*, 9997−10003.

[14] Cramer, C. J.; Truhlar, D. G. *Chem. Rev.* **1999**, *99*, 2161−2200.

## Chapter 5

### Nonergodicity in Electron Capture Dissociation Investigated Using Hydrated Ion Nanocalorimetry

This chapter is reproduced with permission from Ryan D. Leib, William A. Donald, Matthew F. Bush, Jeremy T. O'Brien, and Evan R. Williams "Nonergodicity in electron capture dissociation investigated using hydrated ion nanocalorimetry" *Journal of the American Society for Mass Spectrometry*. **2007**, *18*, 1217-1231. 

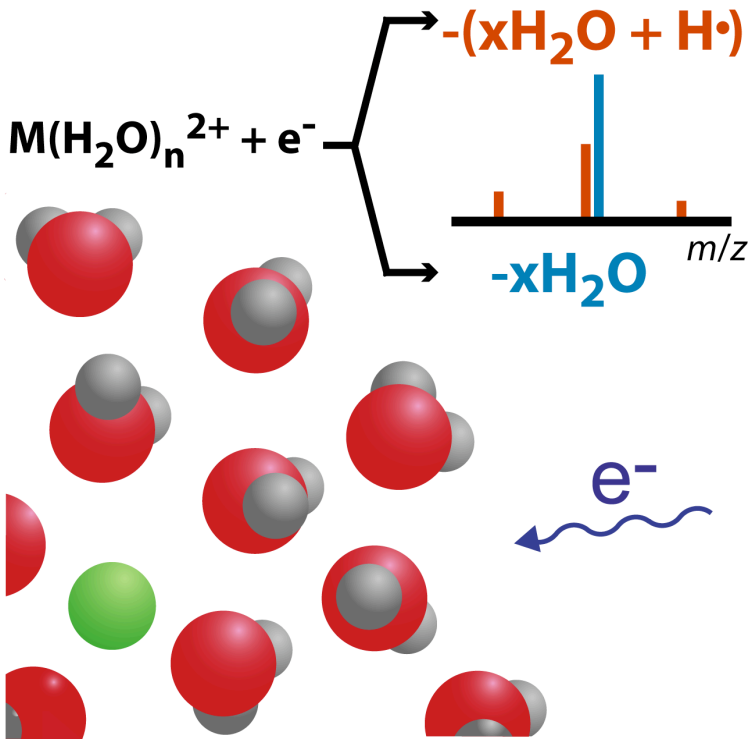

**5.0 Abstract.**

Hydrated divalent magnesium and calcium clusters are used as nanocalorimeters to measure the internal energy deposited into size-selected clusters upon capture of a thermally generated electron. The infrared radiation emitted from the cell and vacuum chamber surfaces as well as from the heated cathode results in some activation of these clusters, but this activation is minimal. No measurable excitation due to inelastic collisions occurs with the low-energy electrons used under these conditions. Two different dissociation pathways are observed for the divalent clusters that capture an electron: loss of water molecules (pathway I) and loss of a H atom and water molecules (pathway II). For $Ca(H_2O)_n^{2+}$, pathway I occurs exclusively for $n \geq 30$ whereas pathway II occurs exclusively for $n \leq 22$ with a sharp transition in the branching ratio for these two processes that occurs for $n \approx 24$. The number of water molecules lost by both pathways increases with increasing cluster size reaching a broad maximum between $n$ = 23 and 32, and then decreases for larger clusters. From the number of water molecules that are lost from the reduced cluster, the average and maximum possible internal energy is determined to be ~4.4 and 5.2 eV, respectively, for $Ca(H_2O)_{30}^{2+}$. This value is approximately the same as the calculated ionization energies of $M(H_2O)_n^+$, M = Mg and Ca, for large $n$ indicating that the vast majority of the recombination energy is partitioned into internal modes of the ion and that the dissociation of these ions is statistical. For smaller clusters, estimates of the dissociation energies for the loss of H and of water molecules are obtained from theory. For $Mg(H_2O)_n^{2+}$, $n$ = 4 – 6, the average internal energy deposition is estimated to be 4.2 – 4.6 eV. The maximum possible energy deposited into the $n$ = 5 cluster is < 7.1 eV, which is significantly less than the calculated recombination energy for this cluster. There does not appear to be a significant trend in the internal energy deposition with cluster size whereas the recombination energy is calculated to increase significantly for clusters with fewer than 10 water molecules. These, and other results, indicate that the dissociation of these smaller clusters is nonergodic.

## 5.1 Introduction.

Advances in protein characterization by mass spectrometry (MS) have been accelerated by new instrumentation and methods of analysis that have blossomed over the last decade. The "bottom-up" approach to protein characterization has been used to identify as many as 7,800 proteins from whole cell lysis of the mouse brain [1]. The effectiveness of the bottom-up method for complex samples can be enhanced by using multidimensional separations. Clemmer and coworkers elegantly demonstrated that combining on-line liquid chromatography (LC) with ion mobility spectrometry and MS can greatly improve separations without increasing analysis times over LC/MS alone [2-4]. In contrast, the "top-down" approach to protein characterization has the advantage that *de novo* sequencing, including the identification and structural localization of labile posttranslational modifications, can be done directly on protein mixtures without proteolysis [5, 6]. This top-down approach has greatly benefited from the development of electron capture dissociation (ECD), a method pioneered by McLafferty and coworkers [6-9]. In a typical ECD experiment, multiply protonated or cationized ions are reduced by the capture of thermally generated electrons to produce odd electron ions. For multiply protonated proteins, electron capture (EC) typically results in generation of "***c***" and "***z***" ions corresponding to cleavage of the protein backbone N-$C_\alpha$ bond. For small proteins, ECD can result in over 90% sequence coverage [9]. Analogous methods that use collisions with anions (ETD) [10, 11] or neutral atoms (ECID) [12, 13] to reduce precursor ions result in similar fragmentation products for proteins.

Although ECD was first demonstrated nearly 10 years ago [7] and has been the subject of extensive reviews [14-17], the mechanism by which fragment ions are formed is still hotly debated. McLafferty and coworkers proposed that capture of an electron by a multiply charged protein results in nonergodic dissociation through high-*n* Rydberg states [18]. In contrast, Tureček and coworkers have argued that the odd electron ions formed by electron capture have very low bond dissociation energies and that dissociation of these ions is rapid even at thermal energies [19-25]. Experimental and computational evidence supporting both of these mechanisms have been reported [26-37], including evidence for some long-lived intermediates from elegant double resonance and H/D scrambling experiments by O'Connor and coworkers [35-37].

Electron capture by a multiply charged ion is the reverse process of ionization of the corresponding ion with one additional electron. For multiply protonated proteins, this recombination energy resulting from EC has been estimated to be 4 – 7 eV [7, 15]. The recombination energy for protonated, lithiated, and cesiated glycine decreases with increasing cation size [38]. The fragment ions formed by ECD of peptides that are cationized with two different cations are consistent with the preferred neutralization of the cation of highest recombination energy [38]. Similar results have been reported by Liu and Hakansson for metalated peptides [33, 34].

A useful parameter to determine the extent to which a dissociation process is ergodic or nonergodic is what fraction of the recombination energy is converted into internal modes of the reduced ion. In principle, it is possible to obtain a measure of the

internal energy deposition of an ion activation method by using "chemical thermometers" [39-46]. Several different approaches for this have been demonstrated. In one method, a measure of the internal energy is obtained from the branching ratio for two or more product ions formed by competing pathways with different and known dissociation enthalpies and entropies [39-41]. For example, the molecular ion of *n*-butyl benzene can dissociate via a direct bond cleavage to form $C_7H_7^+$ (*m*/*z* 91) or via a McLafferty rearrangement to form $C_7H_8^+$ (*m*/*z* 92). The latter process has a lower activation energy but higher entropy; formation of *m*/*z* 92 ion is favored at low internal energies, whereas *m*/*z* 91 is favored at higher internal energies. Thus, the ratio of these two ions serve as a measure of the internal energy deposited into this ion [39-41]. A measure of the internal energy can also be obtained from the abundances of fragment ions formed via consecutive reaction pathways with known critical formation energies [42-45]. For example, activation of $Fe(CO)_5^{+\bullet}$ can result in sequential loss of CO molecules with critical energies ranging from 1.15 eV for the loss of the first CO molecule to 7.58 eV for the loss of all five CO molecules; formation of $FeC^+$ requires 15.7 eV [43]. The abundances of the fragment ions formed by activation of $Fe(CO)_5^{+\bullet}$ or analogous ions provide a measure of the range and magnitude of the internal energy that is deposited into this ion. This method, first demonstrated by Kenttämaa and Cooks [42], has been used to characterize the internal energy distribution resulting from ion-surface and ion-gas collisions [43] as well as other activation methods [44, 45]. The effective internal temperature of an ion can also be obtained from measurements of dissociation kinetics if Arrhenius parameters in the rapid energy exchange limit for the dissociation process are known. For large ions, these parameters can be obtained directly from blackbody infrared radiative dissociation (BIRD) experiments [47] and used to obtain the effective temperature of ions activated by other methods. This method has been used to measure effective temperatures of peptide ions activated by multiple gas-phase collisions [46].

Here, ECD spectra of hydrated clusters of divalent calcium and magnesium clusters are reported as a function of cluster size. Two different dissociation pathways are observed and the branching ratio for these pathways depends on cluster size. We demonstrate that these nanometer-size clusters can be used as calorimeters to measure the energy that is deposited into these ions upon EC. Using this "nanocalorimetry" method, we show that the vast majority of the recombination energy is transferred into internal modes of large clusters and that the dissociation process is ergodic. For smaller clusters, we show that significantly less energy than the potentially available recombination energy is transferred into internal modes of the reduced species and that ECD is nonergodic for these clusters.

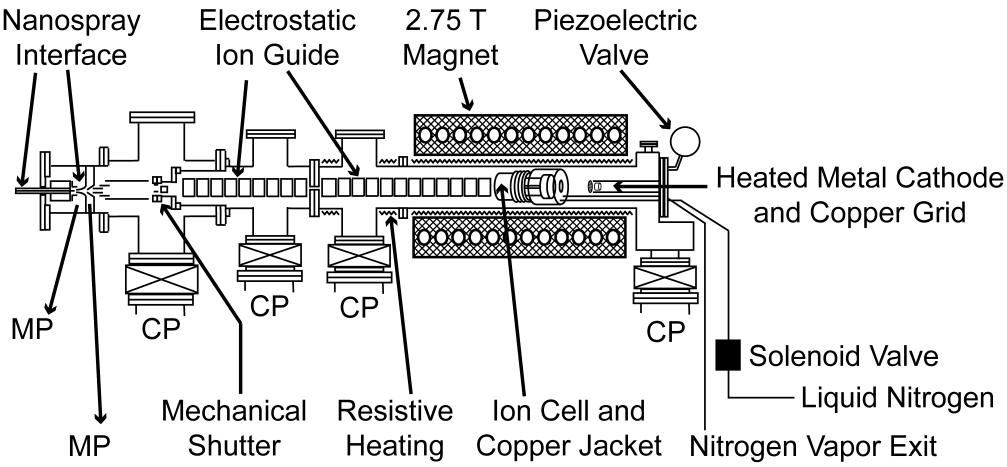


*Figure 5.1. Schematic diagram of the 2.75 T Fourier-transform ion cyclotron resonance mass spectrometer used in these experiments. This instrument has an external electrospray ionization source, a temperature controlled ion cell that is cooled to 130 K with a regulated flow of liquid $N_2$ and a heated metal dispenser cathode mounted on the central axis of the vacuum chamber and positioned 20 cm from the cell center for generation of thermal electrons for ECD. MP and CP indicate mechanical pumps and cryopumps, respectively.*

## 5.2 Experimental Methods.

**5.2.1 Instrument and Methods.** Experiments were performed on a 2.75 Tesla Fourier-transform ion cyclotron resonance (FT/ICR) mass spectrometer with an external electrospray ionization source (Figure 5.1). This instrument, which has a temperature controlled ion cell that can be cooled using a regulated flow of liquid $N_2$ [48] and an electrospray ionization source that is used to produce extensively hydrated ions [49] is described in detail elsewhere. Hydrated divalent calcium and magnesium ions were formed by nanospray from aqueous solutions that are 2 mM in metal ion (from $CaCl_2$ and $MgSO_4$). Tips used for nanospray are produced from pulled borosilicate capillaries that have an inner tip diameter of ~1 μm. A ~550 V potential (relative to the ~115 °C heated metal capillary) is applied to a platinum wire in direct contact with the solution. Hydrated ions are introduced into the ion cell through five stages of differential pumping and accumulated for 4 s during which time $N_2$ gas is introduced at a pressure of ~$10^{-6}$ Torr using a piezoelectric valve to enhance trapping and thermalization of the ions. A mechanical shutter is subsequently closed so that no additional ions are introduced into the cell. The ions then are stored for 6 s to ensure that a steady state internal energy distribution is established and to allow pressure in the instrument to return to < $10^{-8}$ Torr prior to ECD. The temperature of the copper jacket surrounding the ion cell is kept at -140 °C.

For ECD, a 1.0 cm diameter heated dispenser cathode impregnated with barium scandate (Heatwave Labs, Watsonville, CA) was mounted axially with respect to the vacuum chamber 20 cm away from the cell center. A direct current of 3 A is used to heat the dispenser cathode to a temperature of 950 °C. Ion isolation with SWIFT waveforms is followed by a 50 ms delay prior to ECD. To introduce electrons into the cell for ECD, the potential of the cathode housing is pulsed from +10 to -1.4 V for 40 ms. A cathode potential of -1.4 V was found to be optimal for the production of ECD product ions in these experiments. A potential of +9 V was applied to a copper wire mesh mounted 0.5 cm in front of the cathode for all experiments. All potentials are referenced to instrumental ground.

A MIDAS data system was used to acquire 64 K data point transients. The average number of water molecules lost from these ions is determined from a weighted average of the product ion intensities observed. By subtracting the value attributable to BIRD from the weighted average of product ion intensities, the corrected average loss due to EC is obtained.

**5.2.2 Computational Chemistry.** Candidate low-energy structures were determined using conformational searching and chemical intuition. Initial structures of $[MOH(H_2O)_n]^+$, M = Mg and Ca, were generated using Monte Carlo conformation searching with the MMFF94 force field using Macromodel 8.1 (Schrödinger, Inc. Portland, OR). Initial structures of $[M(H_2O)_n]^+$ were generated from low-energy structures of $[Ca(H_2O)_n]^{2+}$, with smaller clusters identified by removing selected water molecules from those structures and substituting Ca with Mg. Additional structures were generated from MP2/6-31G** energy minimized structures reported by Siu and Liu [50].

Candidate structures were energy minimized with hybrid method density functional calculations (B3LYP) using the 6-311++G** basis set. Even electron species were evaluated using restricted spin methods, whereas odd electron species were evaluated using unrestricted spin methods. Vibrational frequencies were calculated to determine zero-point energies. These structures yielded all positive frequency vibrational modes, indicative of local-minima structures. Calculations were performed in Jaguar v6.5 (Schrödinger, Inc. Portland, OR) and Gaussian 03 (Gaussian, Inc. Wallingford, CT) [51] for structures containing Mg and Ca, respectively.

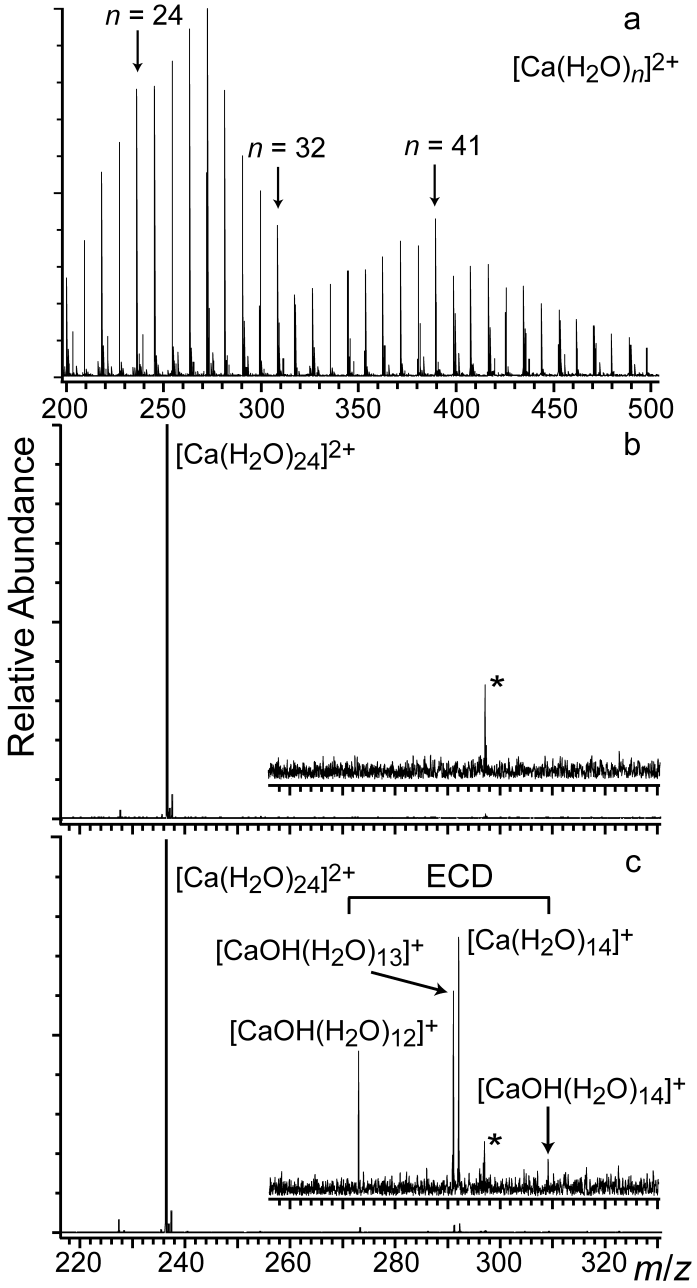


*Figure 5.2. Mass spectra from a) ESI of a 2 mM aqueous $CaCl_2$ showing a broad distribution of $Ca(H_2O)_n^{2+}$ clusters (selected n are labeled); b) SWIFT isolation of $Ca(H_2O)_{24}^{2+}$ and c) ECD of $Ca(H_2O)_{24}^{2+}$ with product ions indicated in the spectrum. A noise peak at ~297 m/z is labeled with an asterisk.*

## 5.3 Results and Discussion.

**5.3.1 Precursor Activation**. Hydrated divalent calcium ions, $Ca(H_2O)_n^{2+}$, were produced using nano ESI of a 2 mM aqueous $CaCl_2$ solution. The resulting cluster distributions are typically broad (Figure 5.2a) and can be shifted to either larger or smaller cluster size by changing instrumental parameters [49]. Low abundances of $CaOH(H_2O)_n^+$ and $H(H_2O)_n^+$ are also observed under these conditions. Ions from $n = 4 – 47$ were formed with sufficient abundance to isolate and measure their ECD spectra. Figure 5.2b shows an isolation spectrum for $Ca(H_2O)_{24}^{2+}$; a fragment ion at $m/z$ 227 corresponding to the loss of a single water molecule from the isolated precursor ion is observed. This ion is predominantly formed by BIRD as a result of infrared (IR) photons emitted from the cell and vacuum chamber surfaces as well as from the heated cathode (950 °C) that is located 20 cm away from the cell center.

To determine the effects of these IR photons on the ion population, $Ca(H_2O)_n^{2+}$, $n = 24$ and 32, were stored in the ion cell for times ranging from 90 ms to 1090 ms both with and without the cathode heated. In both cases, the potential of the cathode was +10 V so that no electrons were introduced into the cell and no ECD occurs. The kinetic data obtained from these experiments are shown in Figure 5.3. Substantial dissociation occurs for both of these ions even without the cathode heated due to blackbody radiation from the cell and surroundings. The dissociation kinetics are first order. Without the cathode heated, the $Ca(H_2O)_{32}^{2+}$ dissociation rate constant is about 60% greater than that for $Ca(H_2O)_{24}^{2+}$. Faster dissociation with increasing cluster size is primarily due to the higher internal energies and faster radiative absorption rates of larger clusters [47], although slightly decreasing binding energies with increasing cluster size may also contribute to this effect. When the cathode is heated to 950 °C, the dissociation rates of these clusters increases by 26% and 40% for the $Ca(H_2O)_{32}^{2+}$ and $Ca(H_2O)_{24}^{2+}$ clusters, respectively. This indicates that substantial activation of the precursor occurs due to absorption of radiation generated from the heated cathode. However, the extent of this activation is minimal for the 90 ms between ion isolation and detection in these ECD experiments. The abundance of the fragment ion corresponding to the loss of a water molecule from $Ca(H_2O)_{24}^{2+}$ is ~2% of the precursor abundance in the isolation mass spectra when the cathode is heated. Loss of a water molecule directly attributable to the heated cathode comprises 1.6% and 1.3% abundance relative to the precursor intensities for the $Ca(H_2O)_{32}^{2+}$ and $Ca(H_2O)_{24}^{2+}$ clusters, respectively. The abundance of this fragment ion increases with increasing cluster size; 9% of the $Ca(H_2O)_{47}^{2+}$ precursor dissociates under these conditions. Thus, the effects of IR emission from the heated cathode are observable, but have minimal impact on these ECD experiments. These effects could be reduced by placing the cathode a greater distance from the ion cell.

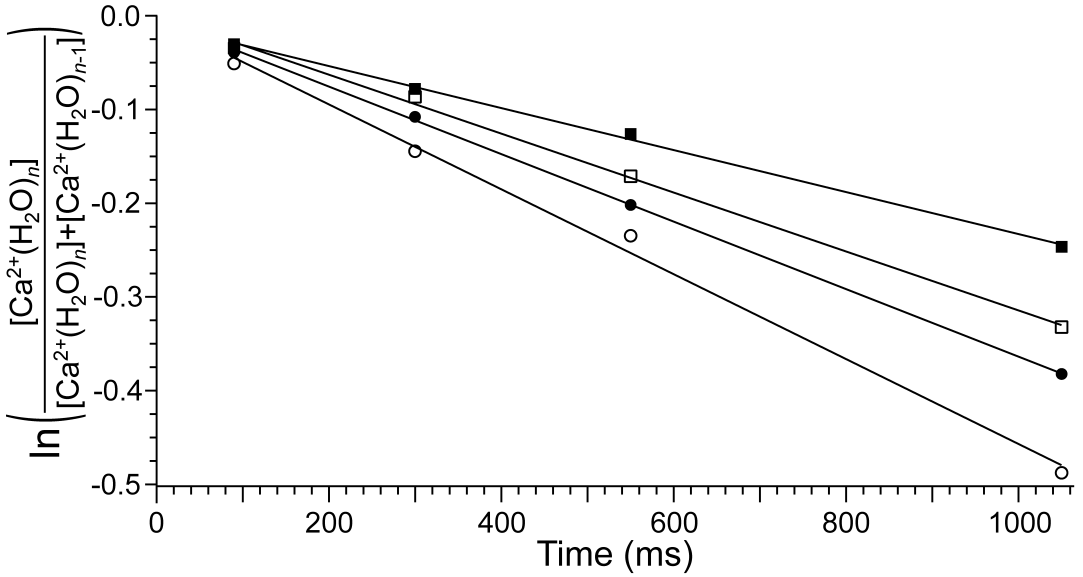


*Figure 5.3. BIRD dissociation kinetics for the loss of a water molecule from $Ca(H_2O)_n^{2+}$, n = 24 and 32, both with the ECD cathode at room temperature and with the cathode heated to 950 ºC but with no electrons introduced into the cell: $Ca(H_2O)_{24}^{2+}$ cathode at room temperature (■) and at 950 ºC (□); $Ca(H_2O)_{32}^{2+}$ cathode at room temperature (●) and at 950 ºC (○).*

In addition to activation by absorption of blackbody radiation, the precursor ions could also potentially be activated by inelastic collisions with electrons. Ion dissociation using low-energy electrons was first demonstrated by Cody and Freiser who termed this method electron impact excitation of ions from organics (EIEIO) [52]. To determine if any EIEIO occurs under the conditions of these ECD experiments, the loss of a water molecule from the isolated precursor ion was compared between experiments with and without electrons injected into the cell. Electrons are introduced into the cell for 40 ms by lowering the potential on the heated cathode from +10 V to -1.4 V. There was no significant difference in the abundance of the product ion corresponding to the loss of a water molecule from the precursor ion under the conditions of this experiment indicating that ion excitation due to EIEIO is negligible. An increase in water loss is observed when the electron kinetic energy is increased to 9 eV. However, no reduced product ions formed by ECD were detected with these conditions.

**5.3.2 Electron Capture Fragmentation Pathways**. As has been noted by others [53, 54], the efficiency of the ECD process is very sensitive to the electron energy, with the filament or cathode producing the most efficient capture conditions for polypeptides at potentials near 0 V. Another broad maximum in polypeptide capture efficiency has been noted at higher voltages, between -3 V to -13 V, and due to the appearance of additional fragmentation products, has been referred to as 'hot' electron capture dissociation [14]. The cathode potential of -1.4 V used in these experiments was selected by maximizing

the efficiency for formation of ECD product ions of $Ca(H_2O)_n^{2+}$; this potential also produced optimum ECD fragment abundances for the polypeptide Substance P under similar experimental conditions.

Capture of an electron by $M(H_2O)_n^{2+}$, M = Ca or Mg, can result in dissociation by two competing pathways (Scheme 5.1):

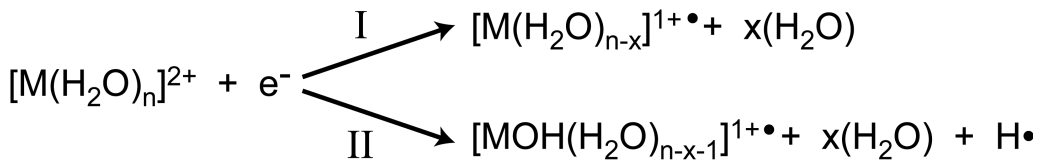


*Scheme 5.1.*

losses of multiple water molecules (pathway I), or ejection of a hydrogen atom forming a hydrated metal hydroxide with a single net charge and loss of multiple water molecules (pathway II). The branching ratio for these two processes depends on cluster size and these data are shown in Figure 5.4. Pathway I exclusively occurs for clusters with $n \geq 30$, whereas pathway II is the exclusive process observed for $n \leq 22$. Between $n = 23$ to 28, both processes are observed and there is a relatively sharp transition in the branching ratio around $n = 24$.

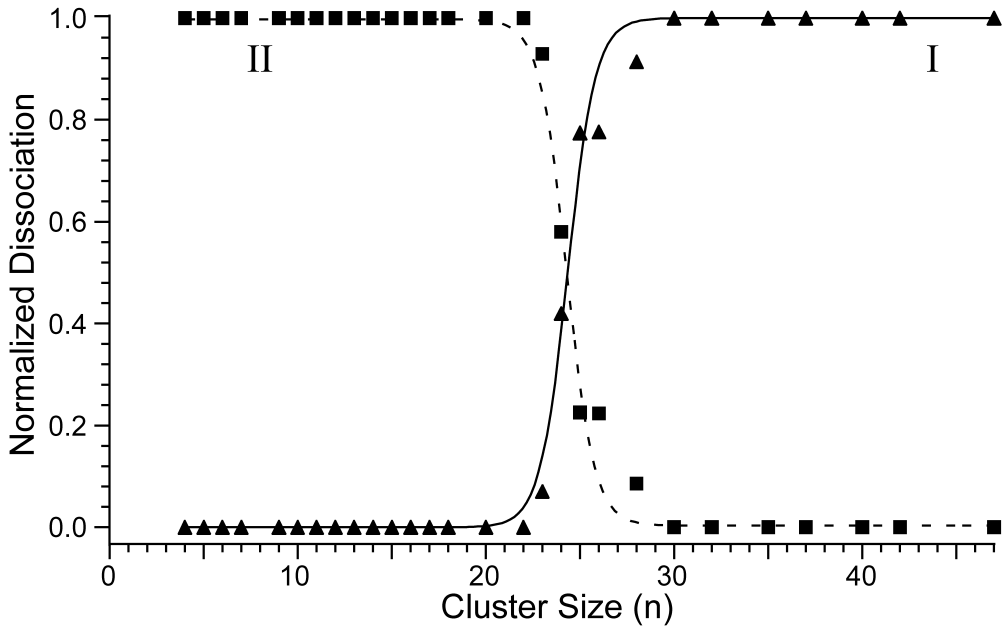


*Figure 5.4. Plot of the normalized product ion intensities from dissociation by pathways I and II (Scheme 5.1) resulting from electron capture by $Ca(H_2O)_n^{2+}$, n = 4 – 47, as a function of cluster size. A rapid transition from the loss of a single H atom and loss of water molecules (■; pathway II) to exclusively loss of water molecules (▲; pathway I) occurs between n = 22 and n = 30. Sigmoidal trend lines were fit to these data as a guide.*

The ECD spectrum of $Ca(H_2O)_{24}^{2+}$, which has products from both dissociation pathways, is shown in Figure 5.2c. In this spectrum, a single product ion that has lost 10 water molecules upon reduction, $Ca(H_2O)_{14}^{+}$, is formed by pathway I. Three product ions, $CaOH(H_2O)_n^{+}$, $n$ = 12 – 14, are formed by pathway II indicating that on average, 10.2 water molecules in addition to the hydrogen atom are lost from the reduced precursor as a result of this process. It should be noted that the natural isotope distribution of calcium does not interfere with distinguishing product ions from these two dissociation pathways. The narrow width of the product ion distributions resulting from electron capture is particularly interesting. For pathway I, the appearance of just a single product ion indicates that a very narrow range of internal energies resulting from EC contributes to the formation of this ion. For pathway II, the formation of three product ions suggests that that the overall internal energy distribution resulting from EC is somewhat broader but still relatively narrow compared to other activation methods [43].

Reactions of hydrated magnesium monocations have been investigated previously [55-57]. Using an expansion source, it was demonstrated that $Mg(H_2O)_n^{+}$ clusters were formed for $n$ = 1 – 5 and $n \geq 15$ whereas $MgOH(H_2O)_n^{+}$ was observed for $n$ = 6 – 14 [56]. In elegant BIRD experiments by Bondybey and coworkers who investigated solvent evaporation from singly charged hydrated magnesium cations, loss of water molecules rapidly occurred at room temperature for large clusters, but below about 21 water molecules, $MgOH(H_2O)_n^{+}$ was formed [57]. Another transition was noted for clusters with $n \leq 6$, where water loss was again the only dissociation pathway observed [57].

**5.3.3 Effects of Cluster Size.** The average number of water molecules lost from the reduced precursor upon EC (from both dissociation channels) as a function of cluster size from $n$ = 4 – 47 are summarized in Figure 5.5. This value increases nearly linearly with cluster size and reaches a broad plateau around $n$ = 23 – 32 from which an average loss of ~10.2 water molecules is observed. The average number of water molecules lost decreases slightly for cluster sizes larger than $n$ = 35. Also shown on this plot are several values obtained for divalent magnesium clusters which closely track the corresponding values for calcium.

The trends in the extent of water loss with cluster size can be qualitatively explained by two competing factors. For smaller clusters, the binding energy of water increases with decreasing cluster size [58-60]. Thus, for the smaller clusters, a fixed internal energy deposition will result in the evaporation of fewer water molecules. This appears to dominate over any increased internal energy deposition that may be expected for smaller clusters (*vide infra*). For larger clusters, the binding energy of water is not expected to change significantly with cluster size [59]. The most labile water molecules in larger clusters are largely shielded from the cation by other water molecules; thus, the binding energy of the outer shell molecules is predominantly determined by inter-water hydrogen bonds. The decrease in the number of water molecules lost from the larger clusters is likely due to the increased degrees of freedom of the precursor [61]. For a given deposited internal energy, the kinetic rate for ion dissociation will decrease with increasing cluster size because the energy can be spread over more internal modes. This will make it possible for competing energy loss mechanisms, such as collisions or

radiative emission, to reduce the energy of the cluster. Under the conditions of these experiments (< $10^{-8}$ Torr, ~130 K), it is expected that radiative emission plays a greater role [47].

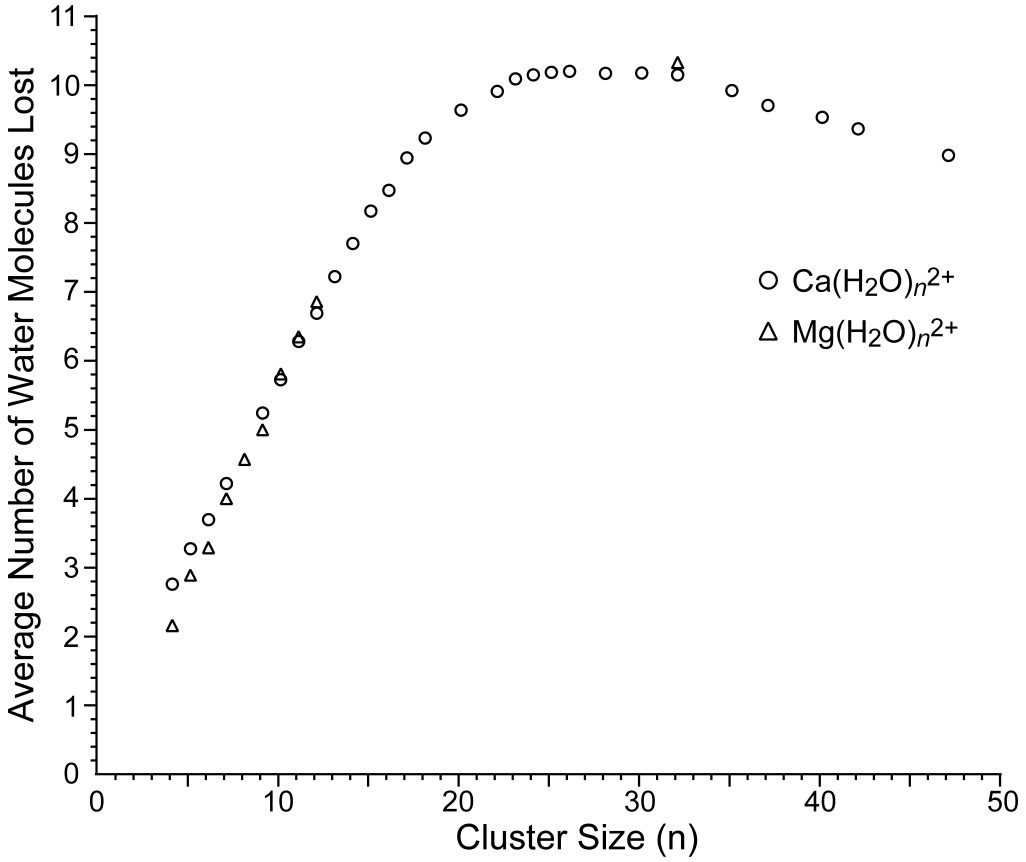


*Figure 5.5. The average number of water molecules lost from the reduced precursor ion due to electron capture by $M(H_2O)_n^{2+}$, M = Ca (○) and M = Mg (Δ), as a function of cluster size. The average number of water molecules lost is determined from both dissociation pathways (Scheme 5.1).*

**5.3.4 Internal Energy Deposition.** In principle, it should be possible to determine the extent to which internal energy is deposited into internal modes of the reduced precursor ions upon electron capture from the distribution of the observed product ions. Specifically, if the threshold dissociation energies for a series of consecutive reactions are known, information about the internal energy deposition can be obtained from the distribution of product ions formed. This method, pioneered by Cooks and coworkers [42, 43], has been used to characterize the internal energy deposition of several activation methods [43-45]. For large clusters, where loss of water molecules is the only process observed, we have shown that the number of water molecules lost from the reduced precursor can be used as a measure of the internal energy deposition in these clusters

[62]. Thus, these nanometer-size clusters can be used as nanocalorimeters to measure energy conversion in ECD or any other process [62].

The binding energies of water to protonated water clusters have been measured using different methods. The sequential binding energies rapidly decrease with cluster size; the proton affinity of water is 165.2 kcal/mol, but loss of a water molecule from a proton-bound dimer requires only 36 kcal/mol [63]. The $6^{th}$, $7^{th}$, and $8^{th}$ water molecule binding enthalpies in protonated water clusters are 13.0, 11.7, and 10.3 kcal/mol, respectively [63]. Castleman and coworkers reported that the sequential binding energies for protonated water clusters with 8 – 28 water molecules range between 9 – 11 kcal/mol [59].

Effects of cation identity on water binding energies are significant for very small clusters, but become negligible for larger clusters. The sixth water binding energies of $M(H_2O)_6^+$, M = Li, Na, and K, are 12.1, 10.7, and 10.0 kcal/mol, respectively [58]. Interestingly, the fourth water binding energies of $M(H_2O)_4^+$ for M = Na, Mg, and Al, are 13.1, 11.5, and 12.5 kcal/mol [60]. This suggests that the binding energy of water does not depend strongly on metal ion identity when the clusters approach a large size. Unfortunately, values for significantly larger clusters, such as those formed here, have not been reported.

An estimate of the binding energy to infinitely large clusters can be obtained from the heat of vaporization of water. This value ranges from 10.8 to 9.7 kcal/mol for temperatures between 0 to 100 °C [64]. The heat of sublimation for hexagonal ice has been reported using a low temperature equation of state developed from thermodynamic equilibrium properties at temperatures ranging from 273.16 to 130 K. The enthalpy of sublimation is relatively constant across these temperatures, ranging from 12.2 to 12.0 kcal/mol [65]. For droplets, the surface energy reduces the vaporization enthalpy from that of the bulk. For neutral water clusters, the evaporation enthalpy of a single water molecule from a cluster of size $n$ can be estimated from the bulk enthalpy of vaporization less a surface energy term which scales as $n^{-1/3}$ [66]. Using a value for the bulk enthalpy of vaporization of hexagonal ice of 11.2 kcal/mol at zero K, the energy required to evaporate a single water molecule from water clusters from $n$ = 20 – 50 is estimated to vary from 9.2 - 9.7 kcal/mol. This suggests that the effects of surface energy are small for clusters in this size range.

Extrapolating bulk physical properties from cluster data can have significant uncertainties. However, these data all suggest that the binding energy of water to the reduced precursors investigated here should be approximately 10 kcal/mol. This value depends on the cluster temperature, size and to a limited extent on shell structures or "magic" numbers observed for some clusters. However, we anticipate that any variations that may be present will be small compared to other uncertainties in our method. Although it is difficult to fully assess the uncertainty in the water binding enthalpies, we estimate this uncertainty to be about ± 10%. For the smaller clusters, where the degrees of freedom are low, the initial effective temperature of the reduced cluster is very high and the effects of temperature on the vaporization energy of water will be more substantial. The energy resolution of this method is also limited by the sequential binding energies of the ligands.

Using this estimated value of roughly 10 kcal/mol per water molecule lost from large clusters, we can determine an average ($E_{avg}$) and an upper limit ($E_{UL}$) to the internal energy deposited into the clusters upon electron capture. For $Ca(H_2O)_{30}^{2+}$, which is in the plateau region of maximum water loss (Figure 5.5), reduction by electron capture results in formation of $Ca(H_2O)_{19}^{+}$ and $Ca(H_2O)_{20}^{+}$ with normalized relative abundances of 0.3 and 1.0, respectively, corresponding to an average of 10.2 water molecules lost. This value must be corrected for residual background dissociation that is due to blackbody radiation (*vide supra*). To do this, we assume that activation of the precursor and the reduced precursor by BIRD is the same; capture of an electron to form the reduced precursor can occur any time during the 40 ms electron irradiation time so that some fraction of the reduced species will be from the precursor that has lost a single water molecule. To the extent that the fragmentation of precursor and the reduced precursor are the same, it is possible to account for dissociation by BIRD. For $Ca(H_2O)_{30}^{2+}$, this correction corresponds to an average water molecule loss of 5%. This value is comparable to the values for other clusters, and varies with cluster size from 1% to 9% for the $Ca(H_2O)_9^{2+}$ and $Ca(H_2O)_{47}^{2+}$ clusters, respectively. Thus, the average water loss from $Ca(H_2O)_{30}^{2+}$ due only to electron capture is $10.23 - 0.05 \approx 10.2$ water molecules. This water loss corresponds to an average internal energy deposition of 10.2 x 10 kcal/mol = 102 kcal/mol (4.4 eV). Formation of the product ion corresponding to the reduced precursor that has lost 11 water molecules requires 110 kcal/mol (4.8 eV). The absence of a product ion corresponding to the loss of 12 water molecules indicates that the maximum possible internal energy that is deposited into $Ca(H_2O)_{30}^{2+}$ upon EC is between 110 and 120 kcal/mol (4.8 – 5.2 eV). It should be emphasized that the uncertainty in the energy values obtained with this method is attributable to the uncertainty in the binding enthalpy of water used to obtain these values from the number of water molecules lost, which we estimate to be about ± 10%. These values are close to 4.5 eV, the value calculated for the vertical ionization energy of $Ca(H_2O)_{29}^{+}$ [62] which is a rough estimate of the recombination energy in this EC experiment. Because the internal energy deposition we obtain from this method is comparable to the estimated recombination energy, we conclude that the vast majority of the recombination energy is deposited into internal modes of the ions, i.e., ECD is ergodic for these larger cluster ions. Additional evidence for ergodic dissociation for the larger clusters is the decreasing number of water molecules lost from the cluster with increasing cluster size (Figure 5.5), consistent with a degree of freedom effect (*vide supra*).

**5.3.5 ECD Energetics for Small $Mg(H_2O)_n^{2+}$ Clusters.** In order to estimate the internal energy that is deposited into the smaller clusters where the loss of a H atom in addition to water loss occurs, dissociation energies for the loss of the H atom and for losses of water must be known. The lowest-energy structures and the barriers for H loss for $Mg(H_2O)_n^{+}$, $n = 1 - 6$, have been calculated by Siu and Liu [50] using MP2/6-31G**. From the reported zero-point corrected energies of these structures, the binding energies of water are determined. The binding energy of water should be approximately equal to the activation energy for dissociation, because any reverse activation barrier should be small. These values are given in Table 5.1. For comparison, experimentally determined bond

*Table 5.1. Zero-point energy corrected water and hydrogen binding energies (in kcal/mol) from B3LYP/6-311++G** calculations for $[X(H_2O)_n]^+$, X = Mg, Ca, MgOH, and CaOH. MP2/6-31G** water binding energies to $[Mg(H_2O)_n]^+$ and hydrogen loss barrier energies from [50], and experimental CID results from [60], are included for comparison.*

| | CID[a] | MP2/6-31G* | | B3LYP/6-311++G** | | | | | |
|---|---|---|---|---|---|---|---|---|---|
| X | Mg | Mg | | Mg | | MgOH | Ca | | CaOH |
| | $H_2O$ | $H_2O$[b] | H | $H_2O$ | H | $H_2O$ | $H_2O$ | H | $H_2O$ |
| *1* | 28.4 ± 3.0 | 36.8 | 71.9[c] | 31.0 | 78.1 | 50.4 | 28.1 | 36.8 | 29.9 |
| *2* | 22.4 ± 1.6 | 30.4 | 49.0[c] | 24.0 | 51.7 | 37.3 | 25.3 | 32.2 | 27.0 |
| *3* | 17.3 ± 2.1 | 26.2 | 33.9[c] | 21.1 | 35.5 | 29.2 | 19.2 | 24.5 | 23.7 |
| *4* | 11.5 ± 2.1 | 19.1 | 31.5[c] (22.0[d]) | 15.0 | 21.3 | 20.6 | 17.5 | 18.2 | 19.6 |
| *5* | --- | 16.5 | 17.9[c] (14.2[d]) | 8.7 | 9.4 | 16.6 | 16.1 | 14.7 | 17.3 |
| *6* | --- | 14.8 | 12.4[e] (6.9[d]) | 24.1 | 17.0 | --- | 17.8 | 15.3 | --- |

[a]Zero K experimental bond dissociation energies from [60] upon collision of $Mg(H_2O)_n^+$, $n$ = 1 – 4, with xenon gas. [b]We calculated MP2/6-31G** energies for $Mg^+$ and $H_2O$. These values and those determined in [50] were used to determine zero-point energy corrected adiabatic water binding energies for these ions.

[c]Dissociation barrier for direct hydrogen loss from the lowest-energy $[Mg(H_2O)_n]^+$ structure determined in [50].

[d]Dissociation barrier for hydrogen loss from $[Mg(H_2O)_n]^+$ allowing structural isomerization barrier prior to hydrogen loss. For selected structures studied, the isomerization barriers were less than the hydrogen loss dissociation barriers [50].

[e]The dissociation barrier for direct hydrogen loss from the lowest energy $[Mg(H_2O)_6]^+$ structure (4+2a) was not reported; the value for a very similar, albeit slightly higher energy, structure (4+2b) is reported instead [50]. Based on the similarities between the two structures, we would expect them to have similar dissociation barriers for direct hydrogen loss.

dissociation energies for loss of water from $Mg(H_2O)_n^+$, $n$ = 1 – 4 [60], are also presented. The activation energy barrier for loss of H is higher than that for the loss of water from $M(H_2O)_n^+$, $n$ = 1 – 5, but loss of a H atom is more energetically favorable for $n$ = 6 and 7. This result is reasonably consistent with the results of BIRD experiments of Bondybey and coworkers [57] where the loss of water was the exclusive loss channel observed for clusters with $n$ < 7, but H atom loss occurred for $n$ = 7 – 21. For smaller clusters, only the loss of water was observed indicating that the activation barrier for loss of a H atom is higher than that for loss of a water molecule for clusters with six or fewer water molecules.

From these calculated dissociation energies, several measures of the internal energy that is deposited into the smaller divalent ion clusters upon EC can be determined. The average value ($E_{avg}$) is determined from the sum of dissociation energies for the loss of H and water weighted by the product ion abundances. The maximum observed energy ($E_{MO}$) is the sum of dissociation energies observed for the smallest product cluster that is observed in these experiments. This cluster is the ion that has lost the maximum number of water molecules from the reduced precursor. An upper limit to the internal energy deposition ($E_{UL}$) can be obtained from the energy required to form the product ion with

one less water molecule relative to the smallest product cluster observed. These energies for $Mg(H_2O)_n^{2+}$, $n = 4 – 6$, are given in Table 5.2.

*Table 5.2. Normalized relative abundances of $MOH(H_2O)_x^+$, M = Mg,Ca, x = 0 – 2, formed by ECD of $M(H_2O)_n^{2+}$, n = 4 – 6, with estimated average ($E_{avg}$), maximum observed ($E_{MO}$), and maximum possible ($E_{UL}$) internal energy depositions (eV) obtained from ligand dissociation energies from A) B3LYP/6-311++G** and B) MP2/6-31G** [50] calculations (Table 5.1).*

| | | | | | Internal Energy Deposition (eV) | | | | | |
|---|---|---|---|---|---|---|---|---|---|---|
| | | | | | A | | | B | | |
| M | n | x = 2 | x = 1 | x = 0 | $E_{avg}$ | $E_{MO}$ | $E_{UL}$ | $E_{avg}$ | $E_{MO}$ | $E_{UL}$ |
| Mg | 4 | --- | 0.84 | 0.16 | 4.16 | 5.99 | --- | 4.46 | 6.40 | --- |
| | 5 | 0.11 | 0.89 | --- | 4.01 | 4.19 | 6.37 | 4.61 | 4.80 | 7.12 |
| | 6 | 0.71 | 0.29 | --- | 4.08 | 5.23 | 7.41 | 4.17 | 5.45 | 7.76 |
| Ca | 4 | --- | 0.24 | 0.76 | 3.98 | 4.29 | --- | --- | --- | --- |
| | 5 | --- | 0.73 | 0.27 | 4.04 | 4.98 | --- | --- | --- | --- |
| | 6 | 0.31 | 0.69 | --- | 4.10 | 4.46 | 5.76 | --- | --- | --- |

An $E_{UL}$ is not reported for $Mg(H_2O)_4^{2+}$ because the smallest product ion that is formed is $MgOH^+$. The dissociation energy of the metal hydroxide is much higher than that for water to the reduced clusters, so $MgOH^+$ could be "hot" and no further dissociation will occur. For $Mg(H_2O)_4^{2+}$, the average values for internal energy deposition of 4.5 eV is not likely to be skewed significantly because the product ion that has a single water molecule attached is the most abundant fragment formed (84%). For $Mg(H_2O)_5^{2+}$ and $Mg(H_2O)_6^{2+}$, no $MgOH^+$ is formed making these ions the best candidates for chemical thermometers of the smaller clusters.

With these caveats, it is interesting to note that there appears to be very little effect of cluster size on the average internal energy deposition resulting from EC. For $Mg(H_2O)_n^{2+}$, this value for $n = 32$ (~4.5 eV) is essentially the same as the values obtained for $n = 4 – 6$ (4.2 – 4.6 eV).

**5.3.6 ECD Energetics for Small $Ca(H_2O)_n^{2+}$ Clusters.** Calculated dissociation energies for the loss of H from $Ca(H_2O)_n^+$ have not been previously reported, but values for H atom and water molecule binding energies to these clusters have [67]. Surprisingly, self-consistent field calculations indicate that loss of a H atom from the clusters is exothermic for $n > 4$ [67]. We evaluated low-energy structures and binding energies for these ions at the B3LYP/6-311++G** level of theory. Lowest-energy structures for both $Ca(H_2O)_n^+$ and $CaOH(H_2O)_n^+$ are shown in Figure 5.6. The structures of $Ca(H_2O)_n^+$, $n = 1 – 3$, and $CaOH(H_2O)_n^+$, $n = 1 – 5$, are the same as those reported by Watanabe *et al.* [67]. For $Ca(H_2O)_4^+$, both levels of theory indicate that $Ca^+$ is solvated by four water molecules in plane with the metal ion, although we found a $D_{2h}$ symmetry to be slightly lower in energy than the $C_s$-symmetry structure with distorted O-Ca-O bond angles identified previously. For $Ca(H_2O)_5^+$ and $Ca(H_2O)_6^+$, our calculations indicate that all water

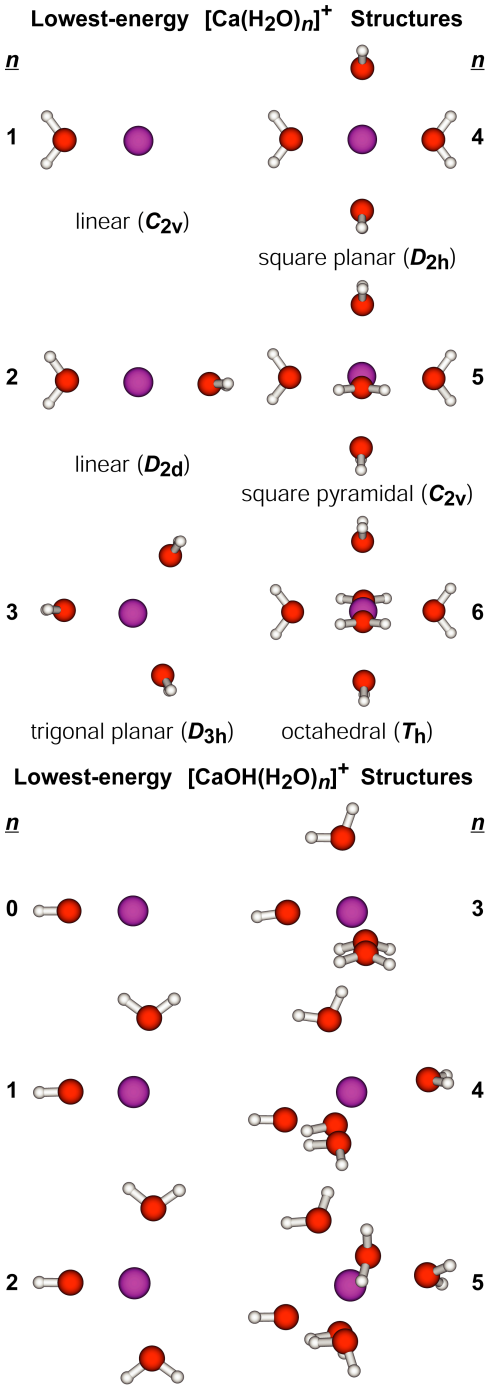


*Figure 5.6. Lowest-energy structures of $Ca(H_2O)_n^+$, n = 1 – 6, and $CaOH(H_2O)_n^+$, n = 1 – 5, at the B3LYP/6-311++G** level of theory. Point groups and inner-shell coordination geometries are included.*

molecules in the lowest-energy structure coordinate directly to the metal ion, whereas the previous calculations indicate that structures with four inner-shell water molecules are lowest in energy. Because Watanabe *et al.* [67] reported relative free energies for structures, it is difficult to directly compare these results.

From these structures, the binding energies of H and a water molecule to $Ca(H_2O)_n^+$ and of a water molecule to $CaOH(H_2O)_n^+$ were determined and these values are given in Table 5.1. These water binding energies are similar to those reported previously, although our values for $Ca(H_2O)_n^+$ are generally slightly higher, whereas our values for $CaOH(H_2O)_n^+$ are generally slightly lower. Our calculated hydrogen atom binding energies for $Ca(H_2O)_n^+$, $n \geq 4$ are substantially higher than those reported by Watanabe *et al*. [67], whereas our values for $n < 4$ are very similar. Our calculations show that the loss of a H atom from $Ca(H_2O)_n^+$, $n = 1 - 6$, is endothermic although these values are lower than the corresponding water molecule binding energies for $n = 5$ and 6.

The values we calculate are binding energies, not activation energies for dissociation. Although these values for the loss of a water molecule should be similar, these values for the loss of a H atom may not. To obtain a rough estimate of the extent to which these values differ, calculations were also done on $Mg(H_2O)_n^+$ and $MgOH(H_2O)_n^+$ at the B3LYP/6-311++G** level of theory. The lowest-energy structures of $Mg(H_2O)_n^+$ are shown in Figure 5.7 and binding energies for H and for water are given in Table 5.1. The lowest-energy structures of $MgOH(H_2O)_n^+$ generally resemble those of $CaOH(H_2O)_n^+$, shown in Figure 5.6, with the notable difference that $MgOH(H_2O)^+$ is linear. It is interesting to compare these results with those from MP2/6-31G** calculations reported previously [50]. Both levels of theory support identical lowest-energy structures for $Mg(H_2O)_n^+$, $n = 1 - 5$, and these structures are consistent with IR photodissociation spectra of $[Mg(H_2O)_n]^+$, $n = 1 - 4$, reported by Inokuch *et al.* [68]. For $n = 6$, the MP2/6-31G** calculations indicate that the lowest-energy structure has a saw horse inner shell, like that in the lowest-energy structure of $[Mg(H_2O)_5]^+$, with two water molecules in the second solvation shell.

The lowest-energy structure of $[Mg(H_2O)_6]^+$ identified with B3LYP/6-311++G** was not considered in the previous report, although another six coordinate structure with reduced symmetry ($C_2$) was calculated to be 5.6 kcal/mol higher in energy than the saw horse structure. The $C_2$-symmetry and saw horse structures (Figure 5.7) are 2.7 and 8.9 kcal/mol higher in energy than the $T_h$-symmetry structure at B3LYP/6-311++G** level of theory. To help determine why these two levels of theory yield such different relative energies, selected structures were also evaluated using the smaller basis set employed in the previous MP2 calculations. At the B3LYP/6-31G** level of theory, the $C_2$-symmetry structure is 0.4 kcal/mol higher in the energy than the saw horse structure, whereas the $C_2$-symmetry structure is 6.2 kcal/mol *lower* in energy than the saw horse structure when the 6-311++G** basis set is used. This indicates that the more complete basis set, which includes diffuse functions and two basis functions per molecular orbital, preferentially stabilizes the $C_2$-symmetry structure by 6.4 kcal/mol. Additionally, the $T_h$-symmetry structure was not stable at the B3LYP/6-31G** level of theory. Upon energy minimization, the water molecules changed orientation relative to the metal ion and more closely resembled those in the $C_2$-symmetry structure. These results indicate that more

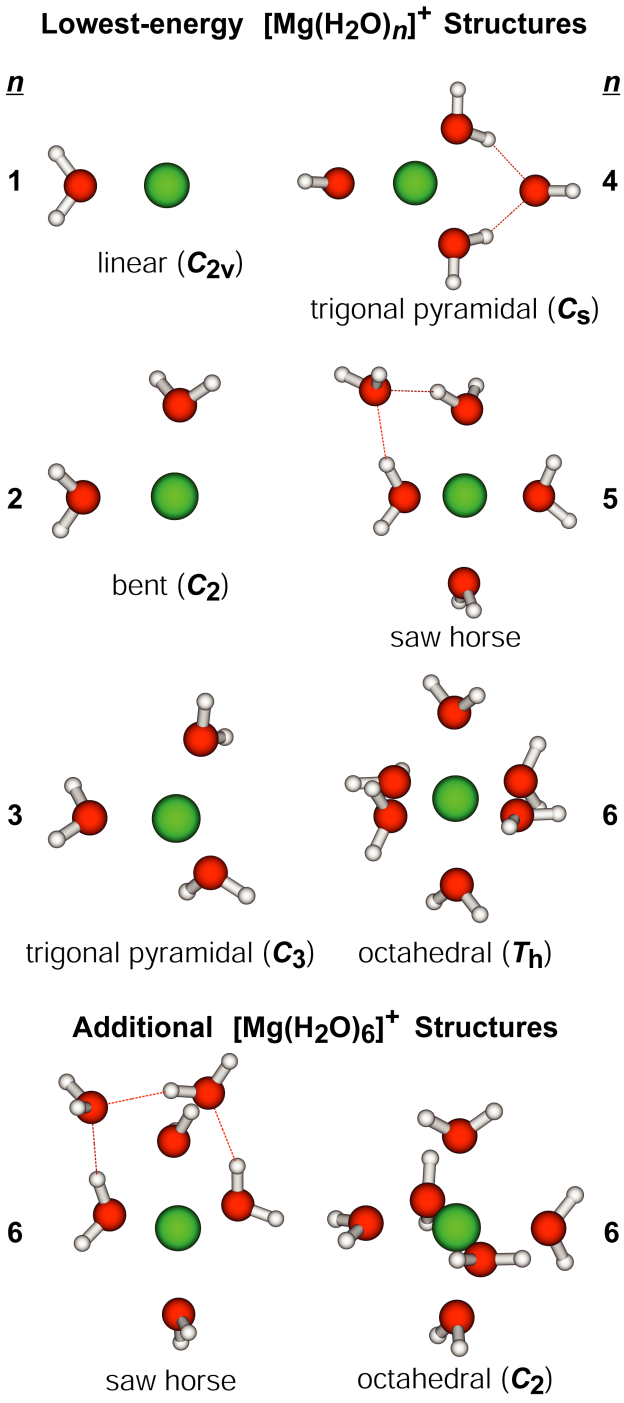


*Figure 5.7. Lowest-energy structure of $Mg(H_2O)_n^+$, n = 1 – 6, at the B3LYP/6-311++G** level of theory. Two higher-energy structures of $Mg(H_2O)_6^+$ are included for comparison. Point groups and inner-shell coordination geometries are included.*

complete basis sets that include diffuse functions are important for determining the relative stabilities of these ions.

Despite the differences in these calculations, the B3LYP/6-311++G** binding energies of water molecules and hydrogen atoms to $Mg(H_2O)_n^+$ are similar to values reported by Siu and Liu [50]. Our values for $Mg(H_2O)_5^+$ are anomalously low, indicating that the lowest-energy structure of this ion may not have been identified. Note that if a lower-energy structure of $[Mg(H_2O)_5]^+$ were identified, this would increase the water and hydrogen binding energies of $[Mg(H_2O)_5]^+$, decrease the water binding energy of $[Mg(H_2O)_6]^+$, but not change the energy difference between the water and hydrogen binding energies of $[Mg(H_2O)_5]^+$. The adiabatic hydrogen binding energies calculated here are within ~10 kcal/mol of the activation barriers for hydrogen loss calculated by Siu and Liu [50] and there is no systematic deviation. This suggests that any reverse activation barrier for H loss is small and that the hydrogen binding energies calculated for $Ca(H_2O)_n^+$ are likely very good approximations for the activation energies for dissociation.

The relative binding energies we calculate for the two competing dissociation processes for $Ca(H_2O)_n^+$ are in excellent agreement with experimental results of Sanekata *et al.* [56]. When $Ca^+$ is reacted with water vapor, the hydrogen loss product $[CaOH(H_2O)_n]^+$ is predominant for $4 < n < 13$ and $[Ca(H_2O)_n]^+$ is primarily observed for the remaining cluster sizes. The switch between mostly $[Ca(H_2O)_n]^+$, $n \leq 4$, to predominantly $[CaOH(H_2O)_4]^+$ , $n > 4$, occurs at the same cluster size expected from the calculated binding energies.

With the caveats stated above, the average ($E_{avg}$), maximum observed ($E_{MO}$), and maximum possible ($E_{UL}$) internal energy deposition from EC by $Ca(H_2O_n)^+$ can be determined. These values as well as values for $Mg(H_2O)_n^+$ determined from binding energies calculated at this same level of theory are given in Table 5.2. The values for $Mg(H_2O)_n^+$ are slightly lower than those calculated using the corresponding values from Siu and Liu [50] although this difference is less than 0.5 eV in most cases. As was noted previously for $Mg(H_2O)_n^+$, there is no significant trend in the average internal energy deposition with cluster size for $Ca(H_2O)_n^+$. It is also interesting to note that the average internal energy deposition for clusters with Mg and Ca are essentially the same.

**5.3.7 Evidence for Nonergodic Dissociation**. Although dissociation via pathway I appears to be ergodic for the larger clusters, three pieces of evidence suggest that pathway II is nonergodic, at least for the smaller clusters. First, the internal energy deposited into the clusters does not depend on cluster size and is significantly less than the calculated ionization energy of the corresponding reduced species for the smaller clusters. Second, the fragmentation pathway for the reduced ions of the smaller clusters is not the same as when these ions are thermally activated. Third, the distribution of product ions observed via pathway II is broader than that for pathway I indicating that the ejected hydrogen atom takes away a broad range of kinetic energies. Each of these pieces of evidence is discussed in more detail below.

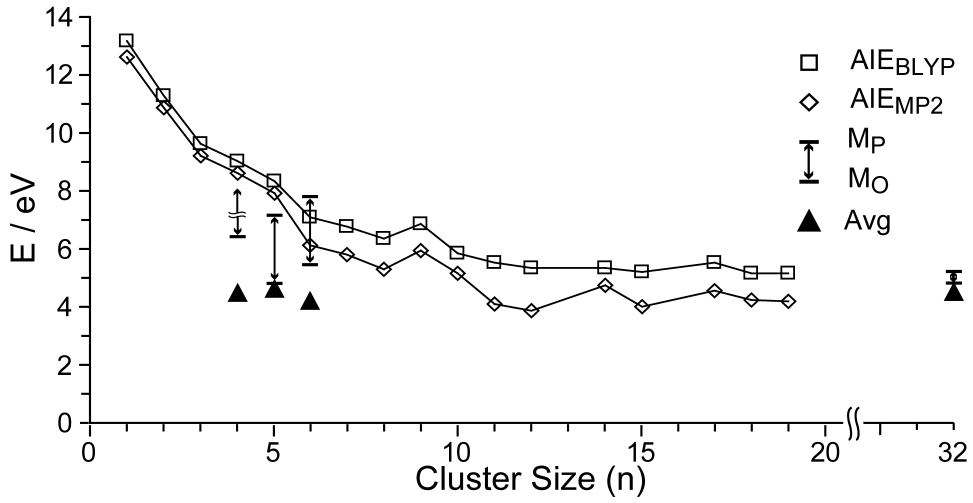


*Figure 5.8. Comparison of the internal energy deposition from electron capture by $Mg(H_2O)_n^{2+}$, n = 4 – 6, 32, with adiabatic ionization energies of $Mg(H_2O)_n^{+}$ from BLYP (□) and MP2 (◊) calculations from [69] as a function of cluster size. The average energy deposition ($E_{avg}$; ▲), as well as the range of energies from the maximum observed ($E_{MO}$) to the maximum possible ($E_{UL}$), are indicated. For $Mg(H_2O)_4^{2+}$, no upper limit ($E_{UL}$) is indicated because $MgOH^+$ is formed. (see text).*

The adiabatic ionization energies of hydrated clusters of $Mg(H_2O)_n^{+}$ have been calculated by Niedner-Schatteburg and coworkers [69]. Results of these calculations as a function of cation size are plotted in Figure 5.8 along with values for the internal energy deposition from EC for selected $Mg(H_2O)_n^{2+}$ clusters measured here. It should be noted that the recombination energy that we obtain with this method in the limit of complete energy randomization should be approximately the same as the adiabatic ionization energy of the reduced cluster. A 50 ms delay after ECD of $Ca(H_2O)_{47}^{2+}$ but before ion detection resulted in no additional water loss. This is sufficient time for solvent reorganization to occur and any energy released from this process results in heating of the cluster. Thus, the recombination energy values we obtain should be comparable to the adiabatic ionization energies calculated by Niedner-Schatteburg and coworkers if all the energy is randomized. The calculated values rapidly decrease with increasing cluster size approaching an asymptotic limit of 3.9 – 4.8 and 5.1 – 5.5 eV for clusters with $n$ = 11 – 19 at the MP2 and BLYP levels of theory, respectively [69]. For $Mg(H_2O)_{32}^{2+}$, we find an average internal energy deposition ($E_{avg}$) of about 4.5 eV and a maximum value of 4.8 – 5.2 eV. These measured values are slightly higher than the recombination energies calculated at the MP2 level, but are comparable to BLYP values for large $n$ [69].

In contrast to the strong trends in calculated ionization energies with cluster size, the experimental data show no significant trend with respect to cluster size. Most striking are the results for $Mg(H_2O)_5^{2+}$ for which our data should provide an accurate measure of the maximum possible internal energy deposition. For this ion, the $E_{avg}$, $E_{MO}$ and $E_{UL}$ deposited upon EC is 4.6, 4.8, and 7.1 eV, respectively (4.0, 4.2, and 6.4 eV using the B3LYP binding energies). If internal energy in excess of 7.1 eV was deposited into this

ion, $MgOH^+$ should have been formed; this ion is not observed. In contrast, the ionization energy of $Mg(H_2O)_5^+$ is calculated to be 7.92 eV [69]. Ionization energies obtained from CC2 and BLYP calculations for this ion are 7.94 and 8.34 eV, respectively [69], indicating that this result does not depend strongly on the type of theory used. The lower value obtained from this experiment suggests that less energy is deposited into $Mg(H_2O)_5^{2+}$ than would be expected if the entire recombination energy that is potentially available in the EC process were converted to internal modes of the ion. Thus, the excess energy could be lost either in the form of kinetic energy of the departing ligands, analogous to what is observed for dissociative electron attachment to water, or by radiative emission. Although water clusters have positive electron affinities [70], the electron affinity of an isolated water molecule is either very small or zero [71]. Electron attachment to an isolated water molecule results in spontaneous dissociation to form predominantly $H^-$ with minor abundances of $O^-$ and $OH^-$ also observed [72]. With increasing incident electron energies, some internal vibration modes can be excited, but the majority of the dissociation energy is carried away by the fragments in the form of kinetic energy [73].

A caveat in this analysis is that the initial effective temperature of the small reduced clusters can be quite high. For $Mg(H_2O)_n^{2+}$, we estimate the effective temperature to be roughly 2900 K and 2000 K for $n$ = 5 and 6, respectively, using calculated values for the electron recombination energy. To obtain a more accurate measure of internal energy deposition from these experimental data, temperature effects on both the bond dissociation energies and on the partitioning of internal energy into translational, vibrational and rotational modes of the products would need to be taken into account. The latter effects could be modeled using phase space theory [74].

The second piece of evidence in support of a nonergodic dissociation process for the smaller clusters is the different dissociation pathways of the precursor ions when thermally activated by BIRD [57] or by collisions with Xe [60] and when formed in an activated state by EC from the doubly charged precursor. As discussed previously, thermal activation of $Mg(H_2O)_n^+$, $n < 7$ results in loss of water molecules (pathway I); loss of H is only observed for $n$ between 7 and 21 (pathway II) [57]. In contrast, $Mg(H_2O)_n^+$, $n$ = 4 – 6, when formed by EC by the corresponding $Mg(H_2O)_n^{2+}$ dissociates exclusively by pathway II. For $n$ = 4, loss of H requires ~32 kcal/mol, whereas loss of a water molecule requires only 19 kcal/mol, and this difference in dissociation energies increases substantially for smaller clusters [50]. Although it is possible that the dissociation entropies are very different for these two processes, both processes are relatively "direct" and should occur through "loose" transition states.

A complicating factor is angular momentum effects that originate from the significantly different masses of $H_2O$ versus H that arise from dissociation via the two different pathways. Information about the energy dependence of the dissociation of small clusters has been reported by Armentrout and coworkers, who used guided ion beam mass spectrometry to measure the sequential binding energies of water to $M(H_2O)_n^+$, M = Na, Mg, and Al, $n$ = 1 – 4 [60]. For $Na(H_2O)_4^+$, loss of one or more water molecules was the only process observed with center of mass collision energies up to 1.5 eV. A second water molecule loss becomes apparent at about 1.2 eV [60]. The third and fourth

sequential binding energies of water to Mg and Na are similar and only loss of water was reported for Mg under similar conditions [60]. These results indicate that $Mg(H_2O)_n^+$, activated by collisions with center of mass collision energies up to 1.5 eV, results in only loss of water despite internal energies that are higher than the binding energy of H to these clusters. Although the maximum energy deposited in these guided ion beam experiments is less than that deposited by EC, it is surprising that this difference alone would result in exclusive dissociation by pathway I for the former and pathway II for the latter if both processes are statistical.

The dissociation of $Mg(H_2O)_n^+$ clusters using visible radiation has also been investigated [56,75,76]. For $n$ = 4 and 5, both dissociation pathways were observed with a branching ratio for pathway II:I of ~4:1 over an energy range of 2.4 – 3.7 and 1.7 – 3.6 eV, respectively [75]. These results, in combination with the aforementioned data, suggest that the loss of H from these clusters occurs directly from electronic excited states formed either by absorption of visible photons by the monovalent cluster or by EC by the corresponding divalent cluster.

A confirmation of the nonergodicity of EC for these clusters would be to measure the collisionally activated dissociation products of the corresponding monovalent clusters at center of mass collision energies comparable to the maximum recombination energy into the divalent cluster upon EC. Different product ions formed from the same precursor ion upon activation to the same internal energy using two different activation methods provides compelling support for nonergodic dissociation.

A third piece of evidence for nonergodic dissociation, although very indirect, is the wider distribution of product ions formed as a result of pathway II versus I (see Figure 5.2c). The internal energy deposition by EC can be quite narrow for the larger cluster ions where often only a single product ion is observed indicating that the width of the energy distribution is less than 10 kcal/mol. This suggests that the kinetic energies of the water molecules that are lost from the cluster via pathway I are low. The broader distribution observed for dissociation via pathway II can be attributed to the H atom carrying away a variable amount of kinetic energy, or possibly a vibrationally excited water molecule accompanying the H atom loss, both of which are consistent with a nonstatistical process.

**5.3.8 Double Resonance Experiments.** To determine the order in which the H atom and water molecules are lost via pathway II, several double resonance experiments were performed. In a double resonance experiment [77, 78], a frequency corresponding to the cyclotron resonance frequency of an ion suspected to be an intermediate in a consecutive dissociation process is continuously irradiated over the course of a dissociation experiment. The disappearance of lower mass ions confirms that the irradiated ion is an intermediary in the formation of those ions. These experiments were done for EC of $Ca(H_2O)_4^{2+}$. Three separate experiments were done where $CaOH^+$ with 1, 2 or 3 water molecules attached were continuously ejected with a single frequency waveform corresponding to the cyclotron frequency of these ions. This waveform had sufficient power to eject an ion from the cell within 100 μs. In each case, the final products were not perturbed by the single frequency waveform, except in the case of ejection of

$CaOH(H_2O)^+$ where this is one of the final products. This suggests that either the ejection of the hydrogen atom occurs after loss of the water molecules, or more likely, that the loss of the hydrogen atom occurs on a timescale that is much shorter than 100 μs.

**5.4 Conclusions.**

The results of the ECD experiments on hydrated divalent magnesium and calcium ions demonstrate that these ions can be used as nanocalorimeters over a wide range of cluster sizes. From the dissociation products, quantitative information about the average and maximum internal energy deposition resulting from EC is obtained. These results clearly show that the range of internal energies deposited is very narrow and that the vast majority of the recombination energy that is available from EC by the divalent precursor ions is converted into internal energy of the reduced precursor for the larger clusters. There is no significant difference in the internal energy deposition as a function of cluster size. The average internal energy deposited into $M(H_2O)_n^{2+}$, M = Mg and Ca, is approximately the same for $n = 4 - 6$ as it is for $n = 32$. In contrast, calculations of the ionization energy of $Mg(H_2O)_n^+$ [69] indicate that the recombination energy should increase rapidly for clusters below $n = 10$. These, and other results, suggest that not all the recombination energy that is available from EC is converted into internal modes of the ion and that the dissociation process for these smaller clusters is nonergodic.

The internal energy deposition values that we obtain from these experiments depend on the dissociation energies of the ligands lost. For the larger clusters, ~10 kcal/mol appears to be a good estimate for the dissociation energy corresponding to the loss of each water molecule from the reduced cluster, although we estimate the uncertainty in this value to be about ± 10%. For the smaller clusters that dissociate by both loss of a H atom and by loss of water molecules, we use calculated values for the dissociation energy because no experimental values are available. The internal energy deposition values that we obtain from these experiments can be revised if more accurate values for the dissociation energies are obtained either through experimental measurements or higher levels of theory. A more detailed investigation into the effects of high internal energy deposition on the translational, vibrational and rotational energies of the products would provide more accurate values for our estimates of the average internal energy deposition from these experimental data. Modeling of the dissociation process, including any partitioning into translational, vibrational and rotational degrees of freedom of the dissociation products with phase space theory, is currently ongoing.

It is interesting to note that the internal energy deposited into Mg and Ca clusters of a given size are essentially indistinguishable. When the electron recombines with the divalent cluster, it is likely that the resulting reduced cluster forms an ion pair consisting of a divalent metal cation with a solvated electron, at least for the larger cluster sizes. Such electrides, which are ionic salts with the electron as an anion [79, 80], have been investigated for many years and a single-crystal electride that is both thermally stable and unreactive has been recently reported [81]. A solvated electron $Mg^{2+}$ pair has also been proposed for gas-phase $Mg(H_2O)_n^+$ for clusters with more than 17 water molecules to explain the change in dissociation reactivity that occurs for clusters of this size [57].

It is also interesting to postulate why dissociation of the small clusters is nonergodic whereas the dissociation of the larger clusters is statistical. Upon electron capture, the large clusters only lose water molecules whereas the smaller clusters lose a H atom and water molecules. The nonstatistical behavior may be due to the processes for loss of a H atom or it may depend on physical properties related to cluster size. Attachment of an electron to the cluster may result in spontaneous ejection of a "hot" H atom analogous to the dissociative electron attachment to an isolated water molecule. The efficiency with which the energy from EC is converted into vibrational modes may be attributable to other physical properties that change as a function of cluster size. Larger clusters have more vibrational modes which may make the transfer of the recombination energy into internal modes more efficient. The energy differences between electronic levels also depend on cluster size. For the octahedral form of $Mg(H_2O)_6^+$, the HOMO-LUMO gap is 0.8 eV and there are 10 unoccupied molecular orbitals with energies that are within 2.5 eV of the HOMO. In contrast, the HOMO-LUMO gap is 2.9 eV for $Mg(H_2O)_4^+$ and there are only 7 unoccupied molecular orbitals that are within 5.0 eV of the HOMO. Thus, the energy differences between electronic excited states decreases with increasing cluster size and this may play a role in the efficiency of energy conversion between excited states and vibrational modes of the cluster.

Finally, it is important to note similarities and differences between these ECD experiments and those done with peptides and proteins. A key distinction between these experiments is that the dissociation processes for the hydrated divalent metal ions are clearly different from those of peptides and proteins. Loss of water molecules resulting from ECD of proteins has been observed [31], but this is a minor process. Product ions corresponding to the loss of a H atom can be the dominant process observed for ECID of diprotonated dipeptides [32], but loss of a H atom is less significant for larger peptides. In larger peptides and proteins, it has been postulated that a hot hydrogen atom may play a role in the formation of product ions [7]. The internal energy deposited into these cluster ions and peptides and protein ions from EC is similar and the process whereby this energy is converted into internal modes may be similar as well. Future experiments on EC of hydrated peptide and protein ions may provide important new information on how ECD occurs in these ions.

### 5.5 Acknowledgements.

The authors thank Professors Peter B. Armentrout, Marcin Majda, William H. Miller, Daniel M. Neumark, Kenneth N. Raymond and Richard J. Saykally for helpful discussions and NSF (CHE-041593) and NIH (R01 GM064712-05) for generous financial support.

**5.6 References.**


[1] Sacksteder, C. A.; Qian, W. J.; Knyushko, T. V.; Wang, H. X.; Chin, M. H.; Lacan, G.; Melega, W. P.; Camp, D. G.; Smith, R. D.; Smith, D. J.; Squier, T. C.; Bigelow, D. J. *Biochemistry* **2006**, *45*, 8009-8022.

[2] Valentine, S. J.; Kulchania, M.; Barnes, C. A. S.; Clemmer, D. E. *Int. J. Mass Spectrom.* **2001**, *212*, 97-109.

[3] Valentine, S. J.; Liu, X. Y.; Plasencia, M. D.; Hilderbrand, A. E.; Kurulugama, R. T.; Koeniger, S. L.; Clemmer, D. E. *Expert Rev. Proteomics* **2005**, *2*, 553-565.

[4] Taraszka, J. A.; Kurulugama, R.; Sowell, R. A.; Valentine, S. J.; Koeniger, S. L.; Arnold, R. J.; Miller, D. F.; Kaufman, T. C.; Clemmer, D. E. *J. Proteome Res*. **2005**, *4*, 1223-1237.

[5] Han, X. M.; Jin, M.; Breuker, K. and McLafferty, F. W. *Science* **2006**, *314*, 109-112.

[6] Ge, Y.; Lawhorn, B. G.; ElNaggar, M.; Strauss, E.; Park, J. H.; Begley, T. P. and McLafferty, F. W. *J. Am. Chem. Soc.* **2002**, *124*, 672-678.

[7] Zubarev, R. A.; Kelleher, N. L. and McLafferty, F. W. *J. Am. Chem. Soc.* **1998**, *120*, 3265-3266.

[8] Zubarev, R. A.; Horn, D. M.; Fridriksson, E. K.; Kelleher, N. L.; Kruger, N. A.; Lewis, M. A.; Carpenter, B. K.; McLafferty, F. W. *Anal. Chem.* **2000**, *72*, 563-573.

[9] Breuker, K.; Oh, H. B.; Horn, D. M.; Cerda, B. A.; McLafferty, F. W. *J. Am. Chem. Soc.* **2002**, *124*, 6407-6420.

[10] Coon, J. J.; Shabanowitz, J.; Hunt, D. F.; Syka, J. E. P. *J. Am. Soc. Mass Spectrom.* **2005**, *16*, 880-882.

[11] Syka, J. E. P.; Coon, J. J.; Schroeder, M. J.; Shabanowitz, J.; Hunt, D. F. *Proc. Natl. Acad. Sci. U.S.A.* **2004**, *101*, 9528-9533.

[12] Hvelplund, P.; Liu, B.; Nielsen, S. B.; Tomita, S. *Int. J. Mass Spectrom.* **2003**, *225*, 83-87.

[13] Hvelplund, P.; Liu, B.; Nielsen, S. B.; Tomita, S.; Cederquist, H.; Jensen, J.; Schmidt, H. T.; Zettergren, H. *Eur. Phys. J. D* **2003**, *22*, 75-79.

[14] Zubarev, R. A. *Mass Spectrom. Rev.* **2003**, *22*, 57-77.

[15] Zubarev, R. A.; Haselmann, K. F.; Budnik, B.; Kjeldsen, F.; Jensen, F. *Eur. J. Mass Spectrom.* **2002**, *8*, 337-349.

[16] Zubarev, R. A. *Curr. Opin. Biotechnol*. **2004**, *15*, 12-16.

[17] Cooper, H. J.; Hakansson, K.; Marshall, A. G. *Mass Spectrom. Rev.* **2005**, *24*, 201-222.

[18] Breuker, K.; Oh, H. B.; Lin, C.; Carpenter, B. K.; McLafferty, F. W. *Proc. Natl. Acad. Sci. U.S.A.* **2004**, *101*, 14011-14016.

[19] Chen, X. H.; Tureček, F. *J. Am. Chem. Soc.* **2006**, *128*, 12520-12530.

[20] Syrstad, E. A.; Tureček, F. *J. Phys. Chem. A* **2001**, *105*, 11144-11155.

[21] Syrstad, E. A.; Stephens, D. D.; Tureček, F. *J. Phys. Chem. A* **2003**, *107*, 115-126.

[22] Syrstad, E. A.; Tureček, F. *J. Am. Soc. Mass Spectrom.* **2005**, *16*, 208-224.

[23] Tureček, F.; Syrstad, E. A.; Seymour, J. L.; Chen, X. H.; Yao, C. X. *J. Mass Spectrom.* **2003**, *38*, 1093-1104.

[24] Tureček, F. *J. Am. Chem. Soc.* **2003**, *125*, 5954-5963.

[25] Tureček, F.; Syrstad, E. A. *J. Am. Chem. Soc.* **2003**, *125*, 3353-3369.

[26] Kruger, N. A.; Zubarev, R. A.; Carpenter, B. K.; Kelleher, N. L.; Horn, D. M.; McLafferty, F. W. *Int. J. Mass Spectrom.* **1999**, *183*, 1-5.

[27] Sobczyk, M.; Simons, J. *Int. J. Mass Spectrom.* **2006**, *253*, 274-280.

[28] Sobczyk, M.; Simons, J. *J. Phys. Chem. B* **2006**, *110*, 7519-7527.

[29] Anusiewicz, I.; Berdys-Kochanska, J.; Skurski, P.; Simons, J. *J. Phys. Chem. A* **2006**, *110*, 1261-1266.

[30] Sawicka, A.; Skurski, P.; Hudgins, R. R.; Simons, J. *J. Phys. Chem. B* **2003**, *107*, 13505-13511.

[31] Robinson, E. W.; Leib, R. D.; Williams, E. R. *J. Am. Soc. Mass Spectrom.* **2006**, *17*, 1469-1479.

[32] Chakraborty, T.; Holm, A. I. S.; Hvelplund, P.; Nielsen, S. B.; Poully, J.-C.; Worm, E. S.; Williams, E. R. *J. Am. Soc. Mass Spectrom.* **2006**, *17*, 1675-1680.

[33] Liu, H.; Hakansson, K. *Anal. Chem.* **2006**, *78*, 7570-7576.

[34] Liu, H.; Hakansson, K. *J. Am. Soc. Mass Spectrom.* **2006**, *17*, 1731-1741.

[35] Leymarie, N.; Costello, C. E.; O'Connor, P. B. *J. Am. Chem. Soc.* **2003**, *125*, 8949-8958.

[36] Lin, C.; O'Connor, P. B.; Cournoyer, J. J. *J. Am. Soc. Mass Spectrom.* **2006**, *17*, 1605-1615.

[37] O'Connor, P. B.; Lin, C.; Cournoyer, J. J.; Pittman, J. L.; Belyayev, M.; Budnik, B. A. *J. Am. Soc. Mass Spectrom.* **2006**, *17*, 576-585.

[38] Iavarone, A. T.; Paech, K.; Williams, E. R. *Anal. Chem.* **2004**, *76*, 2231-2238.

[39] Griffiths, I. W.; Mukhtar, E. S.; March, R. E.; Harris, F. M.; Beynon, J. H. *Int. J. Mass Spectrom. Ion Phys.* **1981**, *39*, 125-132.

[40] Baer, T.; Dutuit, O.; Mestdagh, H.; Rolando, C. *J. Phys. Chem.* **1988**, *92*, 5674-5679.

[41] Chen, J. H.; Hays, J. D.; Dunbar, R. C. *J. Phys. Chem.* **1984**, *88*, 4759-4764.

[42] Kenttämaa, H. I.; Cooks, R. G. *Int. J. Mass Spectrom. Ion Processes* **1985**, *64*, 79-83.

[43] Dekrey, M. J.; Kenttämaa, H. I.; Wysocki, V. H.; Cooks, R. G. *Org. Mass Spectrom.* **1986**, *21*, 193-195.

[44] Beranova, S.; Wesdemiotis, C. *J. Am. Soc. Mass Spectrom.* **1994**, *5*, 1093-1101.

[45] Nguyen, V. Q.; Tureček, F. *J. Mass Spectrom.* **1996**, *31*, 1173-1184.

[46] Schnier, P. D.; Jurchen, J. C.; Williams, E. R. *J. Phys. Chem. B* **1999**, *103*, 737-745.

[47] Price, W. D.; Schnier, P. D.; Jockusch, R. A.; Strittmatter, E. F.; Williams, E. R. *J. Am. Chem. Soc.* **1996**, *118*, 10640-10644.

[48] Wong, R. L.; Paech, K.; Williams, E. R. *Int. J. Mass Spectrom.* **2004**, *232*, 59-66.

[49] Bush, M. F.; Saykally, R. J.; Williams, E. R. *Int. J. Mass Spectrom.* **2006**, *253*, 256-262.

[50] Siu, C. K.; Liu, Z. F. *Chem. Eur. J.* **2002**, *8*, 3177-3186.

[51] Frisch, M. J.; Trucks, G. W.; Schlegel, H. B.; Scuseria, G. E.; Robb, M. A.; Cheeseman, J. R.; Montgomery, J., J. A.; Vreven, T.; Kudin, K. N.; Burant, J. C.; Millam, J. M.; Iyengar, S. S.; Tomasi, J.; Barone, V.; Mennucci, B.; Cossi, M.; Scalmani, G.; Rega, N.; Petersson, G. A.; Nakatsuji, H.; Hada, M.; Ehara, M.; Toyota, K.; Fukuda, R.; Hasegawa, J.; Ishida, M.; Nakajima, T.; Honda, Y.; Kitao, O.; Nakai, H.; Klene, M.; Li, X.; Knox, J. E.; Hratchian, H. P.; Cross, J. B.; Bakken, V.; Adamo, C.; Jaramillo, J.; Gomperts, R.; Stratmann, R. E.; Yazyev, O.; Austin, A. J.; Cammi, R.; Pomelli, C.; Ochterski, J. W.; Ayala, P. Y.; Morokuma, K.; Voth, G. A.; Salvador, P.; Dannenberg, J. J.; Zakrzewski, V. G.; Dapprich, S.; Daniels, A. D.; Strain, M. C.; Farkas, O.; Malick, D. K.; Rabuck, A. D.; Raghavachari, K.; Foresman, J. B.; Ortiz, J. V.; Cui, Q.; Baboul, A. G.; Clifford, S.; Cioslowski, J.; Stefanov, B. B.; Liu, G.; Liashenko, A.; Piskorz, P.; Komaromi, I.; Martin, R. L.; Fox, D. J.; Keith, T.; Al-Laham, M. A.; Peng, C. Y.; Nanayakkara, A.; Challacombe, M.; Gill, P. M. W.; Johnson, B.; Chen, W.; Wong, M. W.; Gonzalez, C.; Pople, J. A. *Gaussian 03, Revision C.02*, Gaussian, Inc., **2004**.

[52] Cody, R. B.; Freiser, B. S. *Anal. Chem.* **1979**, *51*, 547-551.

[53] Polfer, N. C.; Haselmann, K. F.; Zubarev, R. A.; Langridge-Smith, P. R. R. m ion *Rapid Commun. Mass Spectrom*. **2002**, *16*, 936-943.

[54] Kjeldsen, F.; Haselmann, K. F.; Budnik, B. A.; Jensen, F.; Zubarev, R. A. *Chem. Phys. Lett*. **2002**, *356*, 201-206.

[55] Harms, A. C.; Khanna, S. N.; Chen, A. B.; Castleman Jr., A. W. *J. Chem. Phys*. **1994**, *100*, 3540-3544.

[56] Sanekata, M.; Misaizu, F.; Fuke, K.; Iwata, S.; Hashimoto, K. *J. Am. Chem. Soc.* **1995**, *117*, 747-754.

[57] Berg, C.; Beyer, M.; Achatz, U.; Joos, S.; Niedner-Schatteburg, G.; Bondybey, V. E. *Chem. Phys*. **1998**, *239*, 379-392.

[58] Dzidic, I.; Kebarle, P. *J. Phys. Chem.* **1970**, *74*, 1466-1474.

[59] Shi, Z.; Ford, J. V.; Wei, S.; Castleman Jr., A. W. *J. Chem. Phys*. **1993**, *99*, 8009-8015.

[60] Dalleska, N. F.; Tjelta, B. L.; Armentrout, P. B. *J. Phys. Chem.* **1994**, *98*, 4191-4195.

[61] McLafferty, F. W.; Wachs, T.; Lifshitz, C.; Innorta, G.; Irving, P. *J. Am. Chem. Soc.* **1970**, *92*, 6867-6880.

[62] Leib, R. D.; Donald, W. A.; Bush, M. F.; O'Brien, J. T.; Williams, E. R. *J. Am. Chem. Soc.* **2007**, *129*, 4894-4895.

[63] Kebarle, P.; Searles, S. K.; Zolla, A.; Scarborough, J.; Arshadi, M. *J. Mass Spectrom.* **1997**, *32*, 915-921.

[64] Marsh, K. N. "Recommended reference materials for the realization of physiochemical properties."; Blackwell: Oxford, **1987**.

[65] Feistel, R.; Wagner, W. *J. Phys. Chem. Ref. Data* **2006**, *35*, 1021-1047.

[66] Klots, C. E. *J. Chem. Phys.* **1985**, *83*, 5854-5860.

[67] Watanabe, H.; Iwata, S.; Hashimoto, K.; Misaizu, F.; Fuke, K. *J. Am. Chem. Soc.* **1995**, *117*, 755-763.

[68] Inokuchi, Y.; Ohshimo, K.; Misaizu, F.; Nishi, N. *J. Phys. Chem. A* **2004**, *108*, 5034-5040.

[69] Reinhard, B. M.; Niedner-Schatteburg, G. *J. Chem. Phys*. **2003**, *118*, 3571-3582.

[70] Coe, J. V. *Int. Rev. Phys. Chem*. **2001**, *20*, 33-58.

[71] Märk, T. D. *Int. J. Mass Spectrom. Ion Processes* **1991**, *107*, 143-163.

[72] Fedor, J.; Cicman, P.; Coupier, B.; Feil, S.; Winkler, M.; Gluch, K.; Husarik, J.; Jaksch, D.; Farizon, B.; Mason, N. J.; Scheier, P.; Märk, T. D. *J. Phys. B: At. Mol. Phys*. **2006**, *39*, 3935-3944.

[73] Belic, D. S.; Landau, M.; Hall, R. I. *J. Phys. B: At. Mol. Phys*. **1981**, *14*, 175-190.

[74] Baer, T.; Hase, W. L. "Unimolecular reaction dynamics: Theory and experiments."; Oxford University Press: New York, **1996**.

[75] Misaizu, F.; Sanekata, M.; Fuke, K.; Iwata, S. *J. Chem. Phys.* **1994**, *100*, 1161-1170.

[76] Misaizu, F.; Sanekata, M.; Tsukamoto, K.; Fuke, K.; Iwata, S. *J. Phys. Chem.* **1992**, *96*, 8259-8264.

[77] Anders, L. R.; Beauchamp, J. L.; Dunbar, R. C.; Baldeschwieler, J. D. *J. Chem. Phys*. **1966**, *45*, 1062-1063.

[78] Jurchen, J. C.; Garcia, D. E.; Williams, E. R. *J. Am. Soc. Mass Spectrom.* **2003**, *14*, 1373-1386.

[79] Dye, J. L. *Science* **2003**, *301*, 607-608.

[80] Dye, J. L. *Science* **1990**, *247*, 663-668.

[81] Matsuishi, S.; Toda, Y.; Miyakawa, M.; Hayashi, K.; Kamiya, T.; Hirano, M.; Tanaka, I.; Hosono, H. *Science* **2003**, *301*, 626-629.

## Chapter 6

# Direct Quantitation of Peptide Mixtures without Standards using Clusters Formed by Electrospray Ionization Mass Spectrometry



## 6.0 Abstract.

In electrospray ionization mass spectrometry, ion abundances depend on a number of different factors, including analyte surface activity, competition between analytes for charge, solution concentration, as well as instrumental factors, including mass-dependent ion transmission and detection. Here, a novel method for obtaining quantitative information about solution-phase concentrations of peptide mixtures is described and demonstrated for five different peptide mixtures with relative concentrations ranging from 0.05 to 50%. In this method, the abundances of large clusters containing anywhere from zero to thirteen impurity molecules are measured and directly related to the relative solution-phase concentration of the peptides in solution. For clusters containing ~15 or more peptides, the composition of the clusters approaches the statistical value indicating that these clusters are formed nonspecifically and that any differences in ion detection or ionization efficiency is negligible at these large cluster sizes. This method is accurate to within ~20% or better, even when the relative ion intensities of the protonated monomers can differ by over an order of magnitude compared to their solution-phase concentrations. Although less accurate than other quantitation methods that employ internal standards, this method does have the key advantages of speed, simplicity, and the ability to quantitate components in solution even when the identity of the components are unknown.

## 6.1 Introduction.

The ability to accurately and rapidly measure concentrations of individual components in complex mixtures is a key challenge in chemistry. Preparation of small molecules of pharmaceutical interest can result in low molar fraction impurities that stem from unreacted starting materials or intermediates, products from competing side reactions and degraded or modified catalysts [1-3]. Because these diverse minor components may have unintended metabolic effects, impurities must be quantified and if present in sufficient molar excess, removed or structurally identified and shown to be biologically inert [1-3]. In proteomics, protein modifications can be indicative of biological activity as well as provide biomarkers for disease [4-8]. Quantitation of these discrete modifications is highly desirable to determine relative expression levels in living systems. Mass spectrometry (MS) is commonly employed to identify the components of pharmacological or biological mixtures [9-14], and is used to identify thousands of peptides originating from protein digests from whole cells, biological fluids, tissues and organisms [15-29].

Quantitation of nonvolatile or thermally labile molecules using MS can be complicated by differences in ionization efficiency and matrix effects, in which analyte molecules compete for charge with other components in the mixture [30-34], as well as effects of instrumental parameters, including *m*/*z* dependent transmission and detection efficiency [35-38]. In matrix assisted laser desorption/ionization (MALDI), matrix effects can occur as a result of cocrystallization of analytes or in the desorption/ionization process [31,39]. In electrospray ionization (ESI), ion abundances and charge-state distributions can depend on many factors, including the relative surface activities, basicities, surface tension, concentrations and conformations of the analytes and types of solvent [30,40-52].

Relative ion abundances and charge states in ESI mass spectra have been related to the relative surface activites or hydrophobicities of the molecules or ions [30,40-43]. The abundances of anions formed from a solution containing equimolar concentrations of anionic salts trend with the Hofmeister series, with greater dehydration free energies and lower surface affinity correlating to lower relative ion intensity in the gas phase [40]. The ESI intensity of tetraalkyl ammonium halides increases by over an order of magnitude when the hydrophobic chain length increases from methyl to butyl, an effect attributed to the relative solvophobicity of these ions [30]. Differences in charge-state distributions observed for similar size peptides has also been attributed to differences in analyte solvophobicity [30]. Enke and coworkers investigated the effect of peptide surface activity on ion formation by ESI and found that ion intensities of protonated tripeptides decreased with increasing sidechain polarity, indicating that differential partitioning between ions at surfaces vs. in the bulk can affect the observed ion intensity [41]. Addition of basic solvents to peptide and protein containing solutions can result in lower charge state distributions and reduced signal for the peptide or protein ions [44]. The charge state distribution of protein ions formed from denaturing solutions occur at lower *m*/*z* [48-50], which can result in ion abundances that depend on solution composition or pH due to *m/z* dependent detection biases. For low pH solutions in which

proteins are denatured, Pan and McLuckey [53] showed that signal responses of different proteins were better correlated to their solution-phase concentration when normalized for the average charge state of the protein.

Because ion intensities depend on both ionization and instrumental effects, internal standards are typically used to obtain quantitative information from ESI-MS [54-64]. Accurate quantitative information can be obtained by using isotopically labeled analyte molecules as an internal standard. Various methods of introducing isotopic labels have been successfully demonstrated, including chemical modification methods [10,54-58,65], metabolic incorporation [59-61], and "spiking" the sample with a synthetically labeled analyte [63,64]. With isotope coded affinity tags (ICAT) [10,54,55], chemically modified peptides can be selectively retained during an affinity-based chromatographic separation. The abundances of ICAT peptides can be then compared with peptides from other cells that have been modified using a linker with a different isotopic composition which makes possible accurate quantitation of protein expression between the different cell lines. Another common approach to quantitative measurement of relative cell line proteomic expression is stable isotope labeling with amino acids in cell culture (SILAC) [60,61]. In SILAC, a cell line grown in media containing an isotopically enriched amino acid is compared against a line grown in unenriched media making possible direct comparison of expressed proteins. These approaches can yield quantitation accurate to on average better than ~5-10% [61,66]. Mass defect tags, in which chemical modifications incorporating elements, such as Br, can be used to shift the mass of tagged peptides slightly off the exact masses of similar size peptides. This makes possible accurate quantitation even in complex mixtures [57,65]. More generally, preparation of isotopically labeled species for each analyte can be quite time consuming, particularly when an unknown analyte must first be identified. Analog molecules that have similar ionization efficiencies and mass to the analyte can also be used to obtain quantitative information. Lebrilla and coworkers demonstrated that by using a deuterated heptameric maltosaccharide as an internal standard, the concentrations of heptameric fructosaccharides could be obtained to within 1% and other fructo-oligomers in the mixture within 3% using MALDI-MS [67]. Methods to quantitate enantiomeric mixtures using tandem MS or ion mobility MS have also been developed [68-75].

Here, a novel method to obtain quantitative information about relative peptide concentrations in solutions without using standards is demonstrated. In this method, the abundances of *nonspecific*, heterogeneous clusters of molecules are used to obtain accurate solution concentrations. This method is demonstrated on five different peptide mixtures with relative molar fractions ranging from 0.05% to 50%. This method does not require standards, is very fast, reasonably accurate, and can be used to obtain quantitative information about components whose identity is not known.

## 6.2 Experimental Methods.

**6.2.1 Sample Preparation.** Leucine enkephalin, methionine enkephalin, bradykinin, bradykinin fragment 1-8, and bradykinin fragment 2-9 were purchased from Sigma Aldrich Co. (St. Louis, MO); $[ala]_3$-leucine enkephalin and $[lys_6]$-leucine enkephalin

were purchased from VWR (West Chester, PA). Standard 5.00 mM aqueous stock solutions were prepared by weighing the peptides on a microbalance (± 0.01 mg) and then correcting these weights for peptide content using information from the manufacturers' certificate of analysis. All other solutions were prepared using these stock solutions.

**6.2.2 Mass Spectrometry.** Experiments were performed on a 9.4 T FT/ICR mass spectrometer with an external ESI source that is described elsewhere [76,77] Ions are generated by nanoelectrospray (nanoESI) using borosilicate capillaries pulled to a tip with a ~2 μm inner diameter (model P-87 capillary puller, Sutter Instruments, Novato, CA). A small volume of analyte solution, typically ~2-10 μL, is loaded into the capillary, and a platinum wire is inserted into the solution and grounded. The borosilicate capillary is positioned ~2 mm from the source inlet to which a potential of -800 to -1200 V is applied. Ions are accumulated in a hexapole trap for 1.1 s and are subsequently introduced into the ion cell. A pulse of nitrogen gas is introduced through a piezoelectric leak valve to a pressure of ~1 x $10^{-6}$ Torr to assist trapping and thermalization of the ions. Ions from two hexapole injections are accumulated in the cell prior to exciting and detecting the ions. The signal intensity of the peptide clusters is optimized by selectively tuning the DC potential for the external hexapole in a range from 2.8 to 4.0 V [78]. Three mass spectra composed of 50 coadded scans (Predator datastation, NHMFL, Tallahassee, Florida) were acquired at three different DC offset values for each analyte to minimize any effects of transmission efficiency. For experiments where the solution concentration was varied, each mass spectrum was acquired using a new borosilicate capillary to assess effects of tip-to-tip variations and to avoid any sample contamination.

**6.3 Results and Discussion.**

**6.3.1 ESI Mass Spectra.** Solutions (48:48:4 water:methanol:acetic acid) containing leucine enkephalin (LE) and $[ala]_3$-leucine enkephalin ($A_3LE$) were prepared to 2.4 mM total peptide concentration with the fraction of $A_3LE$ ranging from 0.05% to 50%. A nanoESI mass spectrum of one of these solutions in which the molar fraction of $A_3LE$ is 1.0%, obtained under typical experimental conditions, is shown in Figure 6.1a. The ratio of protonated $A_3LE$ to LE in this spectrum is 3.8%, a value much higher than the relative ratio of these peptides in solution. The normalized abundances of the protonated molecular ions as a function of molar fraction of $A_3LE$ in these 2.4 mM solutions are shown in Figure 6.2a. At molar fractions below 1%, the normalized abundance of $(A_3LE + H)^+$ relative to that of $(LE + H)^+$ is about 4 times higher than the relative concentration of these peptides in solution. The deviation between the relative ion abundance and relative solution concentration increases with increasing fractional $A_3LE$ concentration. At molar fractions of 20% and 50%, the $[A_3LE + H]^+/[LE + H]^+$ ratio is 1.7 and 7.3, respectively, corresponding to an approximately eight fold higher relative ion abundance of $(A_3LE + H)^+$ than its relative concentration in solution.

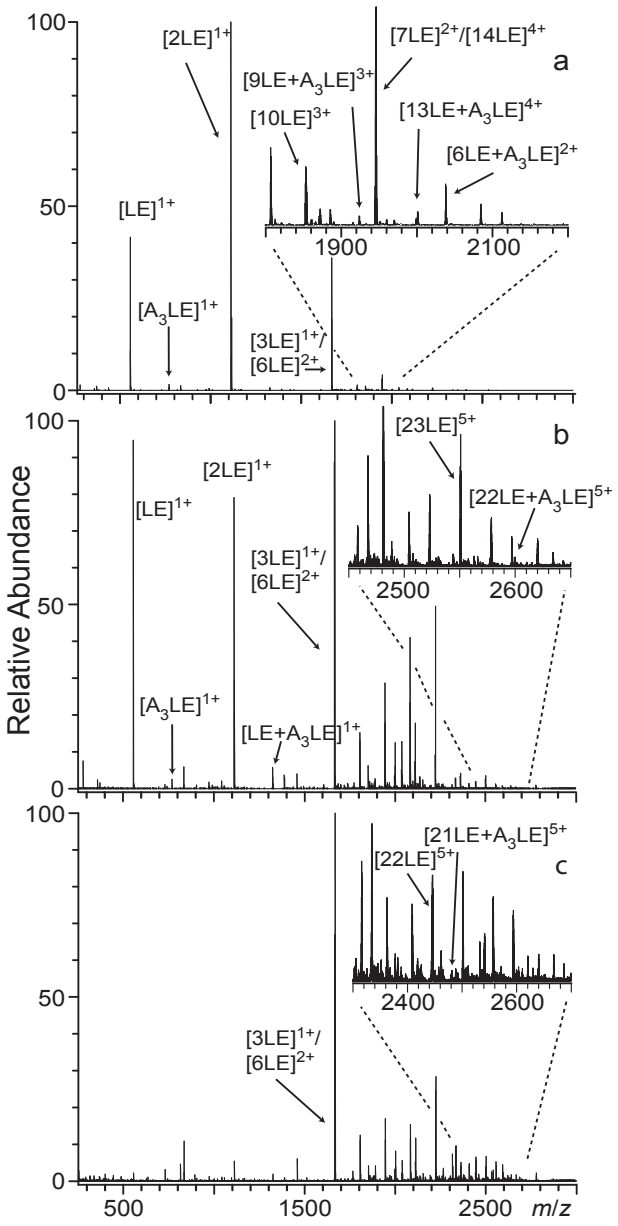


*Figure 6.1. ESI mass spectra of a solution containing 1% molar fraction of [ala]$_3$-leucine enkephalin in leucine enkephalin (2.4 mM total peptide concentration) measured at external accumulation hexapole offset potentials of: a) 2.8 b) 3.6 and c) 4.0 V. Regions of the spectra showing molecular clusters are inset.*

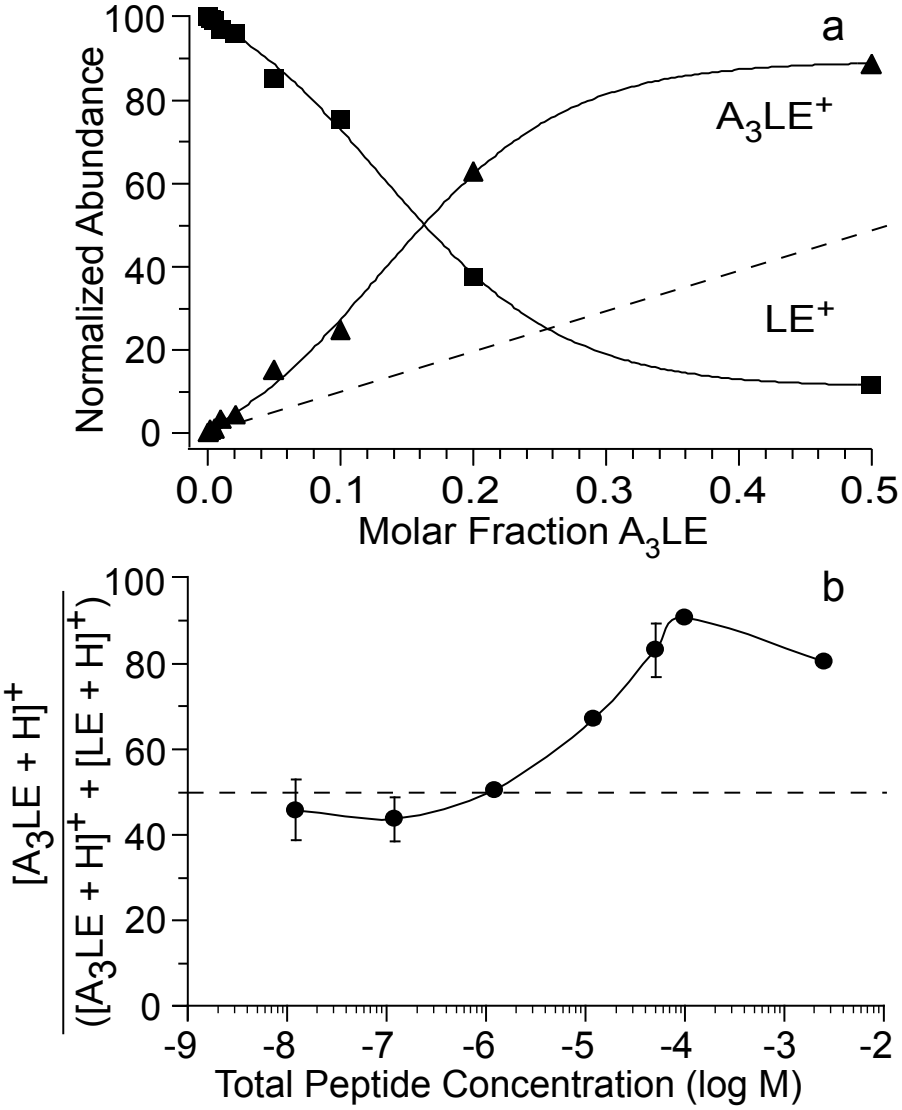


*Figure 6.2. a) Normalized abundances of protonated $A_3LE$ (triangles) and LE (squares) from ESI mass spectra as a function of $A_3LE$ molar fraction for solutions with 2.4 mM total peptide concentration. b) Molar fractions of $A_3LE$ calculated from the abundances of the protonated molecular ions from an equimolar solution with LE as a function of total peptide concentration. Error bars correspond to the standard deviation of three replicate mass spectra obtained from three different nanoelectrospray tips at each solution concentration. Dashed lines represent the ideal trend based on solution concentration.*

There are many factors that contribute to ion abundances in ESI mass spectra, including instrument parameters, detection, transmission and ionization efficiencies and ion suppression in mixtures [30-38,40-50]. The greater propensity to form protonated $A_3LE$ compared to LE in these mixtures may be due to the greater surface activity or hydrophobicity of the former. Alanine is hydrophobic and addition of $A_3$ to LE should increase the surface activity of $A_3LE$ relative to that of LE. Preferential formation of ions that have high surface activities have been reported previously [30,40,41]. At high solution concentration (few hundred μM), ion formation is limited by the excess charge on the ESI droplet surface [51], which appears to enhance this effect presumably because less charge is available for the less surface-active species.

In addition to the protonated molecular ions, abundant ions corresponding to the singly protonated dimer and trimer of LE as well as multiply charged higher order protonated clusters are clearly observed (Figure 6.1a). Heterogeneous clusters, such as the dimer $(A_3LE + LE + H)^+$, are also formed. Cluster formation is common in ESI of concentrated solutions, e.g., ≥100 μM [78-80]. The abundances of the clusters in the ESI spectra can be enhanced by changing several different instrument parameters, including the DC offset potential of the hexapole. This effect is illustrated in Figure 6.1a-c in which the DC offset potential was 2.8, 3.4 and 4.0 V, respectively, with all other conditions the same. Higher order clusters, up to $(LE_{29} + 5H)^{5+}$ and its heterogeneous analogs, are observed. The abundances of lower *m*/*z* ions are significantly attenuated at the higher hexapole DC offset potentials. In addition, the ratio of protonated $A_3LE$ to LE is dramatically decreased. This ratio is 3.8%, 2.7% and <0.3% at these respective potentials. Other instrumental parameters can also influence this ratio as well. These results illustrate that the relative abundance of these protonated molecular ions are an unreliable indicator of their relative abundances in solution.

**6.3.2 Effects of Solution Concentration.** To investigate the effects of solution concentration on the relative ratio of protonated $A_3LE$ to LE, ESI mass spectra were acquired for equimolar mixtures of these two peptides from 10 nM to 2.4 mM total peptide concentration. Different nanoESI tips were used for each solution to avoid sample contamination. Although mass spectra acquired using the same tip are typically reproducible to better than 1%, the use of different tips results in more significant variations in relative ion intensities.

To obtain an estimate of the tip-to-tip variability, three replicate measurements were made using three different tips at each solution concentration. A plot of the normalized ion abundance of protonated $A_3LE$, $[A_3LE + H]^+ / ([A_3LE + H]^+ + [LE + H]^+)$, as a function of solution concentration for this 50/50 mixture, is shown in Figure 6.2b. Error bars correspond to the standard deviation of three replicate measurements. At low concentrations, the uncertainty is higher due to the lower S/N. At higher concentrations, this uncertainty due to tip-to-tip variability is typically a few percent. The high uncertainty at 50 μM is due to one of the three mass spectra being significantly different than the other two, which shows that slight variations in seemingly identical nanospray capillaries can occasionally result in large variations in ion signals. At concentrations above 100 μM, $(A_3LE + H)^+$ is approximately 8 times more abundant than

$(LE + H)^+$ whereas for solutions $\leq 10^{-6}$ M, these abundances are nearly equal, consistent with their equimolar solution-phase concentrations. Thus, the abundances of the protonated molecular ions are more representative of their solution-phase molar fractions when the overall solution concentration is at or below 1 μM. However, this is not always the case for other peptide mixtures.

Mass spectra of four other equimolar peptide mixtures were measured at three different solution concentrations: methionine enkephalin (ME) or [$lys_6$]-leucine enkephalin (KLE) with LE, and bradykinin fragment 1-8 (BK1-8) or bradykinin fragment 2-9 (BK2-9) with bradykinin (BK). The molar fractions derived from the relative protonated molecular ion intensities measured in these experiments are given in Table 6.1. For the ME/LE mixture, molecular ion abundances reflect the molar fraction in solution at all three concentrations. Replacement of leucine by methionine should have little effect on the basicity or surface activity of the peptide, consistent with the similar ionization efficiencies observed. In contrast, the abundances of protonated $A_3$LE and KLE do not reflect well their solution-phase concentrations. Molar fractions derived from these ion abundances are too high at 2.4 mM (80% and 71%, respectively) whereas KLE values are too low (38%) at 1.2 μM. Addition of a lysine residue to LE should significantly affect the physical properties of the peptide resulting in different ionization efficiencies for these two peptides.

**Table 1.** Molar Fraction Calculated from Relative Protonated Molecular Ion Intensities from Equimolar solutions

| Total Peptide Concentration | Bradykinin | | Leucine Enkephalin | | |
|---|---|---|---|---|---|
| | Bradykinin 1-8 | Bradykinin 2-9 | $[Ala]_3$ Enkephalin | Methionine Enkephalin | Lysine Enkephalin |
| 2.4 mM | 68% ± 7% | 55% ± 3% | 80% ± 1% | 46% ± 1% | 71% ± 1% |
| 12. μM | 51% ± 5% | 51% ± 3% | 66% ± 1% | 53% ± 2% | 43% ± 4% |
| 1.2 μM | 55% ± 7% | 67% ± 5% | 50% ± 1% | 55% ± 1% | 38% ± 1% |

For equimolar BK1-8/BK and BK2-9/BK solutions, the relative molecular ion intensities also depend on solution concentration. For BK2-9/BK, the ionic molar fraction is significantly higher than that in solution at 1.2 μM. These data illustrate that using the relative abundance of protonated molecular ions to determine the molar fraction of components in solution can result in significant deviation from the solution-phase concentration. This deviation can be reduced for solution concentrations below 1 μM in some cases. However, the ability to detect low molar fraction components in such dilute solutions can be limited by S/N. In these experiments, the S/N of molecular ions from 50 nM solutions is ~100 for $(LE + H)^+$, which limits detection of minor components to ~2% without modifying the experiment to improve overall S/N.

**6.3.3 Solution Concentration from Cluster Ion Intensities.** A wide range of both homogeneous and heterogeneous cluster ions can typically be formed at high peptide concentrations (Figure 6.1). If the individual constituent molecules are incorporated into these clusters statistically, then the molar fraction of the minor component, $F_m\%$, can be expressed as a binominal expansion for any two clusters of the same number of subunits, $n$, (equation 1);

$$F_m\% = \sqrt[h]{\frac{P(X_h,Y_k)}{p^k \bullet (\frac{n!}{h!(n-h)!})}} \times 100 \qquad (1)$$

where $P(X_h,Y_k)$ is the probability of forming a cluster corresponding to $h$ units of component $X$, and $k$ units of component $Y$ such that $h + k = n$, and $p$ is the observed fraction corresponding to the homogeneous cluster.

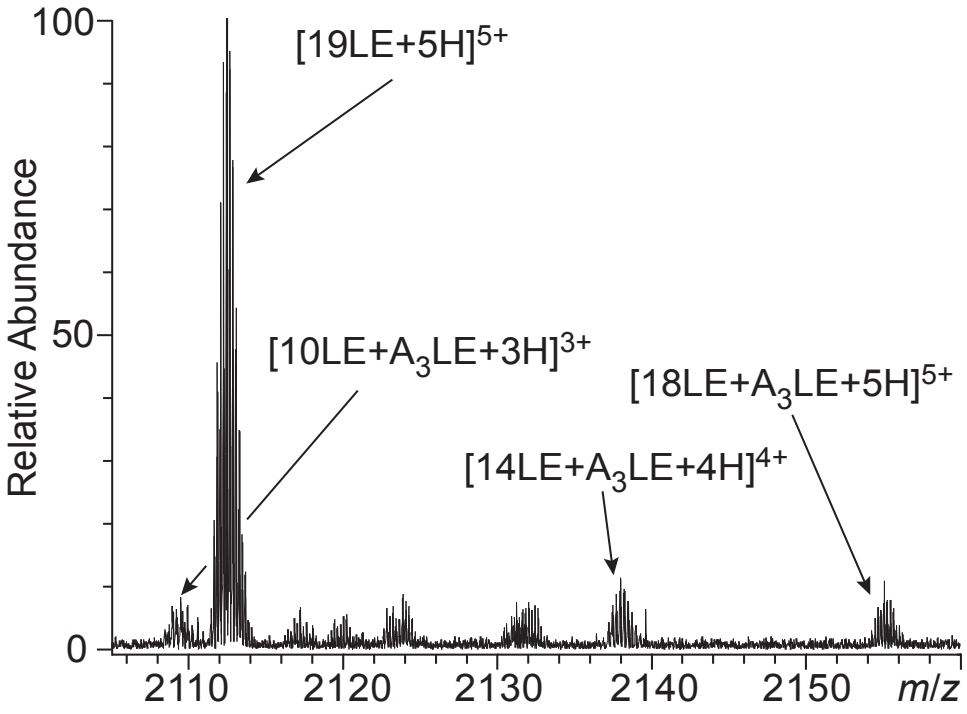


*Figure 6.3. Expanded region of ESI mass spectrum in Figure 6.1a showing homogeneous and heterogeneous clusters with 19 constituent molecules corresponding to $[19LE + 5H]^{5+}$ and $[18LE + A_3LE + 5H]^{5+}$. Minor peaks correspond to adducts, such as $Na^+$, $K^+$ and acetate, and other cluster sizes.*

To illustrate this process, an expansion of the mass spectrum from Figure 6.1a showing clusters for $n$ = 19 obtained from the 2.4 mM 1% $A_3LE$ with LE solution is shown in Figure 6.3. The normalized abundances of $(LE_{19} + 5H)^{5+}$ and $(LE_{18} + A_3LE + 5H)^{5+}$ are 100.0 and 10.2, respectively. No incorporation of additional $A_3LE$ molecules, i.e., $(LE_{17} + A_3LE_2 + 5H)^{5+}$, is observed for this cluster size at this molar fraction. To obtain the fractional incorporation, $P(A_3LE_1,LE_{18})$, the intensity of the cluster that has incorporated a single $A_3LE$ is divided by the sum of that cluster and the homogeneous cluster, i.e., $[LE_{18} + A_3LE + 5H]^{5+} / ([LE_{18} + A_3LE + 5H]^{5+} + [LE_{19} + 5H]^{5+}) = 10.2 / (100.0 + 10.2) = 0.093$. Using this value and the value for the cluster size in the binomial expansion (equation 1) for all three DC offset values, an average value of 0.87% ± 0.32% is obtained, which corresponds to the experimentally determined molar fraction derived from the $n$ = 19 clusters. Similarly, molar fraction values are obtained for each cluster size and these values are shown as a function of cluster size in Figure 6.4.

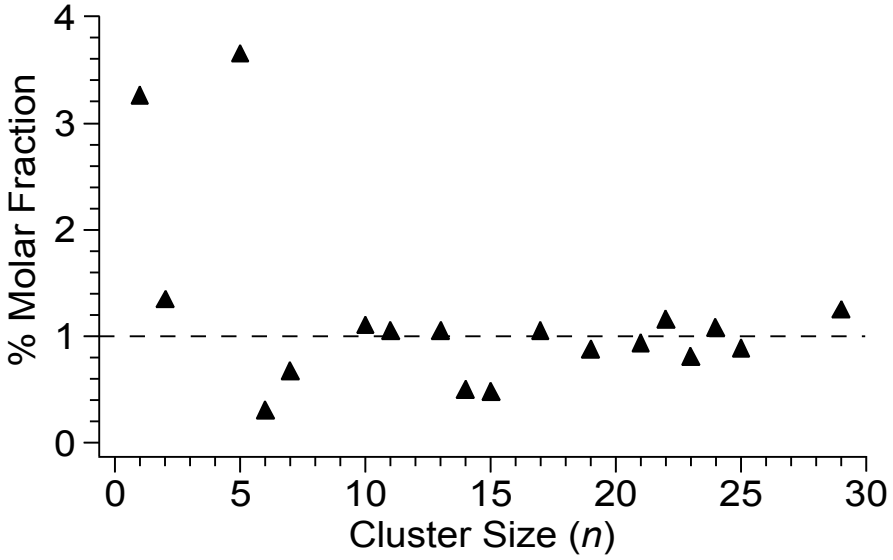


*Figure 6.4. The % molar fraction calculated from the cluster ion intensities assuming statistical incorporation and identical ionization efficiencies obtained from ESI mass spectra of a 1% molar fraction solution of $A_3LE$ in LE (2.4 mM total peptide) as a function of cluster size, n. A dashed line represents the ideal trend based on solution concentration.*

The molar fractions obtained from the cluster data vary significantly for clusters with $n$ < 10. For example, molar fractions of ~3.7% and 0.2% are obtained from the $n$ = 5 and 6 clusters, respectively. However, molar fractions determined from the $n$ = 17 – 29 clusters are similar. The average of the values for the $n$ = 17 – 29 clusters is 1.0 ± 0.3%, consistent with the solution concentration (1.0%). This suggests that these large clusters are not specific and that differences in composition have only a minor effect on relative ionization efficiencies.

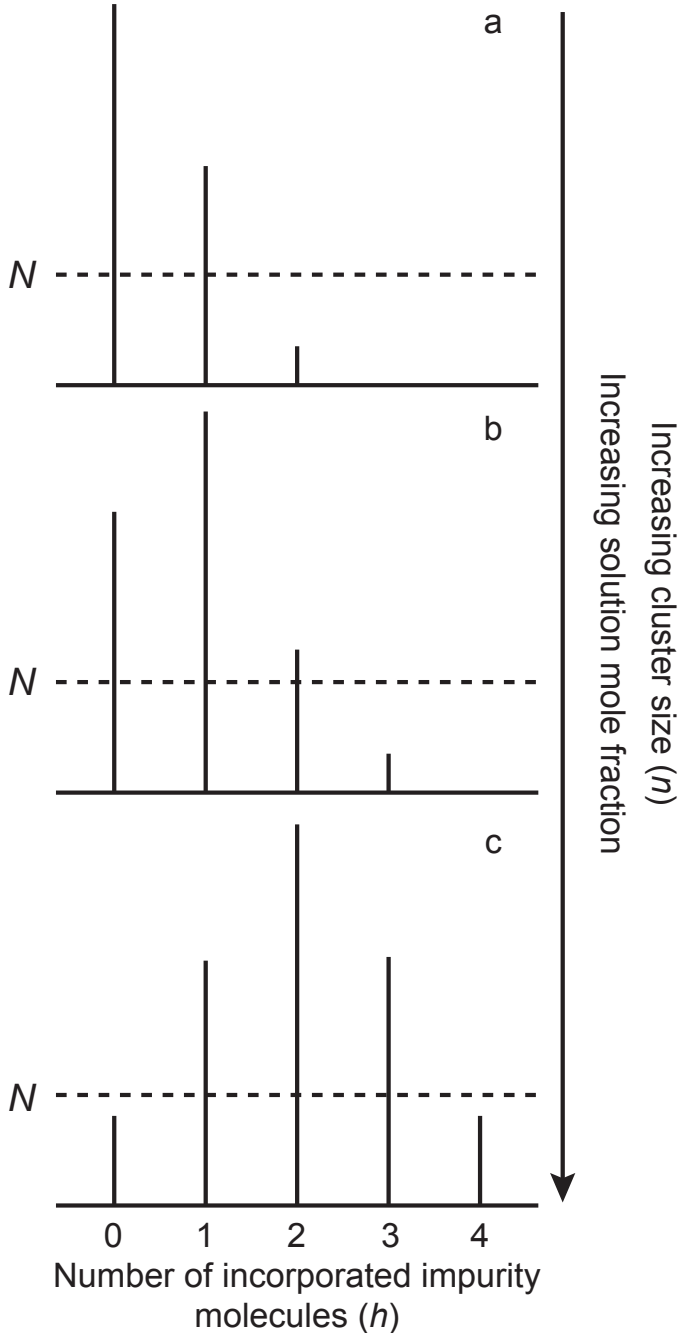


*Figure 6.5. Stickplots representing three theoretical distributions of heterogeneous cluster ions of a given size as a function of increasing cluster size or increasing molar fraction (a-c). Each distribution corresponds to a single cluster size, n, in which each line corresponds to the intensity of a cluster ion that contains some number of impurity molecules, h. The dashed line, N, represents the noise level.*

**6.3.4 Results for Different Molar Fractions.** Molar fractions determined as a function of cluster size were obtained for each solution with $A_3LE$ ranging from 0.05% to 10% of the total peptide concentration with LE as described above. For these concentrations, there are typically two or three different clusters for a given size *n*, with distributions weighted towards clusters with higher extent of incorporation of the more abundant component. In these cases, the effect of noise on the observed ion intensities is small, and the binomial distribution correlates well with the solution molar fraction. This is illustrated in Figure 6.5, which shows representative cluster intensities as a function of cluster composition and solution molar fraction. For low molar fractions, the abundance of the homogeneous cluster is high (Figure 6.5a and b). However, for solutions containing 20% or more of the $A_3LE$ with LE, higher order clusters that contain multiple $A_3LE$ molecules are abundant in the mass spectra and these heterogeneous clusters increase with increasing molar fraction and cluster size. To obtain a discrete value using the binomial expansion, the homogeneous cluster must be observed. However, the homogeneous clusters at the larger cluster sizes are not typically observed for the 20% and 50% molar fraction solutions due to low S/N (Figure 6.5c). For these clusters, a weighted average can be used (equation 2);

$$F_m\% = \frac{\sum_h I_h \times \frac{h}{n}}{\sum_h I_h} \times 100 \qquad (2)$$

where *I* is the intensity of each observed cluster consisting of *n* total peptide molecules with *h* molecules of the minor fraction component. This weighted average method works well for symmetrical distributions, such as those observed at high molar fractions or large cluster sizes, even at relatively low S/N because the center of the distribution can be accurately measured (Figure 6.5c). The asymmetrical distributions observed for lower molar fractions and small clusters are more difficult to accurately measure when the signal-to-noise is low (Figure 6.5a,b). In these cases, the weighted average of these clusters is systematically low. Thus, both methods are used: a binomial expansion when both the homogenous peak and a heterogeneous cluster are observed and a weighted average when no homogeneous cluster is detected. The binomial expansion method should be less sensitive to effects of low S/N because only the high intensity homogeneous and single impurity clusters are used (Figure 6.5a and b).

The $A_3LE$ % molar fraction calculated using the cluster intensities for $n \geq 17$ as a function of % molar fraction in solution is shown in Figure 6.6. These data can be fit to a straight line ($r^2 = 0.97$) with a slope of 0.92. This value is less than 1.0, which indicates that the concentration of $A_3LE$ determined by this method is systematically low. There is also some uncertainty in the solution concentration due to water absorption by the peptide during weighing, although this uncertainty is likely to be small. These data suggest that there may be a slight preference for incorporation of LE into these clusters, although this effect appears to be minor.

In contrast to the results obtained from the cluster data, a linear fit of the molar fractions determined from the protonated molecular ion abundances *vs.* concentration

from these same mass spectra has a slope of 14.2 ($r^2$ = 0.96). Quantitation using this cluster method therefore provides a significantly more accurate measure of the solution-phase concentration than the relative abundances of the protonated molecular ions over a wide range of solution compositions. Because the composition of the large clusters is similar, effects of preferential ionization should be minimal.

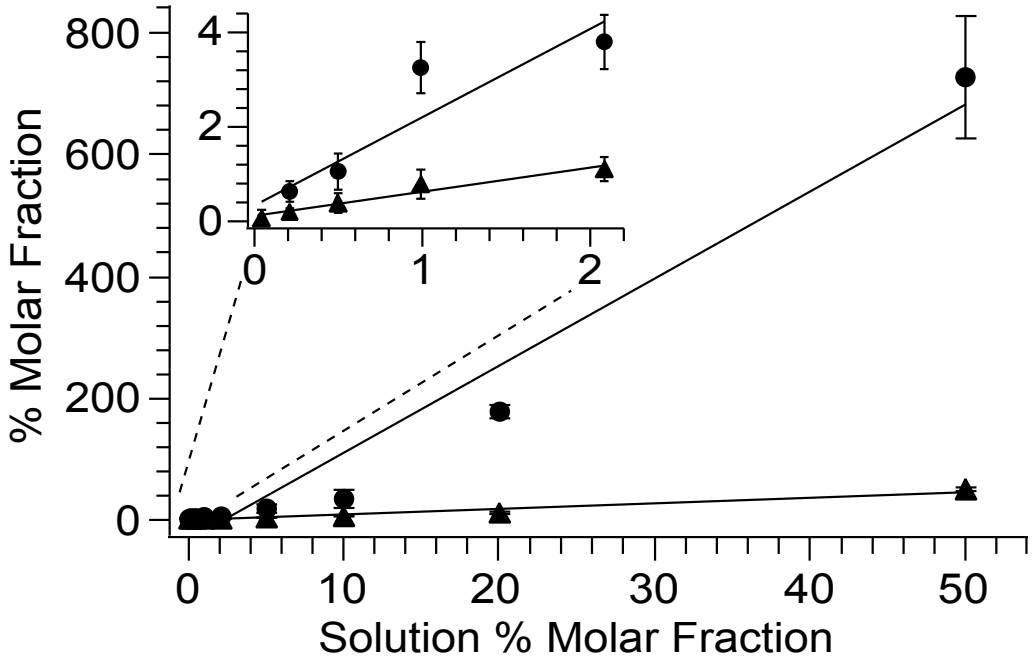


*Figure 6.6. The % molar fraction of $A_3LE$ in LE obtained from the protonated molecular ions (circles) and from the cluster abundances for $n \geq 17$ as a function of the solution % molar fraction. The cluster data is linear with a slope of 0.92 whereas the protonated molecular ion data has a slope of 14.2 and is not well fit to a line. Error bars correspond to a standard deviation of three replicate spectra at different DC offset voltages of 2.8, 3.6 and 4.0.*

**6.3.5 Effects of Analyte Identity.** To investigate the generality of this method, analogous experiments were performed on four additional peptide mixtures. Solutions containing various molar fractions of either ME or KLE with LE, and either BK1-8 or BK2-9 with BK were prepared and three replicate mass spectra at the three hexapole DC offset values were obtained. These peptides were chosen to investigate effects of surface activity and basicity. As was observed for $A_3LE$ in LE, the molar fraction obtained from the cluster ion intensities varies with cluster size for smaller clusters. In each case, the protonated molecular ions and clusters with $n \leq 10$ result in measured molar fractions that are significantly different from those expected based on solution concentration. Data for 1% molar fraction BK1-8 in BK are shown in Figure 6.7. The molar fraction value obtained from $n$ = 4 and 8 is 5.2% and 4.3%, respectively, and are significantly higher

than the solution value of 1%. Similar results were obtained for the smaller clusters formed from solutions containing the other peptides, suggesting that preferential incorporation of some peptides into the smaller clusters occurs.

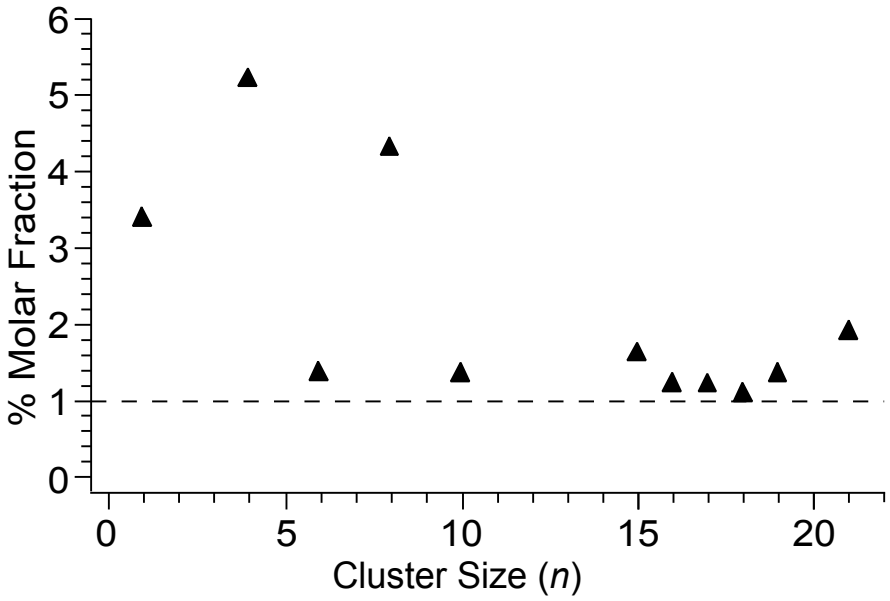


*Figure 6.7. The % molar fraction calculated from cluster ion intensities obtained from ESI mass spectra of a 1% molar fraction BK1-8 with BK (2.4 mM total peptide concentration) as a function of cluster size, n. A dashed line represents the ideal trend based on solution concentration, assuming statistical incorporation of subunits into clusters.*

The molar fraction calculated for the larger cluster ions approaches solution values for all the mixtures, indicating that effects of cluster specificity and ionization effects are minor for these larger clusters. Clusters formed from the 1% solution of BK1-8 in BK with $n \geq 15$ are relatively constant with an average value of 1.4 ± 0.3. Similar results are obtained for the other solutions, but the cluster size where the value becomes constant depends on the analyte identities. Clusters sizes of $n \geq 12$, 20 and 15 were used to obtain the molar fractions for solutions containing ME with LE, KLE with LE and BK2-9 with BK, respectively. The lower cluster size for ME with LE is likely because substitution of a leucine for a methionine should have a relatively small effect on cluster specificity or ionization efficiency. The larger cluster size for KLE in LE is likely due to a more significant change to the physical properties of these peptides. The % molar fractions determined from the cluster data, as well as the values determined from the protonated molecular ion intensities, are plotted against the solution % molar fractions in Figure 6.8a-d for these solutions.

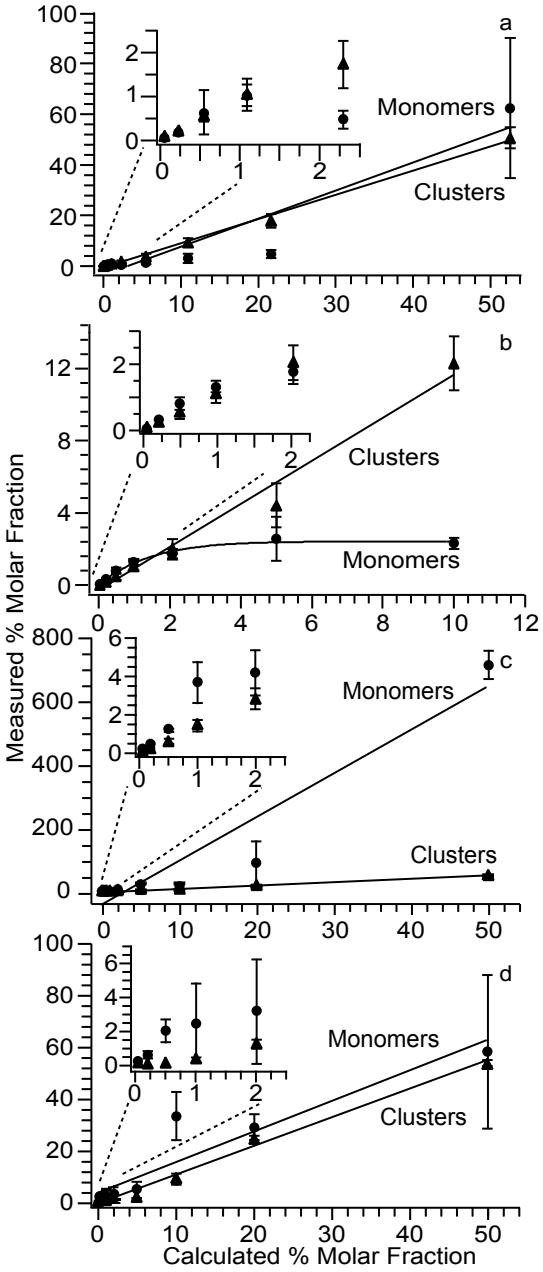


*Figure 6.8. The % molar fractions calculated from the protonated molecular ions (squares) and cluster ions (triangles) as a function of the % molar fraction in solution for two component mixtures consisting of a) ME with LE, b) BK2-9 with BK, c) BK1-8 with BK and d) KLE with LE. Data from clusters with n ≥ 12, 15, 15 and 20 subunits were used for these respective mixtures. Best-fit slopes of 0.95, 1.19, 1.08 and 1.10 are obtained for the cluster data a-d, respectively (see text).*

For all four of these mixtures, the data for the protonated molecular ions are not well fit by a line. The slope of these data for the protonated molecular ions from solutions containing BK1-8/BK and BK2-9/BK are 13.7 ($r^2 = 0.92$) and 0.2 ($r^2 = 0.64$), respectively, and for solutions containing ME with LE and KLE with LE the slopes are 1.11 ($r^2 = 0.88$) and 1.18 ($r^2 = 0.88$), respectively. These results show that the relative protonated molecular ion abundances can either be significantly higher or lower than their corresponding solution-phase concentration. However, molar fractions obtained from the cluster data are linear, and the slope of best fit lines are 0.95 ($r^2 > 0.99$), 1.19 ($r^2 = 0.98$), 1.08 ($r^2 > 0.99$) and 1.10 ($r^2 > 0.99$) for solutions containing ME, BK2-9, BK1-8 and KLE, respectively. Thus, the molar fractions obtained from the cluster ion data are within ~10% of the solution-phase concentrations over a four-order of magnitude range in solution molar fraction for four of the five peptide mixtures investigated, and within 20% over a three-order of magnitude range for BK2-9 in BK. These results indicate that this cluster method should be a general and robust technique to obtain reasonably accurate quantitative information about peptide concentration in solution without the need for standards or knowledge of molecular identity.

**6.4 Conclusions.**

Quantitation of peptides in solution using MS is complicated by differences in the physical properties of the molecules, which can result in preferential ionization of some components in a mixture as well as instrumental effects including *m*/*z* dependent ion transmission and detection efficiency. These effects can be reduced by using the abundances of large, nonspecific clusters from which accurate measures of the solution-phase concentrations can be obtained. For five different peptide mixtures, the relative solution-phase concentrations obtained from the abundances of large clusters are accurate to within ~20%. In contrast, the relative abundances of the protonated molecular ions differ from the relative solution-phase concentrations by more than an order of magnitude.

Although the accuracy of this method is lower than that obtainable by using standards, this method has several important advantages: 1) it does not require either an internal nor an external standard which greatly reduces the time and effort necessary to obtain quantitative information, 2) the components do not need to be identified in order to measure their relative solution-phase concentration and 3) effects of instrument or detector mass bias are significantly reduced which is of key importance when the charge states or masses of peptides differ significantly. Although this method requires high concentration solutions to produce large clusters, only a few picomoles of sample are consumed using nanoESI at typical flow rates of ~5 nL/min.

The accuracy of this method should be improved by obtaining data from even larger clusters. Systematic error due to effects of the asymmetry of the cluster distributions is reduced at higher S/N. Both of these improvements would increase the resolution and dynamic range of the method and could make possible simultaneous quantitation of multiple impurities in a single mixture. This method should be equally applicable to smaller molecules, such as pharmaceuticals, for which larger clusters could

be produced and analyzed to provide rapid quantitative information about possible impurities without having to use standards or even knowing the identity of the impurities. Results from the large peptide clusters also provide compelling support for the use of ion abundances in MS to obtain accurate measures of protein modifications or adducts where relatively minor chemical changes to a large protein should have only minor effects on ionization.

**6.5 Acknowledgements.**

The authors are grateful to Dr. Gregory T. Blakney for assistance in the development of the Predator datastation and to generous financial support from the National Institutes of Health (R01GM064712).

## 6.6 References.


[1] Görög, S. *Anal. Bioanal. Chem.* **2003**, *377*, 852-862.

[2] Görög, S. *J. Pharm. Biomed. Anal.* **2008**, 247-253.

[3] Qiu, F.; Norwood, D. L. *J. Liq. Chromatogr. Relat. Technol.* **2007**, *30*, 877-935.

[4] Freitas, M. A.; Sklenar, A. R.; Parthun, M. R. *J. Cell. Biochem.* **2004**, *92*, 691-700.

[5] Jensen, O. N. *Nat. Rev. Mol. Cell Biol.* **2006**, *7*, 391-403.

[6] Hanash, S. *Nature* **2003**, *422*, 226-232.

[7] Zhou, H.; Watts, J. D.; Aebersold, R. *Nat. Biotechnol.* **2001**, *19*, 375-378.

[8] Kelleher, N. L.; Hicks, L. M. *Curr. Opin. Chem. Biol.* **2005**, *9*, 424-430.

[9] Aebersold, R.; Mann, M. *Nature* **2003**, *422*, 198-207.

[10] Gygi, S. P.; Rist, B.; Gerber, S. A.; Tureček, F.; Gelb, M. H.; Aebersold, R. *Nat. Biotechnol.* **1999**, *17*, 994-999.

[11] Olah, T. V.; McLoughlin, D. A.; Gilbert, J. D. *Rapid Commun. Mass Spectrom.* **1997**, *11*, 17-23.

[12] Wiener, M. C.; Sachs, J. R.; Deyanova, E. G.; Yates, N. A. *Anal. Chem.* **2004**, *76*, 6085-6096.

[13] Liu, H.; Sadygov, R. G.; Yates, J. R., III *Anal. Chem.* **2004**, *76*, 4193-4201.

[14] Moresco, J. J.; Dong, M.-Q.; Yates, J. R., III *Am. J. Clin. Nutr.* **2008**, *88*, 597-604.

[15] Petyuk, V. A.; Qian, W.-J.; Hinault, C.; Gritsenko, M. A.; Singhal, M.; Monroe, M. E.; Camp, D. G., II; Kulkarni, R. N.; Smith, R. D. *J. Proteome Res.* **2008**, *7*, 3114-3126.

[16] Metz, T. O.; Jacobs, J. M.; Gritsenko, M. A.; Fontès, G.; Qian, W. J.; Camp, D. G.; Poitout, V.; Smith, R. D. *J. Proteome Res.* **2006**, *5*, 3345-3354.

[17] Petyuk, V. A.; Qian, W.-J.; Chin, M. H.; Wang, H.; Livesay, E. A.; Monroe, M. E.; Adkins, J. N.; Jaitly, N.; Anderson, D. J.; Camp, D. G., II; Smith, D. J.; Smith, R. D. *Genome Res.* **2007**, *17*, 328-336.

[18] Strittmatter, E. F.; Ferguson, P. L.; Tang, K.; Smith, R. D. *J. Am. Soc. Mass Spectrom.* **2003**, *14*, 980-991.

[19] Ishihama, Y.; Sato, T.; Tabata, T.; Miyamoto, N.; Sagane, K.; Nagasu, T.; Oda, Y. *Nat. Biotechnol.* **2005**, *23*, 617-621.

[20] Patrie, S. M.; Ferguson, J. T.; Robinson, D. E.; Whipple, D.; Rother, M.; Metcalf, W. W.; Kelleher, N. L. *Mol. Cell. Proteomics* **2006**, *5*, 14-25.

[21] Parks, B. A.; Jiang, L.; Thomas, P. M.; Wenger, C. D.; Roth, M. J.; Boyne, M. T., II; Burke, P. V.; Kwast, K. E.; Kelleher, N. L. *Anal. Chem.* **2007**, *79*, 7984-7991.

[22] Forbes, A. J.; Patrie, S. M.; Taylor, G. K.; Kim, Y.-B.; Jiang, L.; Kelleher, N. L. *Proc. Natl. Acad. Sci. U.S.A.* **2004**, *101*, 2678-2683.

[23] Dong, M.-Q.; Venable, J. D.; Au, N.; Xu, T.; Park, S. K.; Cociorva, D.; Johnson, J. R.; Dillin, A.; Yates, J. R., III *Science* **2007**, *317*, 660-663.

[24] Liao, L.; McClatchy, D. B.; Park, S. K.; Xu, T.; Lu, B.; Yates, J. R., III *J. Proteome Res.* **2008**, *7*, 4743-4755.

[25] Denny, P.; Hagen, F. K.; Hardt, M.; Liao, L.; Yan, W.; Arellanno, M.; Bassilian, S.; Bedi, G. S.; Boontheung, P.; Cociorva, D.; Delahunty, C. M.; Denny, T.; Dunsmore, J.; Faull, K. F.; Gilligan, J.; Gonzalez-Begne, M.; Halgand, F.; Hall, S. C.; Han, X.; Henson, B.; Hewel, J.; Hu, S.; Jeffrey, S.; Jiang, J.; Loo, J. A.; Loo, R. R. O.; Malamud, D.; Melvin, J. E.; Miroshnychenko, O.; Navazesh, M.; Niles, R.; Park, S. K.; Prakobphol, A.; Ramachandran, P.; Richert, M.; Robinson, S.; Sondej, M.; Souda, P.; Sullivan, M. A.; Takashima, J.; Than, S.; Wang, J.; Whitelegge, J. P.; Witkowska, H. E.; Wolinsky, L.; Xie, Y.; Xu, T.; Yu, W.; Ytterberg, J.; Wong, D. T.; Yates, J. R., III; Fisher, S. J. *J. Proteome Res.* **2008**, *7*, 1994-2006.

[26] Zhai, B.; Villén, J.; Beausoleil, S. A.; Mintseris, J.; Gygi, S. P. *J. Proteome Res.* **2008**, *7*, 1675-1682.

[27] Swaney, D. L.; McAlister, G. C.; Coon, J. J. *Nat. Methods* **2008**, *5*, 959-964.

[28] Savitski, M. M.; Nielsen, M. L.; Kjeldsen, F.; Zubarev, R. A. *J. Proteome Res.* **2005**, *4*, 2348-2354.

[29] Krijgsveld, J.; Ketting, R. F.; Mahmoudi, T.; Johansen, J.; Artal-Sanz, M.; Verrijzer, C. P.; Plasterk, R. H. A.; Heck, A. J. R. *Nat. Biotechnol.* **2003**, *21*, 927-931.

[30] Fenn, J. B. *J. Am. Soc. Mass Spectrom.* **1993**, *4*, 524-535.

[31] Cohen, S. L.; Chait, B. T. *Anal. Chem.* **1996**, *68*, 31-37.

[32] Kebarle, P. *J. Mass Spectrom.* **2000**, *35*, 804-817.

[33] Smith, R. D.; Shen, Y.; Tang, K. *Acc. Chem. Res.* **2004**, *37*, 269-278.

[34] King, R.; Bonfiglio, R.; Fernandez-Metzler, C.; Miller-Stein, C.; Olah, T. *J. Am. Soc. Mass Spectrom.* **2000**, *11*, 942-950.

[35] Belov, M. E.; Nikolaev, E. N.; Harkewicz, R.; Masselon, C. D.; Alving, K.; Smith, R. D. *Int. J. Mass Spectrom.* **2001**, *208*, 205-225.

[36] Page, J. S.; Kelly, R. T.; Tang, K.; Smith, R. D. *J. Am. Soc. Mass Spectrom.* **2007**, *18*, 1582-1590.

[37] Axelsson, J.; Scrivener, E.; Haddleton, D. M.; Derrick, P. J. *Macromolecules* **1996**, *29*, 8875-8882.

[38] Marshall, A. G.; Hendrickson, C. L.; Jackson, G. S. *Mass Spectrom. Rev.* **1998**, *17*, 1-35.

[39] Tang, K.; Allman, S. L.; Jones, R. B.; Chen, C. H. *Anal. Chem.* **1993**, *65*, 2164-2166.

[40] Cheng, J.; Vecitis, C. D.; Hoffmann, M. R.; Colussi, A. J. *J. Phys. Chem. B* **2006**, *110*, 25598-25602.

[41] Cech, N. B.; Enke, C. G. *Anal. Chem.* **2000**, *72*, 2717-2723.

[42] Cech, N. B.; Enke, C. G. *Mass Spectrom. Rev.* **2001**, *20*, 362-387.

[43] Kuprowski, M. C.; Boys, B. L.; Konermann, L. *J. Am. Soc. Mass Spectrom.* **2007**, *18*, 1279-1285.

[44] Iavarone, A. T.; Jurchen, J. C.; Williams, E. R. *J. Am. Soc. Mass Spectrom.* **2000**, *11*, 976-985.

[45] Iavarone, A. T.; Jurchen, J. C.; Williams, E. R. *Anal. Chem.* **2001**, *73*, 1455-1460.

[46] Iavarone, A. T.; Williams, E. R. *Int. J. Mass Spectrom.* **2002**, *219*, 63-72.

[47] Kebarle, P.; Peschke, M. *Anal. Chim. Acta* **2000**, *406*, 11-35.

[48] Loo, J. A.; Loo, R. R. O.; Udseth, H. R.; Edmonds, C. G.; Smith, R. D. *Rapid Commun. Mass Spectrom.* **1991**, *5*, 101-105.

[49] Konermann, L.; Douglas, D. J. *Biochemistry* **1997**, *36*, 12296-12302.

[50] Dobo, A.; Kaltashov, I. A. *Anal. Chem.* **2001**, *73*, 4763-4773.

[51] Tang, L.; Kebarle, P. *Anal. Chem.* **1993**, *65*, 3654-3668.

[52] Iavarone, A. T.; Williams, E. R. *J. Am. Chem. Soc.* **2003**, *125*, 2319-2327.

[53] Pan, P.; McLuckey, S. A. *Anal. Chem.* **2003**, *75*, 1491-1499.

[54] Han, D. K.; Eng, J.; Zhou, H.; Aebersold, R. *Nat. Biotechnol.* **2001**, *19*, 946-951.

[55] Gygi, S. P.; Rist, B.; Griffin, T. J.; Eng, J.; Aebersold, R. *J. Proteome Res.* **2002**, *1*, 47-54.

[56] DeSouza, L.; Diehl, G.; Rodrigues, M. J.; Guo, J.; Romaschin, A. D.; Colgan, T. J.; Siu, K. W. M. *J. Proteome Res.* **2005**, *4*, 377-386.

[57] Hall, M. P.; Ashrafi, S.; Obegi, I.; Petesch, R.; Peterson, J. N.; Schneider, L. V. *J. Mass Spectrom.* **2003**, *38*, 809-816.

[58] Rodgers, R. P.; Blumer, E. N.; Hendrickson, C. L.; Marshall, A. G. *J. Am. Soc. Mass Spectrom.* **2000**, *11*, 835-840.

[59] Oda, Y.; Huang, K.; Cross, F. R.; Cowburn, D.; Chait, B. T. *Proc. Natl. Acad. Sci. U.S.A.* **1999**, *96*, 6591-6596.

[60] Ong, S.-E.; Blagoev, B.; Kratchmarova, I.; Kristensen, D. B.; Steen, H.; Pandey, A.; Mann, M. *Mol. Cell. Proteomics* **2002**, *1*, 376-386.

[61] Ong, S.-E.; Kratchmarova, I.; Mann, M. *J. Proteome Res.* **2003**, *2*, 173-181.

[62] Ong, S.-E.; Mann, M. *Nat. Chem. Biol.* **2005**, *1*, 252-262.

[63] Ji, J.; Chakraborty, A.; Geng, M.; Zhang, X.; Amini, A.; Bina, M.; Regnier, F. *J. Chromatogr. B* **2000**, *745*, 197-210.

[64] Havliš, J.; Shevchenko, A. *Anal. Chem.* **2004**, *76*, 3029-3036.

[65] Hernandez, H.; Niehauser, S.; Boltz, S. A.; Gawandi, V.; Phillips, R. S.; Amster, I. J. *Anal. Chem.* **2006**, *78*, 3417-3423.

[66] Yi, E. C.; Li, X.-J.; Cooke, K.; Lee, H.; Raught, B.; Page, A.; Aneliunas, V.; Hieter, P.; Goodlett, D. R.; Aebersold, R. *Proteomics* **2005**, *5*, 380-387.

[67] Seipert, R. R.; Barboza, M.; Ninonuevo, M. R.; LoCascio, R. G.; Mills, D. A.; Freeman, S. L.; German, J. B.; Lebrilla, C. B. *Anal. Chem.* **2008**, *80*, 159-165.

[68] Zhang, D.; Tao, W. A.; Cooks, R. G. *Int. J. Mass Spectrom.* **2001**, *204*, 159-169.

[69] Augusti, D. V.; Carazza, F.; Augusti, R.; Tao, W. A.; Cooks, R. G. *Anal. Chem.* **2002**, *74*, 3458-3462.

[70] Augusti, D. V.; Augusti, R.; Carazza, F.; Cooks, R. G. *Chem. Commun.* **2002**, 2242-2243.

[71] Dwivedi, P.; Wu, C.; Matz, L. M.; Clowers, B. H.; Siems, W. F.; Hill, H. H., Jr. *Anal. Chem.* **2006**, *78*, 8200-8206.

[72] Grigorean, G.; Ramirez, J.; Ahn, S. H.; Lebrilla, C. B. *Anal. Chem.* **2000**, *72*, 4275-4281.

[73] Ahn, S.; Ramirez, J.; Grigorean, G.; Lebrilla, C. B. *J. Am. Soc. Mass Spectrom.* **2001**, *12*, 278-287.

[74] Guo, J.; Wu, J.; Siuzdak, G.; Finn, M. G. *Angew. Chem.-Int. Edit.* **1999**, *38*, 1755-1758.

[75] Mie, A.; Jörntén-Karlsson, M.; Axelsson, B.-O.; Ray, A.; Reimann, C. T. *Anal. Chem.* **2007**, *79*, 2850-2858.

[76] Jurchen, J. C.; Williams, E. R. *J. Am. Chem. Soc.* **2003**, *125*, 2817-2826.

[77] Robinson, E. W.; Williams, E. R. *J. Am. Soc. Mass Spectrom.* **2005**, *16*, 1427-1437.

[78] Jurchen, J. C.; Garcia, D. E.; Williams, E. R. *J. Am. Soc. Mass Spectrom.* **2003**, *14*, 1373-1386.

[79] Baker, E. S.; Bernstein, S. L.; Bowers, M. T. *J. Am. Soc. Mass Spectrom.* **2005**, *16*, 989-997.

[80] Liu, B.; Hvelplund, P.; Nielsen, S. B. *J. Am. Soc. Mass Spectrom.* **2005**, *16*, 1840-1845.

## Chapter 7

### Simultaneous Quantitation of Amino Acid Mixtures using Clustering Agents

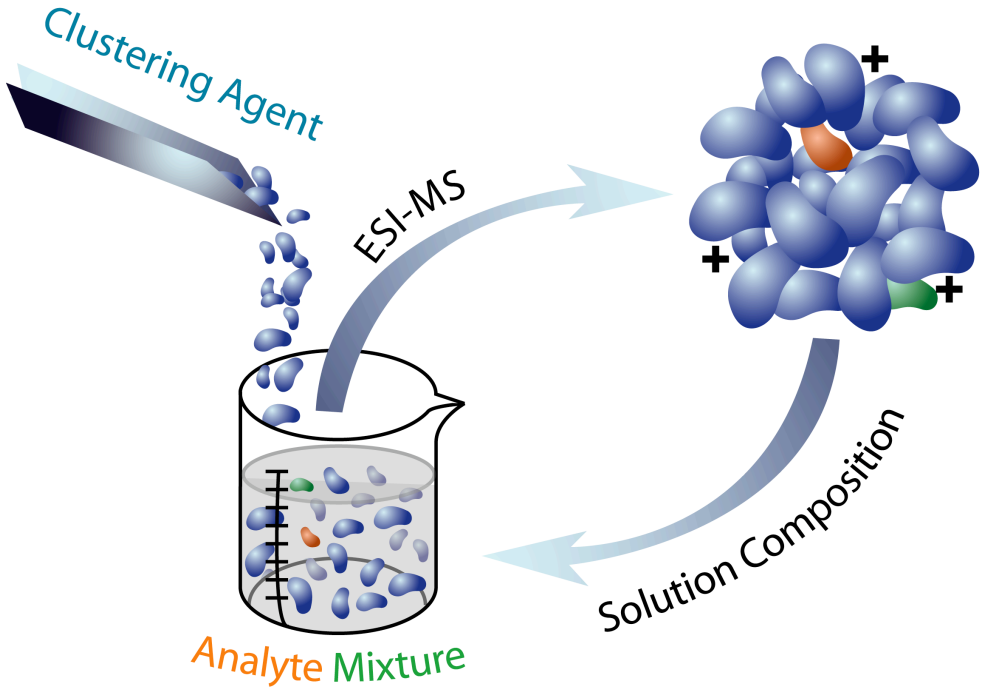


**7.0 Abstract.**

A method that uses the abundances of large clusters formed in electrospray ionization to determine the solution-phase molar fractions of amino acids in multi-component mixtures is demonstrated. For solutions containing either four or ten amino acids, the relative abundances of protonated molecules differed from their solution-phase molar fractions by up to 30 fold and 100 fold, respectively. For the four-component mixture, the molar fractions determined from the abundances of larger clusters consisting of 19 or more molecules were within 25% of the solution-phase molar fractions indicating that the composition of these clusters statistically reflects the relative concentrations of these amino acids in solution and ionization and detection biases are significantly reduced. Lower accuracy was obtained for the ten-component mixture where values determined from the cluster abundances were typically within a factor of three of their solution molar fractions. The lower accuracy of this method with the more complex mixture may be due to specific clustering effects owing to the heterogeneity as a result of significantly different physical properties of the components or it may be the result of lower S/N for the more heterogeneous clusters and not including the low-abundance more highly heterogeneous clusters in this analysis. Although not as accurate as using traditional standards, this clustering method may find applications when suitable standards are not readily available.

## 7.1 Introduction.

Mass spectrometry is widely used to identify compounds with known structures or elucidate the structures of previously unknown compounds [1-10], even those present in complex mixtures [1,2]. Elemental composition can be obtained from exact mass measurements [2-5] and tandem mass spectrometry can provide detailed information about structure [6-10]. However, obtaining quantitative information directly from ion abundances can be more challenging due to a number of effects, including relative ionization efficiencies, matrix effects due to the presence of other molecules, and mass-dependent ion transmission and detection efficiencies. Quantitation can be especially challenging when the efficiency of the ionization method depends significantly on both molecular structure and the matrix, as is the case for both electrospray ionization (ESI) [11-14] and matrix-assisted laser desorption ionization [15-18].

In ESI, a variety of factors can affect ionization efficiency and charging [12,13,19-29], such as basicity of the solvent and analyte, solvent surface tension, and analyte surface activity, which can all result in preferential ionization or suppression of individual components in mixtures. Separation methods, such as liquid chromatography, can be used to reduce matrix effects and are commonly used with complex mixtures [30,31], but increase analysis time and do not necessarily eliminate matrix effects or effects of differential ionization efficiencies [14,32].

Accurate quantitation can be done by using carefully chosen and/or specifically prepared standards [31-44]. Typically, standards are selected to closely mimic the physical properties of the analyte, with the most robust quantitation done using isotopically labeled forms of the analyte as internal standards [38-41]. Both internal and external standards are used in a variety of analytical applications of mass spectrometry [42-44]. However, suitable standards may not always be readily available, such as with newly discovered natural products, illicit or restricted compounds, or new products and intermediates formed by organic synthesis, which can make it difficult to rapidly obtain accurate quantitation with mass spectrometry.

We recently introduced a new approach to obtaining quantitative measurements of analyte molar fractions directly from an ESI mass spectrum without using traditional standards [45-47]. A clustering agent, such as an amino acid, is added to a solution in significant molar excess, at a concentration typically around 1 to 10 mM. Abundant homogenous clusters of the added agent are formed, as are heterogeneous clusters that contain primarily the clustering agent but also one or more analyte molecules. Smaller clusters often exhibit preferential incorporation of some components, or can preferentially ionize depending on the cluster composition. But these effects become smaller with increasing cluster size where incorporation of analyte molecules into the cluster becomes more statistical and reflects the relative ratios of components in solution. The abundances of these nonspecific clusters can be used to obtain the molar fractions of the components in solution [45]. Even when serine, which is known to form specific chirally selective structures at small cluster size [48-50], is used as a clustering agent, the composition of large clusters can be used to obtain solution molar fractions of other amino acids that are accurate to within ~20% of the solution value [46]. By adding a

known amount of the clustering agent to the solution, the absolute concentration of an analyte can be determined [47]. This method has been demonstrated on solutions containing individual amino acids and peptides, and has been applied to the direct analysis of active ingredients in Tamiflu and other pharmaceutical tablets, where the ionization/detection efficiency of individual components differed by up to 100 fold, but the dosages of the active ingredients in each of the tablets were determined to typically better than 20% accuracy [47]. Although not as accurate as methods that use more traditional standards, this method has the advantages that it is fast, it can be used for mixtures containing unknown analytes, and can be used when suitable standards may not be readily available, such as schedule I or II controlled substances, or designer drugs that have not been previously characterized. Here, we investigate the viability of this cluster agent approach for obtaining simultaneous quantitative information from more complex solution mixtures containing up to 10 components.

## 7.2 Experimental Methods.

**7.2.1 Mass Spectrometry.** All mass spectra were obtained using a 9.4 T Fourier transform ion cyclotron resonance (FT/ICR) mass spectrometer that has been described elsewhere [45,51]. Aqueous stock solutions containing glycine, alanine, serine, threonine, leucine, lysine, histidine, phenylalanine, arginine and tryptophan (Sigma Aldrich, St. Louis, MO) were prepared at 6 mM. Mixed analyte solutions were prepared from these stock solutions and diluted to a final concentration of 3 mM. Ions were formed by nanoelectrospray ionization using ~10 μL of aqueous solution loaded into borosilicate capillaries pulled to a tip inner diameter of ~2 μm. The borosilicate capillary is positioned ~2-3 mm away from the source inlet and electrospray is initiated by applying approximately -1 kV to the source inlet. A platinum wire in direct contact with the analyte solution in the borosilicate capillary is grounded. Ions are accumulated in an external hexapole for 1.5 s prior to injection and trapping within the ion cell. Trapping of clusters is enhanced by pulsing $N_2$ gas through a piezoelectric valve to increase the cell pressure transiently to ~1 x $10^{-6}$ Torr, after which the cell pressure returns to ~1 x $10^{-9}$ Torr prior to ion detection. Spectra were signal averaged to increase the signal-to-noise ratio.

## 7.3 Results and Discussion.

**7.3.1 Solution Concentrations and Cluster Abundances.** If a cluster is formed statistically from a solution containing two or more components, the cluster abundance can be used to determine the relative concentration of the components in solution if the effects of differential ionization, detection, and ion transmission are small, which should occur when one of the components is dominant within the clusters. For a two-component mixture, molar fractions can be obtained using either a binomial expansion, or more rigorously, a weighted average [45]; in cases where the absolute concentration of one component is known, the absolute concentrations of the other component can be readily obtained. In the same way, cluster ion abundances from solutions containing more than

two components can also be used to determine absolute molar fractions for each component. In Figure 7.1a and b, theoretical ion abundances for clusters containing the same number of subunits, *n*, are shown for two different two-analyte mixtures that share the same majority 'clustering agent,' C, but one of two different minority analytes, A and B, respectively. In both cases, homogeneous clusters composed only of the clustering agent C are formed, as well as a series of heterogeneous clusters still composed of *n* subunits, but containing one or more analyte molecules. The mass difference between each of these clusters is the difference in the molecular weight of a single clustering agent molecule and a single analyte molecule, denoted by A-C and B-C in the two spectra, respectively. Multiple incorporations of an analyte are also expected if the cluster size or the analyte solution molar fraction are sufficiently large, resulting in additional clusters separated by integer values of the mass difference between the clustering agent and the analyte. To obtain a solution percent molar fraction, $F_m\%$, from either of these theoretical cluster distributions, the weighted average in Equation 1 can be used:

$$F_m\% = \frac{\sum_h I_h \frac{h}{n}}{\sum_h I_h} \times 100 \qquad (1)$$

where *I* is the ion abundance of each cluster, *n* is the number of molecules in the cluster and *h* is the number of minority analyte molecules incorporated into the cluster.

When clusters are formed from a solution containing more than two components, the above weighted average can still be used iteratively for each analyte to obtain solution molar fractions from the resulting distribution of clusters as long as *all* cluster ions at a given *n* containing the specific analyte are included. As an example, Figure 7.1c shows a theoretical cluster distribution formed for a solution containing the clustering agent C and both analytes A and B for the same number of subunits *n*. Note that the addition of the second analyte greatly reduces the abundance of the homogeneous clustering agent peak because the clustering agent is now largely present in the heterogeneous clusters, including a cluster corresponding to the incorporation of both minority analytes, with a mass difference of A + B – 2C.

Although this analysis can be continued iteratively for additional incorporations of minority components into a cluster, (*e.g.* A + A + B – 3C, A + B + B – 3C), these higher order analyte incorporations should be highly unlikely when the clustering agent is added in large excess, *e.g.*, in these experiments, greater than ~17 fold. An excess of clustering agent reduces the observed spectral overlap between cluster ions containing multiple heterogeneous components by shifting most of the observed ion abundance into the homogeneous cluster and heterogeneous clusters containing only one or two analyte molecules. Only the incorporation of up to two minority analyte components is considered in these analyses.

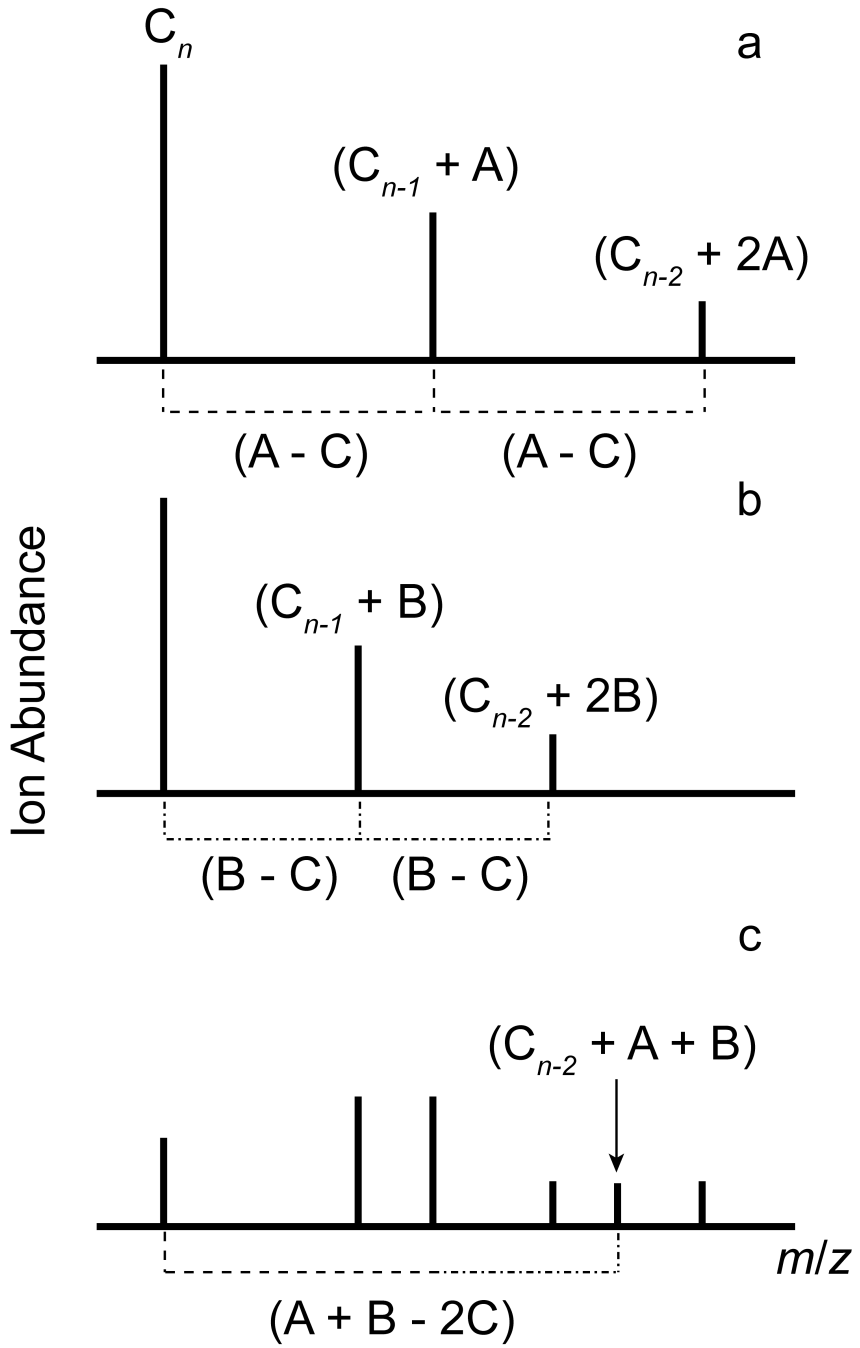


*Figure 7.1. Stickplots representing mass spectra of homogeneous and heterogeneous clusters of size n formed statistically from solutions containing a clustering agent C and (a) a single analyte A and (b) a single analyte B, and (c) both analytes A and B. Dashed lines denote mass differences between homogeneous and heterogeneous clusters that incorporate each of the analytes and mixtures of analytes. Total ion abundance is the same in all three stickplots.*

**7.3.2 Molar Fractions for Four-Component Mixtures.** An ESI mass spectrum of a solution containing four amino acids, serine, histidine, arginine and leucine, prepared at an approximately 95/2/2/1 ratio is shown in Figure 7.2. In addition to the protonated molecules, homogeneous and heterogeneous cluster ions, from dimers to clusters containing up to ~35 molecules are observed. The heterogeneous clusters consist of primarily serine and one or two other analyte molecules (see inset). For this four-component mixture, ten clusters of a given *n* are used to calculate relative solution phase molar fractions: the homogeneous cluster, the three heterogeneous clusters containing only one minority component, *i.e.*, either histidine, arginine or leucine, and the six possible heterogeneous clusters containing either two of the same minority component, *e.g.*, two histidines, or two different minority components, *e.g.*, an arginine and a leucine. Because the serine clustering agent is present in significant excess, the majority of the heterogeneous cluster ion abundance corresponds to the incorporation of a single analyte. Greater ion abundance of clusters containing multiple different analytes would be expected at either larger cluster sizes or at higher relative molar fractions. For example, ten clusters with $n = 29$ are observed: a homogeneous serine cluster, as well as nine heterogeneous clusters corresponding to the incorporation of up to two analyte molecules. Using the abundances of these ten clusters in Eq 1, solution molar fractions of 1.36%, 1.78%, and 1.05% are determined for arginine, histidine and leucine, respectively. Excluding the six heterogeneous clusters corresponding to multiple incorporations and using only the abundances of the four clusters corresponding to the homogeneous cluster and the incorporation of a single analyte molecule in Eq 1 results in solution molar fractions of 0.56%, 1.18% and 0.47% for arginine, histidine and leucine, respectively. Thus, without including the contribution of clusters containing multiple analyte molecules, the solution molar fractions obtained by this method are artificially low because a significant amount of ion abundance is present in clusters containing multiple analyte molecules.

Solution molar fractions for each analyte at various cluster sizes were obtained by solving Eq 1 iteratively for each analyte in the mixture and these values are shown in Figure 7.3. The most intense protonated molecule is not the clustering agent serine but arginine, which comprises 61% of the molecular ion abundance even though it is present at only a 2% solution molar fraction, a 30-fold excess. Histidine also ionizes efficiently, comprising 33% relative molecular ion abundance, 15-fold higher than its molar fraction in solution. Interestingly, the relative ion abundance of protonated leucine is ~1%, although the similarity between relative protonated molecule abundance and solution molar fraction for this analyte is almost certainly coincidental. Previous results for leucine-serine mixtures showed a strong enhancement in formation of protonated leucine, 54-fold in excess of its solution molar fraction [46]. As a result of the anomalously high ion abundances of arginine and histidine, protonated serine, the primary component of the mixture, is only ~5% relative abundance, 19-fold less than its 95% solution molar fraction. The anomalously high abundances of the protonated arginine and histidine relative to the clustering agent are likely due to their high basicity, although differences in surface activity and instrumental parameters can also affect relative ion abundances.

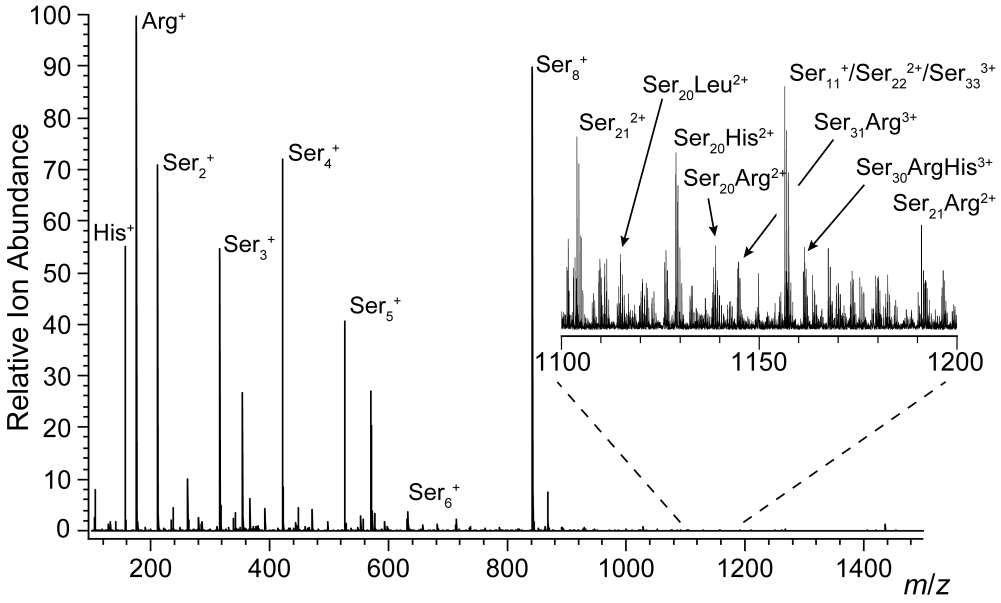


*Figure 7.2. ESI mass spectrum of a solution containing serine, histidine, arginine and leucine in a 95/2/2/1 ratio, respectively. Expanded region shows homogeneous and heterogeneous cluster ions of varying size, with specific clusters denoted.*

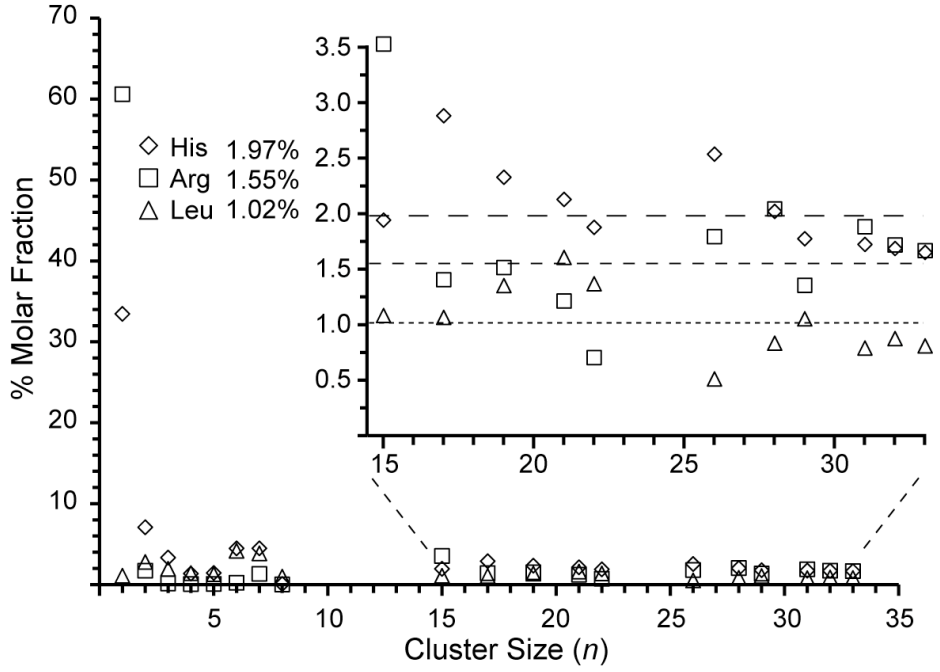


*Figure 7.3. Percent molar fractions obtained from the cluster abundances formed by ESI of a solution containing serine, histidine, arginine and leucine in a 95/2/2/1 molar fraction, respectively, as a function of cluster size. Dashed lines indicate the average molar fractions obtained from cluster measurements of the n = 19 through 33 for histidine (1.97%), arginine (1.55%), and leucine (1.02%).*

In contrast to the protonated molecules, the cluster compositions rapidly reflect the relative solution molar fraction with increasing cluster size. Even though serine is only ~5% of the molecular ion signal, it represents 88% and 96% of the composition of all dimers and trimers, respectively. This indicates that incorporation of molecules present in the solution into the cluster ions is more statistical, although some specificity is still observed at these small sizes. For example, dimers of serine and histidine appear to be preferentially formed, comprising 11% of all dimer ions, corresponding to a ~6% molar fraction. Arginine is preferentially excluded from the trimer, comprising only 0.3% of the ion abundance, corresponding to a 0.1% molar fraction.

For the octameric clusters, histidine and arginine both incorporate at a much lower ratio than expected statistically, resulting in measured molar fractions of 0.08% and 0.01%, respectively. Leucine, however, incorporates statistically at ~1%. As has been reported previously, the serine octamer typically forms a chirally selective specific structure that has been demonstrated to exclude a number of other amino acids that disrupt the octamer structure [48-50].

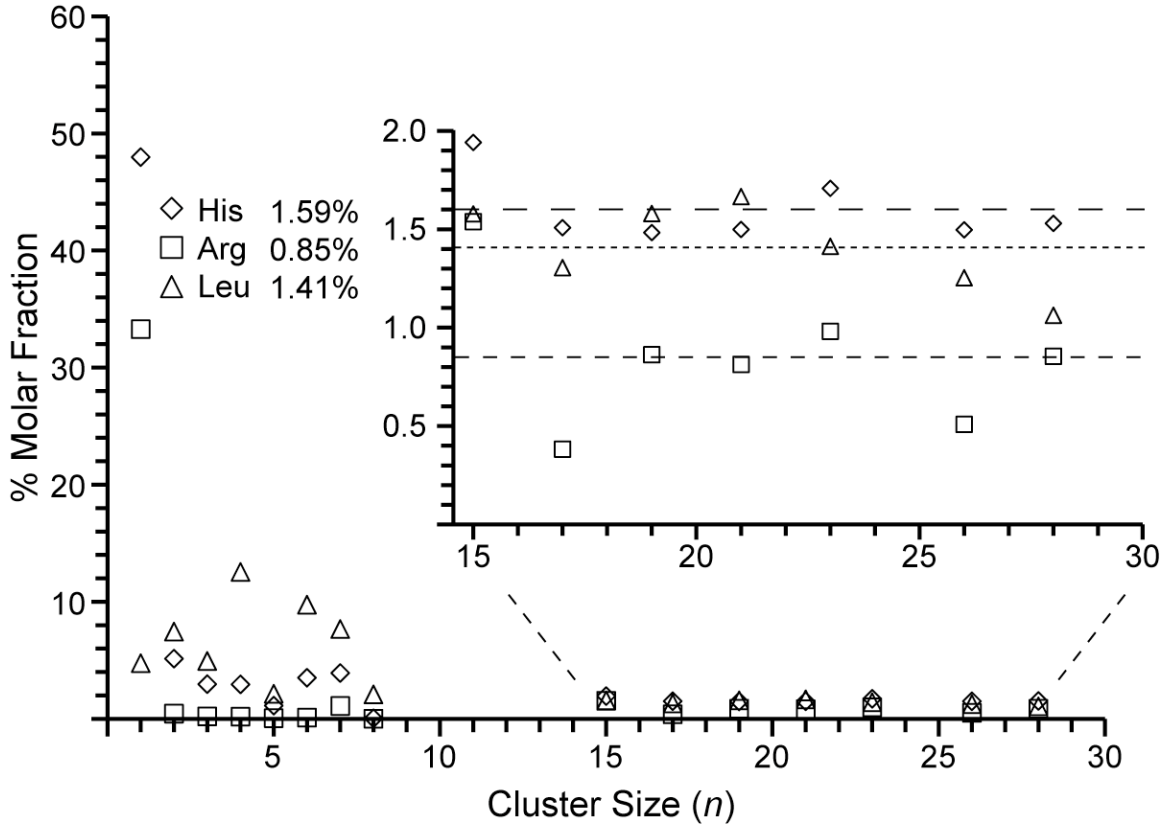


*Figure 7.4. Percent molar fractions obtained from the cluster abundances formed by ESI of a solution containing serine, histidine, arginine and leucine in a 95/2/1/2 ratio, respectively, as a function of cluster size. Dashed lines indicate the average molar fractions obtained from cluster measurements of the n = 19 through 28 clusters for histidine (1.59%), leucine (1.41%), and arginine (0.85%).*

For cluster ions with $n$ between 19 and 33 (Figure 7.3, inset), average molar fractions of 1.97%, 1.55%, and 1.02% are obtained for arginine, histidine and leucine, respectively. At these larger cluster sizes, the compositions are largely independent of cluster size, and correlate well with the solution values of 1.93%, 1.95%, and 0.90% for these respective analytes. Thus, the composition of large, gas-phase clusters reflects the solution composition to within 25% accuracy.

To determine if the cluster compositions are sensitive to small changes in the solution composition, an ESI mass spectrum of a mixture of serine, histidine, arginine and leucine in an approximately 95/2/1/2 ratio, respectively, was obtained, and the percent molar fractions calculated from this spectrum are shown in Figure 7.4. For the protonated molecules, histidine is 48% of the total ion abundance, with arginine and leucine comprising 33% and 5%, respectively, inconsistent with their 2/1/2 solution ratios. However, values obtained from large cluster ions with $n$ = 19-28 are 1.59%, 0.85%, and 1.41% for histidine, arginine and leucine respectively, reasonably consistent with their respective solution molar fractions of 1.93%, 0.98% and 1.81%. The slightly lower values obtained in this experiment are likely an artifact of the low cluster ion S/N ratio. Noise disproportionately affects low signal-to-noise ratio heterogeneous peaks [45], such as those observed here, resulting in slightly lower values when analyzed by a weighted average. Improving the S/N through additional signal averaging or reducing chemical noise due to the other nonspecific adducts, such as salts, would likely improve the accuracy of these measurements. Even with these caveats, the abundances and composition of the cluster ions can be used to obtain a moderately accurate measure of solution molar fractions (~20% for histidine) whereas the abundances of protonated molecules can differ dramatically from their solution molar fractions (30 fold for histidine). These results show that this cluster method can be used to measure small changes in relative solution concentration of the analytes.

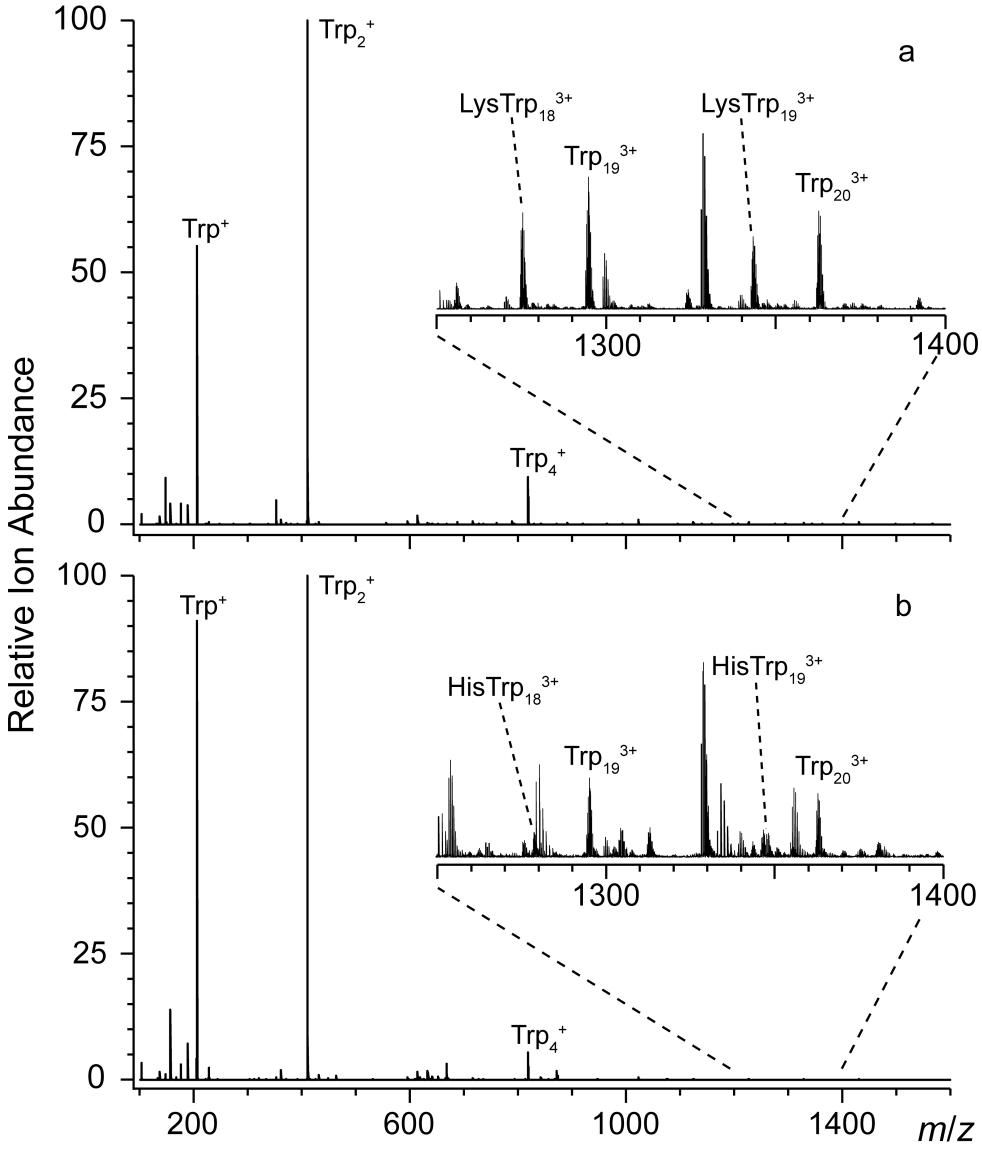


*Figure 7.5. ESI mass spectra of solutions containing tryptophan, lysine, histidine, glycine, alanine, serine, threonine, leucine, phenylalanine and arginine in differing ratios: (a) 87/5/1/1/1/1/1/1/1/1 and (b) 87/1/5/1/1/1/1/1/1/1, respectively. An expanded region of the spectrum shows homogeneous and heterogeneous clusters with selected clusters denoted (see text).*

**7.3.3 Solution Molar Fractions from More Complex Mixtures.** To investigate the extent to which this clustering agent method can be applied to more complex mixtures, two solutions were prepared. Each solution contained ten components: a clustering agent (tryptophan; 87%) and different concentrations of nine other amino acids. The minority components glycine, alanine, serine, threonine, leucine, lysine, histidine, phenylalanine and arginine are 1/1/1/1/1/5/1/1/1 and 1/1/1/1/1/1/5/1/1 percent, respectively, and ESI mass spectra of these two solutions are shown in Figure 7.5a and 7.5b, respectively. Tryptophan was selected as a clustering agent because its mass is roughly twice that of serine. The resulting increase in *m*/*z* spacing between each homogeneous cluster reduces spectral overlap of the many possible heterogeneous clusters that could be formed.

For the protonated molecules, significant differences between the relative abundance and the solution molar fraction are observed. For some analytes, ionization efficiency is significantly enhanced. Protonated arginine is present at a 1% molar fraction in both solutions but has relative abundances of 6% and 3% from the two solutions, respectively. The solution molar fractions of lysine and histidine are each 5% in these respective solutions, yet their relative protonated molecule signals are both 13%. For many of the other analytes, ionization is suppressed. Both protonated alanine and protonated threonine have relative abundances of 0.02% and 0.01% in the respective solutions, corresponding to 50 and 100 fold suppressions in their ion abundance relative to their solution molar fractions. Thus, as was observed for the four-component mixtures, the relative abundances of the protonated molecules correlate poorly with solution molar fraction in these more complex mixtures.

*Table 7.1. Clustering Agent Percent Molar Fractions from Solutions Containing Nine Analytes.*

| Gly | Ala | Ser | Thr | Leu | Lys | His | Phe | Arg |
|---|---|---|---|---|---|---|---|---|
| 0.84[a] | 0.43[a] | 0.53[a] | 0.48[a] | 0.35[a] | 1.71[a] | 0.42[a] | 0.27[a] | 0.75[a] |
| (1.00) | (1.11) | (1.01) | (1.05) | (1.07) | (5.09) | (0.98) | (1.09) | (0.98) |
| 0.79[b] | 0.49[b] | 0.85[b] | 0.36[b] | 0.77[b] | 0.55[b] | 1.60[b] | 0.70[b] | 0.54[b] |
| (1.00) | (1.11) | (1.01) | (1.05) | (1.07) | (1.02) | (4.90) | (1.10) | (0.98) |

[a] Percent molar fraction obtained from clusters with $n$ = 17 through 22 observed in the mass spectrum from Figure 5a. Solution values are listed in parentheses.
[b] Percent molar fraction obtained from clusters with $n$ = 17 through 22 observed in the mass spectrum from Figure 5b. Solution values are listed in parentheses.

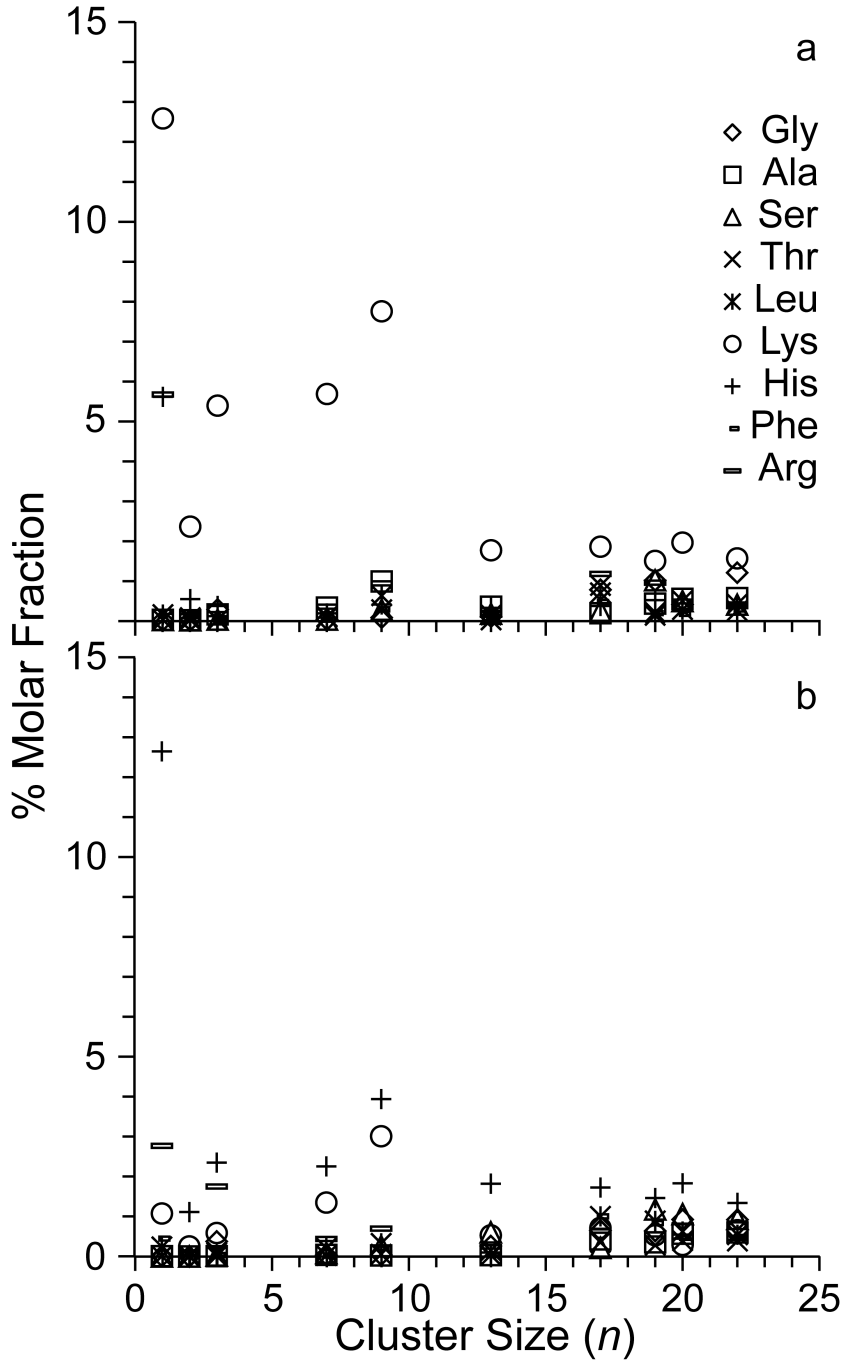


*Figure 6. Percent molar fractions obtained from clusters formed from solutions containing tryptophan, lysine, histidine, glycine, alanine, serine, threonine, leucine, phenylalanine and arginine in differing ratios: (a) 87/5/1/1/1/1/1/1/1/1 and (b) 87/1/5/1/1/1/1/1/1/1, respectively, as a function of cluster size.*

In addition to the protonated molecules, cluster ions with *n* up to 22 are also formed from these solutions (Figure 7.5). Homogeneous cluster ions containing only tryptophan are observed, as are a host of heterogeneous cluster ions corresponding to the incorporation of 1 or 2 analyte molecules into a tryptophan cluster. The molar fractions determined from these cluster ions for each of the nine analytes are shown as a function of cluster size in Figure 7.6. At small *n*, formation of homogeneous tryptophan clusters is favorable, and most heterogeneous clusters are suppressed. However, the abundances and composition of heterogeneous clusters begins to more closely reflect the solution molar fractions at larger cluster sizes. For $n = 17$ and larger, the average solution molar fraction obtained from clusters by this method is within 25% for glycine and within a factor of ~2 for most other analytes (Table 7.1).

Although mole fractions obtained from the cluster data provide a significantly more reliable indication of solution composition compared to the individual protonated molecule abundances, these values are not as accurate as those obtained for less complex mixtures. There is evidence for either specific incorporation of molecules into the clusters or possible differences in ionization efficiency for heterogeneous clusters of the same size. For example, expanded regions of the mass spectra showing homogeneous and heterogeneous clusters for $n = 19$ and 20 are inset in Figure 5a and b. Even though lysine and histidine are the same 5% solution molar fraction in their respective solutions, the abundances of heterogeneous clusters containing a single lysine (Figure 5a) or a single histidine (Figure 5b) differ significantly compared to their corresponding homogeneous tryptophan clusters. For the $n = 20$ clusters, the heterogeneous peak containing a single lysine (a) or histidine (b) should be 1.15 times *more* abundant than the homogeneous tryptophan cluster if these cluster compositions are statistical. However, the respective relative abundances are 74% and 29% (Figure 5, insets). This indicates that incorporation of both lysine and histidine into this large tryptophan cluster is hindered, and that incorporation of histidine is less favorable than lysine.

Additional evidence for specific incorporation into tryptophan clusters is found at other cluster sizes. This suggests that clusters formed from these mixtures may not just occur as a sequential addition of individual amino acids. Large clusters could also be formed through the aggregation of smaller clusters, such as dimers and trimers. Small clusters more readily form specific structures and incorporation of these specific structures into larger clusters would skew the observed ion abundances of larger heterogeneous clusters to reflect the less statistical incorporation.

Although lysine and histidine show different extents of incorporation into the various heterogeneous clusters, the measured molar fractions obtained for lysine and histidine are essentially the same: 1.7% and 1.6%, respectively, for clusters with $n = 17$ through 22. Even though specific cluster formation occurs, the sum total composition analysis over a wide range of cluster sizes more accurately reflects solution molar fraction than data for an individual cluster size. This suggests that cluster formation may occur stoichiometrically, if not statistically at each cluster size, which is consistent with these clusters being predominately formed by a charged residue mechanism, as has been reported previously [46,50]. Although this method is clearly not as accurate as techniques using traditional standards, this method offers a significantly more reliable

indicator of solution composition than the abundances of individual protonated molecules and provides rapid, albeit rough, quantitative information even from relatively complex mixtures.

## 7.4 Conclusions.

The compositions of mixtures containing either four or ten amino acids were analyzed by using the abundances of both homogeneous and heterogeneous cluster formed by ESI. Although the relative abundances of some of the protonated molecules differed from their molar fractions in solution by as much as two orders of magnitude, the molar fractions determined from larger clusters were within 25% for the four-component solutions although poorer accuracy was obtained for the ten-component mixtures where the solution molar fractions could typically be determined within a factor of three. This indicates that the accuracy of this cluster quantitation method decreases with increasing mixture complexity, but it can still provide some quantitative information directly from an ESI mass spectrum.

There are several challenges in extending this method to more complex mixtures. With increasing mixture complexity, the ion signal is spread into many additional clusters reducing the overall signal-to-noise ratio of a given cluster. This also increases the resolving power required to separate all the different clusters. Preferential incorporation of some components into the clusters may occur for solutions that contain molecules that have vastly different physical properties. Multiple measurements using different clustering agents may reduce error associated with specific incorporation of some analytes.

Although not as accurate as traditional methods using either internal or external standards, this cluster quantitation method does have the advantages that the analytes do not need to be identified, and quantitative information for all analytes can be obtained simultaneously. This cluster quantitation method may be advantageous when combined with separations or when there is a limited number of unknown analytes, such as mixtures containing intermediates and side reaction products generated during the synthesis of organic or pharmaceutical molecules, or with illicit drugs of unknown structure.

## 7.5 Acknowledgements.

The authors are grateful for financial support from the National Institutes of Health (Grant R01 GM064712-08)

**7.6 References.**


[1] Domon, B.; Aebersold, R. *Science* **2006**, *312*, 212-217.

[2] Marshall, A. G.; Rodgers, R. P. *Acc. Chem. Res.* **2003**, *37*, 53-59.

[3] Kim, S.; Rodgers, R. P.; Marshall, A. G. *Int. J. Mass Spectrom.* **2006**, *251*, 260-265.

[4] Conrads, T. P.; Anderson, G. A.; Veenstra, T. D.; Pasa-Tolic, L.; Smith, R. D. *Anal. Chem.* **2000**, *72*, 3349-3354.

[5] Hernandez, H.; Niehauser, S.; Boltz, S. A.; Gawandi, V.; Phillips, R. S.; Amster, I. J. *Anal. Chem.* **2006**, *78*, 3417-3423.

[6] Hoke, S. H.; Wood, J. M.; Cooks, R. G.; Li, X. H.; Chang, C. J. *Anal. Chem.* **1992**, *64*, 2313-2315.

[7] Reid, G. E.; McLuckey, S. A. *J. Mass Spectrom.* **2002**, *37*, 663-675.

[8] Breuker, K.; Jin, M.; Han, X. M.; Jiang, H. H.; McLafferty, F. W. *J. Am. Soc. Mass Spectrom.* **2008**, *19*, 1045-1053.

[9] Sleno, L.; Volmer, D. A. *Rapid Commun. Mass Spectrom.* **2005**, *19*, 1928-1936.

[10] Kelleher, N. L.; Lin, H. Y.; Valaskovic, G. A.; Aaserud, D. J.; Fridriksson, E. K.; McLafferty, F. W. *J. Am. Chem. Soc.* **1999**, *121*, 806-812.

[11] Iavarone, A. T.; Udekwu, O. A.; Williams, E. R. *Anal. Chem.* **2004**, *76*, 3944-3950.

[12] Konermann, L.; Douglas, D. J. *Biochemistry* **1997**, *36*, 12296-12302.

[13] Cech, N. B.; Enke, C. G. *Anal. Chem.* **2000**, *72*, 2717-2723.

[14] Taylor, P. J. *Clin. Biochem.* **2005**, *38*, 328-334.

[15] Cohen, S. L.; Chait, B. T. *Anal. Chem.* **1996**, *68*, 31-37.

[16] Tang, K.; Allman, S. L.; Jones, R. B.; Chen, C. H. *Anal. Chem.* **1993**, *65*, 2164-2166.

[17] Wang, M. Z.; Fitzgerald, M. C. *Anal. Chem.* **2001**, *73*, 625-631.

[18] Knochenmuss, R.; Stortelder, A.; Breuker, K.; Zenobi, R. *J. Mass Spectrom.* **2000**, *35*, 1237-1245.

[19] Fenn, J. B. *J. Am. Soc. Mass Spectrom.* **1993**, *4*, 524-535.

[20] Cech, N. B.; Enke, C. G. *Anal. Chem.* **2001**, *73*, 4632-4639.

[21] Page, J. S.; Kelly, R. T.; Tang, K.; Smith, R. D. *J. Am. Soc. Mass Spectrom.* **2007**, *18*, 1582-1590.

[22] Cheng, J.; Vecitis, C. D.; Hoffmann, M. R.; Colussi, A. J. *J. Phys. Chem. B* **2006**, *110*, 25598-25602.

[23] Iavarone, A. T.; Williams, E. R. *J. Am. Chem. Soc.* **2003**, *125*, 2319-2327.

[24] Kebarle, P. *J. Mass Spectrom.* **2000**, *35*, 804-817.

[25] Pan, P.; McLuckey, S. A. *Anal. Chem.* **2003**, *75*, 5468-5474.

[26] King, R.; Bonfiglio, R.; Fernandez-Metzler, C.; Miller-Stein, C.; Olah, T. *J. Am. Soc. Mass Spectrom.* **2000**, *11*, 942-950.

[27] Cech, N. B.; Enke, C. G. *Mass Spectrom. Rev.* **2001**, *20*, 362-387.

[28] Hogan, C. J.; Carroll, J. A.; Rohrs, H. W.; Biswas, P.; Gross, M. L. *Anal. Chem.* **2009**, *81*, 369-377.

[29] Iavarone, A. T.; Jurchen, J. C.; Williams, E. R. *J. Am. Soc. Mass Spectrom.* **2000**, *11*, 976-985.

[30] Lee, M. S.; Kerns, E. H. *Mass Spectrom. Rev.* **1999**, *18*, 187-279.

[31] Smith, R. D.; Anderson, G. A.; Lipton, M. S.; Pasa-Tolic, L.; Shen, Y.; Conrads, T. P.; Veenstra, T. D.; Udseth, H. R. *Proteomics* **2002**, *2*, 513-523.

[32] Matuszewski, B. K.; Constanzer, M. L.; Chavez-Eng, C. M. *Anal. Chem.* **2003**, *75*, 3019-3030.

[33] Regnier, F. E.; Riggs, L.; Zhang, R. J.; Xiong, L.; Liu, P. R.; Chakraborty, A.; Seeley, E.; Sioma, C.; Thompson, R. A. *J. Mass Spectrom.* **2002**, *37*, 133-145.

[34] Zhang, L. K.; Gross, M. L. *J. Am. Soc. Mass Spectrom.* **2000**, *11*, 854-865.

[35] Marshall, J.; Franks, J.; Abell, I.; Tye, C. *J. Anal. At. Spectrom.* **1991**, *6*, 145-150.

[36] Conrads, T. P.; Alving, K.; Veenstra, T. D.; Belov, M. E.; Anderson, G. A.; Anderson, D. J.; Lipton, M. S.; Pasa-Tolic, L.; Udseth, H. R.; Chrisler, W. B.; Thrall, B. D.; Smith, R. D. *Anal. Chem.* **2001**, *73*, 2132-2139.

[37] Keshishian, H.; Addona, T.; Burgess, M.; Kuhn, E.; Carr, S. A. *Mol. Cell. Proteomics* **2007**, *6*, 2212-2229.

[38] Bantscheff, M.; Schirle, M.; Sweetman, G.; Rick, J.; Kuster, B. *Anal. Bioanal. Chem.* **2007**, *389*, 1017-1031.

[39] Oda, Y.; Huang, K.; Cross, F. R.; Cowburn, D.; Chait, B. T. *Proc. Natl. Acad. Sci. U. S. A.* **1999**, *96*, 6591-6596.

[40] Gygi, S. P.; Rist, B.; Gerber, S. A.; Turecek, F.; Gelb, M. H.; Aebersold, R. *Nature Biotech.* **1999**, *17*, 994-999.

[41] Ong, S. E.; Blagoev, B.; Kratchmarova, I.; Kristensen, D. B.; Steen, H.; Pandey, A.; Mann, M. *Mol. Cell. Proteomics* **2002**, *1*, 376-386.

[42] Lill, J. *Mass Spectrom. Rev.* **2003**, *22*, 182-194.

[43] Maurer, H. H. *J. Chromatogr. B* **1998**, *713*, 3-25.

[44] Hopfgartner, G.; Bourgogne, E. *Mass Spectrom. Rev.* **2003**, *22*, 195-214.

[45] Leib, R. D.; Flick, T. G.; Williams, E. R. *Anal. Chem.* **2009**, *81*, 3965-3972.

[46] Flick, T. G.; Leib, R. D.; Williams, E. R. *Anal. Chem.* **2009**, *81*, 8434-8440.

[47] Flick, T. G.; Leib, R. D.; Williams, E. R. *Anal. Chem.* **2010**, *82*, 1179-1182.

[48] Nanita, S. C.; Cooks, R. G. *Angew. Chem. Int. Ed.* **2006**, *45*, 554-569.

[49] Hodyss, R.; Julian, R. R.; Beauchamp, J. L. *Chirality* **2001**, *13*, 703-706.

[50] Spencer, E. A. C.; Ly, T.; Julian, R. R. *Int. J. Mass Spectrom.* **2008**, *270*, 166-172.

[51] Robinson, E. W.; Williams, E. R. *J. Am. Soc. Mass Spectrom.* **2005**, *16*, 1427-1437.

# Chapter 8

## Future Prospects and Concluding Remarks.

This dissertation represents the first steps for two new techniques that use clusters of ions to obtain previously unknown characteristics of ion energetics and mixture composition. They provide a significant improvement on previous estimations or measures in terms of simplicity, specificity and speed of analysis, although in some cases at the sacrifice of some accuracy. Both of the methods presented in this dissertation are inherently general: the identity of the analyte within the cluster does not in principle affect the ability to make the measurement. This means that reactions that are difficult to perform in bulk, such as the one-electron reduction of Fe, are now readily achievable in the gas phase, and can be compared subsequently with other bulk-like measurements. Further, the cluster quantitation approaches seem particularly useful in cases where the analyte is unknown or more traditional standards are not readily available.

To take full advantage of the ion nanocalorimetry method, a variety of extensions of these experiments are already being explored. Continuing on the work presented in Chapter 4, a variety of thermodynamic methods have been devised using ionic clusters to elucidate the electrochemical series using these gas-phase measurements, and the first direct and fully experimental measures of the absolute standard hydrogen electrode have already been obtained by comparison of bulk relative redox reactions with gas-phase ion-electron nanocalorimetry experiments. This nanocalorimetry method has also been applied to characterize stable, hydrated ion electron pair formation, resulting in a direct measure of the absolute electron solvation enthalpy, the solvation energy of the proton, the effect of electron kinetic energy on the electron capture process, and the energy of fluorescent photons released after absorption by a hydrated fluorophore. Another interesting avenue for further exploration is the ability to hydrate species with multiple reaction pathways and quantify the thermodynamic differences between these reactions. This work has already begun in peptides, and could likely be extended to other small molecules, sugars, and nucleic acids.

An important improvement as these experiments continue would be to upgrade the existing 2.7 T FT/ICR MS datastation from its current 256k MIDAS system to a 8M PDAS like that described in Chapter 2 for the 9.4 T FT/ICR MS. This easy, inexpensive improvement should offer significantly higher resolving powers particularly at large $m/z$, and with the improved filter design will likely improve the signal-to-noise ratio by at least an order of magnitude.

When using this method to characterize hydrated species, one of the most critical improvements is to be able to perform this technique on larger clusters. Improvements to the existing instrumentation to allow access to such clusters are currently underway; the replacement of the 2.7 T magnet with a 7 T magnet should

allow storage of clusters approximately an order of magnitude larger than those studied here, assuming they can be stored for sufficient time to make the measurement before dissociation. Additional improvements to the cold ion cell design may further this pursuit. This should allow species to be studied in increasingly 'bulk-like' solutions, allowing these studies to approach ever closer to a direct description of solution reactivity by means of a simple gas-phase measurement.

Another interesting direction to take this nanocalorimetry technique is to use it to investigate ion structure. In the bulk, peptide and protein structure is thought to depend heavily on the local hydration environment, and this hydrated cluster method allows the sequential attachment of waters to investigate solvation effects. This is particularly advantageous in structures where the ion's charge is diffused over multiple charge carrier sites, such as with multiply protonated proteins. A good model system for this type of structure is diammonium alkanes. Figure 8.1 shows the waters lost following electron attachment for various cluster sizes of two diammonium alkanes, 1,7 diammoniumheptane and 1,12 diammoniumdodecane. At large sizes, the loss of water from the alkanes depends very little on the differences in the alkane chain length, *e.g.*, on average losing 9.4 and 9.5 waters for the $n$ = 40 clusters of the heptane and dodecane, respectively.

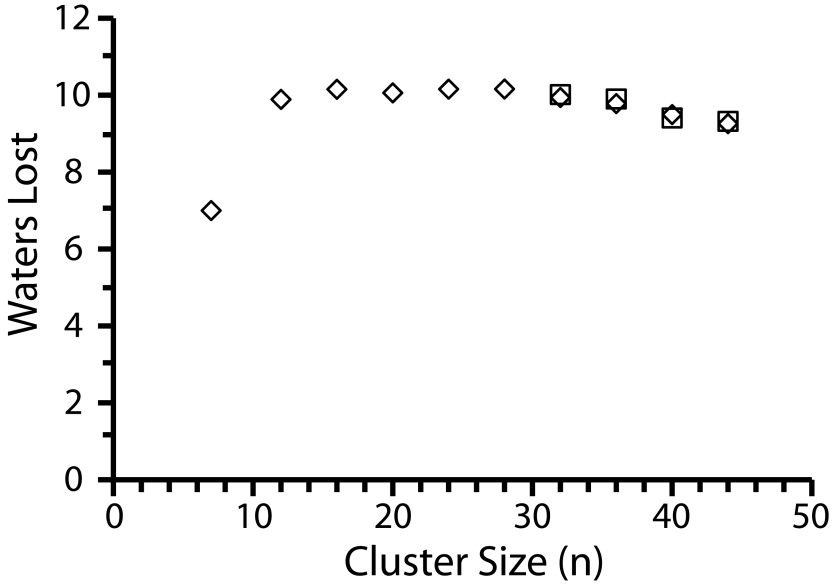


Figure 8.1. Water loss with respect to cluster size for 1,7 diammoniumalkane (squares) and 1,12 diammonium alkane (diamonds).

This result provides insight into the structure of these large cluster ions. Without water attachment, the doubly charged alkane should be highly constrained by Coulomb interactions between the two protons, with the heptane clearly more restricted by the closer proximity of the two charge carriers. Addition of even a

handful of waters to diammoniumdodecane appears to overcome this Coulomb repulsion, as the loss of water does not depend significantly on cluster size. If Coulomb interactions dominated at larger cluster sizes, the cluster would be split into two discrete water clusters around the ammonium moieties, resembling a "barbell" type structure. Upon reduction of one of the charge sites, this structure would likely spontaneously lose its attached waters, roughly half the total number of waters attached. Instead, the observed water loss suggests that the waters bridge between both ammonium moieties prior to electron capture, and therefore the reduction of one of the charge sites to an ammonia does not result in excessive loss from that site because the waters are stabilized through a network of hydrogen bonds to the other charge carrier.

Additional support for this "pincher" solvation structure, where both charge sites are interacting with the same water cluster, is found in the observed H radical loss, regardless of cluster size or alkane length. One possible explanation for the observed H radical loss here is that the radical formed from reduction of the charge carrier takes place near the surface of the droplet, allowing for the H radical to be easily lost from the cluster. If the charges were buried further into the cluster, H radical loss would be less likely, particularly as cluster size increased.

Two additional experiments seem beneficial to test this structural hypothesis. First, a rigid linker could be used between the two charged moieties to force separation between the charge carriers and reduce the likelihood of bridging waters between them. Assuming that each water is only interacting with a single charge site, approximately one half of all waters would be lost following the reduction, regardless of size. A second useful experiment would be to use infrared ion spectroscopy of the smaller doubly charged clusters to obtain additional structural characterization of these species as the water-binding network is formed. This may help elucidate the transition between the "barbell" separated structure and the "pincher" charge-solvated structure.

In cases where the energetic resolution of this nanocalorimetry technique is critical to describing energetically similar but distinct pathways, another interesting option to improve the energy resolution is found by changing the solvent used to form the cluster. By moving to a solvent such as methanol, the binding energy of each molecule to the cluster would roughly halve, resulting in a two-fold improvement in energy resolution obtained by similar measurements.

By the same token, cluster quantitation is likely improved by determining a set of small molecules that are readily attainable and useful as clustering agents. Here, amino acids and peptides are explored, but other clustering agents such as small organic molecules may prove very promising. Use of a readily available, homologous clustering agents related to the analytes expected to be present in the mixture would likely improve the statistical incorporation into clusters and reduce any observed differences in ionization efficiency. This sort of approach could help extend this technique into pharmaceutical and forensic applications.

Further, forensic and pharmaceutical mixtures–where the number of components in, *e.g.*, an illicit drug mixture, pill or synthetic step, is relatively discrete–seem to be the ideal place to apply this quantitation method. In both cases, traditional standards may not be available due to either restricted access or insufficient available quantities, and rapid screening is ideal. This approach has already been successfully applied to a variety of pharmaceutical pill mixtures to accurately quantify active ingredients [1]. Expanding into analysis of forensic or organic synthesis mixtures is an interesting next step.

Similarly, use of this method in security applications is of particular interest, especially given the invasive nature of security procedures currently being employed at state buildings and airports. Mass spectrometry is already widely accepted as a reasonable detection method for explosives and other illicit materials; implementing cluster quantitation methods delivered through atmospheric pressure or surface sampling technologies seems a viable alternative. In these cases, using clustering agent solutions on passengers or their belongings would likely reduce false positives, allowing for improved security with less privacy invasion.

**References.**

[1] Flick, T. G.; Leib, R. D.; Williams, E. R. *Anal. Chem*. **2010**, *82*, 1179-1182.